

NASA Technical Paper 1704

# The Effect of Throat Contouring on Two-Dimensional Converging-Diverging Nozzles at Static Conditions

Mary L. Mason, Lawrence E. Putnam,  
and Richard J. Re

AUGUST 1980

CASE FILE  
COPY

**NASA**

NASA Technical Paper 1704

# The Effect of Throat Contouring on Two-Dimensional Converging-Diverging Nozzles at Static Conditions

Mary L. Mason, Lawrence E. Putnam,  
and Richard J. Re  
*Langley Research Center  
Hampton, Virginia*



National Aeronautics  
and Space Administration

**Scientific and Technical  
Information Branch**

1980

## SUMMARY

An experiment has been conducted at static conditions to determine the nozzle internal-performance effect of throat contouring, the result of increasing the circular-arc throat radius. Five nonaxisymmetric converging-diverging nozzles were tested in the static-test facility of the Langley 16-Foot Transonic Tunnel. Internal-performance data were recorded at nozzle pressure ratios up to 9.0. Data are presented as internal thrust ratios, discharge coefficients, and static-pressure distributions. Throat contouring resulted in a positive effect on discharge coefficient but showed no significant improvement in internal thrust ratio except in cases of internal flow separation. As an illustration of the use of the data, a two-dimensional inviscid theory was applied to the five converging-diverging nozzles. The generally good comparisons of data with theoretical results indicate that two-dimensional inviscid theory can be applied successfully to the prediction of two-dimensional converging-diverging nozzle internal flow.

## INTRODUCTION

Multiengine, highly maneuverable jet aircraft must operate efficiently over a wide range of power settings and Mach numbers. Such aircraft require a propulsion exhaust-nozzle system with a variable geometry for high performance at different throttle settings. The axisymmetric nozzle has generally been implemented in the conventional multiengine jet configuration. Axisymmetric nozzles are relatively lightweight, have high internal performance, and facilitate integration of the nozzle with the jet engine. However, the application of an axisymmetric nozzle system to a typical multiengine jet configuration produces certain aircraft performance penalties, such as high aft-end drag (refs. 1, 2, and 3). The integration of multiple nozzles with the airframe results in a complex aft-end flow field, a source of considerable external drag. The aft-end drag effect is increased by the boattail "gutter" interfairing, which is generally required between the jet engines or nozzles (ref. 4).

Investigations of the effects of nozzle design on twin-engine jet aircraft performance (refs. 5 to 13) indicate that a high level of nozzle performance, without considerable aft-end drag, results from use of the nonaxisymmetric nozzle concept. The nonaxisymmetric nozzle geometry is more efficiently integrated into the airframe, eliminating the boattail gutter interfairing. Installation of the nonaxisymmetric nozzle allows design options for thrust vectoring and thrust reversing, capabilities which improve the maneuverability and handling of the aircraft.

Most of the experimental investigations of nonaxisymmetric nozzle performance concerned the installed and isolated performance of specific nozzle designs at realistic nozzle power settings. Recent investigations (refs. 14 and 15) provided detailed parametric data on some internal design geometry

variables. Such parametric investigations establish an internal-performance data base for nozzle design optimization.

The parametric analyses included investigation of the two-dimensional converging-diverging (2-D C-D) nozzle geometry, one of the basic nonaxisymmetric nozzle types. However, the current 2-D C-D nozzle data base does not include the performance effect of a systematic variation in nozzle throat contour. Therefore, an experiment has been conducted to determine the effects on internal performance of contouring the nozzle throat by varying throat radius. Two 2-D C-D nozzles having high internal performance (ref. 15) were selected as suitable geometries. Five additional nozzles of similar design were fabricated with different throat radii. These five nozzles, which involved two different throat radius values, were tested in the static-test facility of the Langley 16-Foot Transonic Tunnel. Internal-performance data are presented as discharge coefficients, internal thrust ratios, and static-pressure distributions.

A two-dimensional, inviscid computational model for the calculation of internal nozzle flow (ref. 16) was applied to the five configurations. The computational results are compared with the experimental data at selected experimental conditions.

#### SYMBOLS

All forces and angles are referenced to the model center line. The center line serves as the body axis. A detailed discussion of the data reduction and calibration is given in reference 14. Extensive definitions of forces, angles, and propulsion relationships used in this report are also discussed in reference 14.

$A_e$	nozzle-exit area, $\text{cm}^2$
$A_t$	nozzle-throat area, $\text{cm}^2$
$A_e/A_t$	nozzle expansion ratio
$F$	gross thrust along body axis, N

$F_i$	ideal isentropic gross thrust,	$w_p \sqrt{RT_{t,j} \left( \frac{2\gamma}{\gamma-1} \right) \left[ 1 - \left( \frac{p_\infty}{p_{t,j}} \right)^{\frac{\gamma-1}{\gamma}} \right]}$	, N
-------	--------------------------------	--	-----

$h_e$	half-height at nozzle exit, cm
$h_i$	half-height at nozzle-connect station, cm
$h_t$	half-height at nozzle throat, cm
$h_1$	height from nozzle center line to beginning of throat-contour section, cm

$h_2$	height from nozzle center line to end of throat-contour section, cm
$l$	length from nozzle-connect station to nozzle-exit station, cm
$l_e$	length from nozzle-throat station to nozzle-exit station, cm
$l_t$	length from nozzle-connect station to nozzle-throat station, cm
$l_1$	length from nozzle-connect station to beginning of throat-contour section, cm
$l_2$	length from beginning of throat-contour section to nozzle-throat station, cm
$l_3$	length from nozzle-throat station to end of throat-contour section, cm
$l_4$	length from end of throat-contour section to nozzle-exit station, cm
$M_d$	design Mach number
$NPR_d$	design nozzle pressure ratio $P_{t,j}/P_\infty$
$p$	local static pressure, Pa
$P_{t,j}$	jet total pressure, Pa
$P_\infty$	ambient pressure, Pa
$R$	gas constant (for $\gamma = 1.3997$ ), 287.3 J/kg-K
$r_c$	nozzle circular-arc throat radius, cm
$T_{t,j}$	jet total temperature, K
$w_i$	ideal mass-flow rate, kg/sec
$w_p$	measured mass-flow rate, kg/sec
$w_t$	nozzle-throat width, 10.157 cm
$x$	axial distance measured from nozzle throat, positive downstream, cm
$y$	lateral distance from model center line, positive to left looking upstream, cm
$z$	vertical distance measured from model center line, positive up, cm
$\gamma$	ratio of specific heats, 1.3997 for air
$\epsilon$	nozzle divergence angle, deg
$\theta$	nozzle convergence angle, deg

## Configuration designations:

2-D C-D	two-dimensional converging-diverging
A1,A2	low-divergence-angle 2-D C-D nozzle configurations
B1,B2,B3	high-divergence-angle 2-D C-D nozzle configurations

## APPARATUS AND METHODS

### Static-Test Facility

The experimental investigation was conducted in the static-test facility of the Langley 16-Foot Transonic Tunnel. The test area is located in a room with a high ceiling and a large, open doorway. Pressurized air is directed into and through the nozzle model, and the resulting jet exhausts to atmospheric conditions through the doorway.

The static-test facility uses the same clean, dry-air supply as that used in the 16-Foot Transonic Tunnel (ref. 17). The air-control system, also similar to that of the 16-Foot Tunnel, includes valving, filters, and a heat exchanger for maintaining a constant stagnation temperature in the exhaust jet. During the experiment, data were recorded on a 96-channel magnetic-tape data-acquisition system.

### Single-Engine Propulsion Simulation System

The experimental nozzles were mounted on a single-engine air-powered nacelle model. A sketch of the nacelle model, with a typical converging-diverging nozzle installed, is given in figure 1. For this experiment, the body shell of the model was removed from station 0.0 to station 52.07.

An external high-pressure air system provided a continuous flow of clean, dry air which was kept at a controlled temperature of 300 K and pressurized up to 1013 kPa. The airflow entered a high-pressure plenum chamber through six supply lines in the nozzle support system (see fig. 1). The airflow direction was perpendicular to the model axis. The flow then discharged into a low-pressure plenum through eight multiholed sonic nozzles, spaced equally around the high-pressure plenum. The low-pressure plenum, which had a circular cross section, was mounted to a force balance. This procedure minimizes forces which result from the transfer of axial momentum as the air passes from a high-pressure region to a low-pressure region. Two flexible metal bellows seal the system and compensate for axial forces due to the pressurization.

The air flowed from the low-pressure plenum through a transition section, a choke plate, and an instrumentation section to simulate exhaust-jet flow from the nozzle exit. The same transition and instrumentation sections were used for all five nozzle configurations tested in this investigation. The transition section provided a regular flow path from the circular low-pressure plenum to the rectangular choke plate and instrumentation section, illustrated in

figure 1. The instrumentation section had a constant cross-sectional area of  $35.75 \text{ cm}^2$  with a width-to-height ratio of 1.437. The geometry of the instrumentation region was identical to the nozzle airflow entrance. All five nozzle configurations were attached to the instrumentation section at model station 104.47.

### Nozzle Design

Five two-dimensional converging-diverging (2-D C-D) nozzles were investigated in this experiment. Each nozzle consisted of four basic parts designed to define the internal flow-field geometry. A typical 2-D C-D nozzle is shown as part of the experimental apparatus in figure 1. The two upper and lower components are designated as flaps in this report, since these components are used to vary the nozzle geometry in realistic nozzle configurations. Two sidewalls, which are also shown in figure 1, complete the nozzle internal geometry. For all configurations in this experiment, fixed flaps and sidewalls were used. The sidewall length was always equal to the total nozzle length.

Two converging-diverging nozzles, A1 and B1, were used as the baseline nozzle geometries in this experiment. Three nozzles, A2, B2, and B3, which were modified from the baseline designs, were also tested. Sketches of the baseline nozzles, photographs of all five configurations, and tables defining internal and external geometries are given in figure 2. Both baseline configurations had the same throat area, circular-arc throat radius, convergence angle  $\theta$ , and total nozzle length.

The baseline configurations were modified by increasing the circular-arc throat radius while keeping all geometric parameters constant except for  $\theta$  and  $\epsilon$ . Increasing the circular-arc radius from 0.68 cm to 2.74 cm contours the nozzle throat region and increases both  $\theta$  and  $\epsilon$ . For both modified configurations A2 and B2, the circular-arc radius was increased to 2.74. B3, the fifth nozzle for this investigation, was generated from B1 by increasing the circular-arc radius to 2.74 while keeping  $\epsilon$  fixed. In this case, rounding the throat decreases  $\theta$  and increases the total nozzle length. The design parameters which varied in this experiment are presented in the following table for the five configurations:

Parameter	A1	A2	B1	B2	B3
$A_e/A_t$	1.09	1.09	1.80	1.80	1.80
$l$ , cm	11.56	11.56	11.56	11.56	12.25
$M_d$	1.35	1.35	2.08	2.08	2.08
$NPR_d$	2.97	2.97	8.81	8.81	8.81
$r_c$ , cm	.68	2.74	.68	2.74	2.74
$\theta$ , deg	20.84	22.33	20.84	22.33	20.42
$\epsilon$ , deg	1.21	1.21	10.85	11.24	10.85

## Instrumentation

A sketch of the nozzle instrumentation section is included in figure 1. A three-component strain-gage balance was used to measure the forces and moments on the nacelle model and nozzle downstream of station 52.07 cm. Three rakes of total-pressure probes were used to measure the jet total pressure at a fixed station in the instrumentation section. A four-probe rake through the upper surface of the instrumentation section recorded the jet total pressure; a three-probe rake was used on the side; and a three-probe rake was used in the corner. The jet total temperature was measured by a thermocouple which was also located in the instrumentation section.

Internal static-pressure orifices were located on both the upper and lower flaps and on the sidewalls for all five nozzle configurations. Three rows of orifices were placed longitudinally along the upper and lower flaps. On both the right and left sidewalls, a single row of orifices ran along the horizontal center line. Sketches of the nozzle components with the pressure orifice rows are presented in figure 3. Tables defining the locations of the orifices for each configuration are included in the figure.

## Data Reduction

Data were recorded at intervals of increasing jet total pressure. Several repeat points were taken as the jet total pressure was decreased from the maximum level. At each data point, all data values were recorded simultaneously on magnetic tape. Approximately 11 frames of data, taken at a rate of 2 frames per second, were recorded for each data point. The averaged value of these 11 frames of data was used in subsequent computations.

The internal thrust ratio  $F/F_i$ , defined as the ratio of the actual nozzle thrust to the computed ideal nozzle thrust, and the discharge coefficient  $w_p/w_i$ , the ratio of the measured mass-flow rate to ideal mass-flow rate, are the basic nozzle performance parameters. The nozzle thrust parameter  $F$  represents the measured balance axial force corrected for weight tares and balance interactions. However, small bellows tares on axial, normal, and pitch balance components result from a small pressure gradient between the ends of the bellows when internal velocities are high. Bellows tares on the three balance components also result from minor differences in the forward and aft bellows spring constants when the bellows are pressurized. The magnitudes of these bellows tares were calculated by testing calibration nozzles with known performance over a range of normal forces and pitching moments. This procedure is described in detail in reference 14. The balance data were then corrected using an algorithm similar to the balance correction procedure discussed in reference 14.

Several measurements were used in calculating the nozzle mass flow  $w_p$ . The pressure and temperature in the high-pressure plenum of the propulsion simulation system were measured before the airflow was discharged through the eight sonic nozzles into the low-pressure plenum (see fig. 1). The discharge coefficients of the sonic nozzles were determined by testing circular calibration nozzles with known flow characteristics. The sonic-nozzle discharge coefficients



were combined with the temperatures and pressures measured in the high-pressure plenum to determine the mass flow.

## RESULTS AND DISCUSSION

### Basic Data

Basic data for each of the five nozzle configurations are presented as nozzle internal thrust ratio  $F/F_i$  and discharge coefficient  $w_p/w_i$ . The data for nozzles A1 and A2, which have small divergence angles and low expansion ratios, are given in figure 4. The data for nozzles B1, B2, and B3, which have large divergence angles and large expansion ratios, are given in figure 5. The internal-thrust-ratio data and discharge-coefficient data are presented as functions of nozzle pressure ratio.

The discharge-coefficient data in figures 4 and 5 show some variation with nozzle geometry. However, as should be expected,  $w_p/w_i$  is independent of nozzle divergence angle and nozzle pressure ratio since the nozzles were choked for all experimental data. Contouring at the nozzle throat by increasing the circular-arc radius has a positive effect on the discharge coefficient. This positive effect is apparent in the comparison of A2 discharge coefficients with A1 values in figure 4 and in the comparison of B2  $w_p/w_i$  values with B1 values in figure 5. Comparing B3  $w_p/w_i$  values with B1 values shows a less significant increase in discharge coefficient. Although B3 and B2 have the same value of throat radius, the  $w_p/w_i$  levels for B3 are lower than for B2. This inconsistency in the effect of throat radius on discharge coefficient is not fully understood.

The internal-thrust-ratio data show more variation with nozzle pressure ratio than the discharge-coefficient data. Therefore, thrust ratio as a function of nozzle pressure ratio is used to evaluate the isolated static performance of each nozzle. In figure 4, the profiles of  $F/F_i$  as a function of nozzle pressure ratio show little difference in internal performance between nozzles A1 and A2. Both configurations have thrust-ratio data profiles which peak near the design nozzle pressure ratio of 2.97 and gradually decrease as nozzle pressure ratio increases. The similarity of the  $F/F_i$  profiles indicates that contouring the nozzle throat by increasing the throat radius has little effect on the nozzle internal thrust ratio for the 2-D C-D nozzle with low divergence angle.

In figure 5, the  $F/F_i$  plots for the nozzles with high divergence angle show definite variation with throat contouring below the design nozzle pressure ratio. The thrust-ratio data have basically the same behavior for all three nozzles B1, B2, and B3. For each configuration, the value of  $F/F_i$  increases from a minimum at the lowest nozzle pressure ratios to a peak level near the design nozzle pressure ratio of 8.81. Each of the three configurations has the same maximum thrust ratio. However, the level of the minimum thrust ratio at the lower nozzle-pressure-ratio settings depends on the nozzle geometry. A comparison of nozzles B2 and B1 shows that the minimum  $F/F_i$  for nozzle B2 is greater than the minimum value for nozzle B1. This increase in minimum thrust ratio from B1 to B2 is a major effect of throat contouring. A comparison of B3

with B2 shows an increase in minimum  $F/F_i$  from B2 to B3. For nozzle B3, increasing the total nozzle length in addition to increasing the nozzle throat radius results in the optimal minimum  $F/F_i$  for all three high-divergence-angle nozzles. In general, throat contouring has a favorable effect on  $F/F_i$  for the nozzles with high divergence angles at the lower nozzle pressure ratios. At higher nozzle pressure ratios near design, throat contouring has no significant effect on thrust ratio.

### Internal Static-Pressure Distributions

The effects of throat contouring are also evident in plots of internal local static pressure. Detailed listings of internal static-pressure data for all five configurations are presented in tables I to V. Data are given at each of the pressure orifice locations shown in figure 3 and span the full range of experimental nozzle-pressure-ratio settings.

Comparisons of internal static-pressure distributions along the upper-flap axial center line are presented in figure 6 for nozzles A1 and A2, in figure 7 for B1 and B2, and in figure 8 for B1 and B3. The data are presented as local static pressure normalized by jet total pressure,  $p/p_{t,j}$ , and are plotted as a function of  $x$  normalized by  $l_e$ , the distance from the nozzle throat to nozzle exit. Only the static pressures on the upper-flap center line are considered in this comparison, since the center-line pressures generally reflect the basic flow trends for the five configurations. For A1 and A2, the  $p/p_{t,j}$  profiles vary little with nozzle pressure ratio. As a result, only the comparison of A1 and A2 at a nozzle pressure ratio of approximately 6.0 is presented in figure 6. However, for B1, B2, and B3, the nozzles with high divergence angles, the internal flow separates at the lower nozzle pressure ratios. The separation from the nozzle wall is indicated by a sharp rise in  $p/p_{t,j}$  just downstream of the nozzle throat. As a result, two cases of pressure distributions are presented in figure 7, comparing B1 and B2, and in figure 8, comparing B1 and B3. The lower nozzle pressure ratio case, near 2.0, illustrates  $p/p_{t,j}$  behavior when internal flow separation occurs. The higher nozzle pressure ratio case, near 6.0, illustrates the pressure distribution profile without separation.

When the nozzle internal flow is separated, contouring at the nozzle throat increases the magnitude of the pressures on the divergent flap. Contouring also affects the separation location. The flow for the contoured nozzle separates upstream of the separation point for the sharper nozzle with a small throat radius. The integrated effect of the differences in the magnitude of the separation pressure gradient and in the separation location results in a slight improvement in the nozzle internal performance for the contoured nozzles B2 and B3 at low nozzle pressure ratios. This improvement for the nozzles with separated flow was evident in the  $F/F_i$  data plots in figure 5.

When the internal flow does not separate, illustrated by the  $p/p_{t,j}$  plots at a nozzle pressure ratio of approximately 6.0 in figures 6, 7, and 8, there are no large differences in the compared pressure profiles. At higher nozzle pressure ratios, the effects of contouring occur upstream of the nozzle throat and in the vicinity of the throat. Static pressures near the throat

are generally higher for the contoured nozzles than for the baseline nozzles. However, when there is no internal flow separation, the average effect of throat contouring on the internal static pressures is negligible. This lack of significant effect of throat contouring for the unseparated internal flow cases at higher nozzle pressure ratios was also evident in the  $F/F_i$  profiles in figures 4 and 5.

Static-pressure data were recorded on the flaps at three different spanwise locations and on both the right and left sidewalls, as shown in figure 3. On the flaps, each row of static pressures corresponded to a different value of  $y/w_t/2.0$ . On the sidewalls, the row of static pressures ran along the horizontal center line. Comparing the three rows of static-pressure data for each flap and the right and left center-line data for the sidewalls may indicate dominant three-dimensional effects in the internal flow. Selected plots of pressure distributions along the upper and lower flaps and on the right and left sidewalls are presented in figures 9 to 13. In each figure,  $p/p_{t,j}$  along each row is plotted as a function of  $x/l_e$ . Results for the low-divergence-angle nozzles are given in figure 9 for A1 and in figure 10 for A2. Plots for the high-divergence-angle nozzles are presented in two cases to show static-pressure behavior with and without the occurrence of internal flow separation. Data for B1 are given in figure 11; B2 data are given in figure 12; and B3 data are given in figure 13.

At a nozzle pressure ratio near 6.0, nozzles A1 and A2 show almost no variation in  $p/p_{t,j}$  across the flaps or along the sidewalls. The static-pressure distributions are independent of spanwise location, which indicates that the flow is essentially two-dimensional for the low-divergence-angle nozzles. The most pronounced three-dimensional effect in the static-pressure profiles is evident in figure 11 for the high-divergence-angle nozzle B1. When the internal flow is separated at a nozzle pressure ratio near 2.0, the combination of the sharp nozzle throat and the high divergence angle results in considerable variation in  $p/p_{t,j}$  across the flaps. This variation in static pressure with spanwise location is not apparent in the high nozzle-pressure-ratio unseparated case in figure 11. Nozzles B2 and B3 show a similar three-dimensional effect for the separated cases, although the magnitude of the spanwise variation in  $p/p_{t,j}$  are smaller than for configuration B1. As discussed for B1, the three-dimensional effect in B2 and B3 is no longer evident when the internal flow remains attached. Thus, the internal flow for all five 2-D C-D nozzles is predominantly two-dimensional, with three-dimensional effects apparent in the static-pressure data only in the case of internal flow separation at low nozzle pressure ratios.

## Comparison of Experimental Data With Two-Dimensional

### Inviscid Theory

A two-dimensional inviscid computational model was applied to each of the five 2-D C-D nozzle configurations. The theoretical results, in the form of internal thrust ratios and static-pressure distributions, were then compared with the experimental data. The comparisons of theory and experimental data give insight into the internal flow-field behavior and illustrate both the

application of the experimental data to theory evaluation and the application of computational models in assessing the internal performance of nozzle designs.

Since the experimental data exhibit essentially two-dimensional behavior, the two-dimensional, inviscid, time-dependent theory of Cline (ref. 16) was used for nozzle performance predictions. The theory applies the two-dimensional, inviscid Euler equations to the calculation of internal nozzle flow and exhaust jet for converging, converging-diverging, and wedge-plug nozzle geometries. Shock effects are modeled using a "shock-smearing" technique which incorporates an explicit artificial viscosity. Earlier application of the inviscid theory to a nonaxisymmetric wedge nozzle showed good agreement of data and theory in internal flow regions (ref. 18).

Comparisons of theoretical internal thrust ratio with the experimental  $F/F_i$  results are given in figure 14 for nozzles A1 and A2 and in figure 15 for B1, B2, and B3. The theoretical thrust ratio was calculated from the two-dimensional inviscid gross thrust normalized by a theoretical ideal gross thrust. The theoretical ideal thrust was computed from the geometric ideal mass flow necessary for complete expansion to ambient pressure. No experimental data were used in the computation of the theoretical ideal thrust ratio. (Note that the experimental values of  $F/F_i$  can be referred to the theoretical ideal thrust by multiplying the theoretical result by the experimental discharge coefficient.)

The theoretical results were calculated for nozzle pressure ratios of 2.97 to 9.0. The theory was not applied to lower nozzle pressure ratios with known internal flow separation since the inviscid theory is inadequate for modeling the viscous effects of separated flow regions. The comparison of theoretical internal thrust ratio with the  $F/F_i$  data is optimal near design conditions. The theory matches the  $F/F_i$  data peaks except for nozzles A2 and B2; in these cases, the theoretical results are higher than the data values.

To assess the general effect of throat contouring on internal thrust ratio, the theoretical analysis was expanded to include two additional values of throat radius, 1.37 cm and 2.05 cm. The inviscid theory was applied to four additional nozzle geometries which incorporated the new throat radii. Two of the modified geometries were based on the low-divergence-angle baseline nozzle A1; the other two were based on the high-divergence-angle baseline nozzle B1.

The effect of throat contouring on internal thrust ratio is presented in figure 16. Experimental and theoretical internal thrust ratios are presented as a function of the nozzle throat radius. Results are presented in separate cases for the low-divergence-angle nozzles and for the high-divergence-angle nozzles. In each case, theoretical results are presented for throat radii of 0.68, 1.37, 2.05, and 2.74. The theory was applied only at the design nozzle pressure ratio of 2.97 for the low-divergence-angle nozzles and 8.81 for the high-divergence-angle nozzles. These  $F/F_i$  data are presented only for the experimental throat radii of 0.68 and 2.74. Results are presented for both nozzles B2 and B3 in the high-divergence-angle case.

The experimental data show almost no variation in  $F/F_i$  with throat radius. The theoretical results, however, show some changes in thrust ratio

as throat radius increases. As discussed previously and shown in figures 14 and 15, thrust ratios for the contoured nozzles A2 and B2 were generally higher than the data over the full nozzle-pressure-ratio range. Thus, variations observed at design conditions in figure 16 are probably due to inviscid limitations of the theory. Small changes in the theoretical internal thrust ratio with throat radius may be attributed to the theory rather than to the effect of throat radius. In general, both the experimental and theoretical results indicate that throat radius, and therefore throat contouring, has no significant effect on internal thrust ratio.

Figures 17 and 18 present comparisons of experimental and theoretical  $p/p_{t,j}$  along the upper-flap center line for A1 and A2. Figures 19, 20, and 21 present the same data-theory comparisons for B1, B2, and B3. The theory was applied only at design conditions, when the internal flow was not separated, while the data represented four cases of nozzle-pressure-ratio settings. The theoretical static-pressure distributions follow the basic flow trends in the data, matching the static-pressure highs and lows. Poor data-theory agreement generally occurs in the vicinity of the nozzle throat and is due to the inviscid limitations of the theory.

In figures 22 to 26, for each of the five configurations, the theoretical static pressures along the center line of the nozzle interior are compared with the data on the left sidewall center line. The theory was again applied at design conditions; the experimental data are shown at four values of nozzle pressure ratio. The data-theory agreement is generally good, with poorest comparisons downstream of the nozzle throat, as discussed previously. The good agreement of theoretical  $p/p_{t,j}$  profiles along the interior center line with sidewall data emphasizes the predominantly two-dimensional nature of the nozzle internal flow for all five configurations. The overall good agreement between theory and experimental data in regions without separated flow indicates that the two-dimensional, inviscid, time-dependent theory may be successfully applied to the 2-D C-D nozzle geometry for internal flow prediction.

#### CONCLUDING REMARKS

An experiment has been conducted to determine the internal-performance effect of throat contouring by increasing the circular-arc throat radius of nonaxisymmetric converging-diverging nozzles. Five two-dimensional converging-diverging nozzles were tested at static conditions in the static-test facility of the Langley 16-Foot Transonic Tunnel. Internal-performance data were recorded for a range of nozzle pressure ratios up to 9.0. Data are presented as internal thrust ratios, discharge coefficients, and static-pressure distributions. Comparing internal-performance data for the five nozzles shows that throat contouring results in improved values of discharge coefficient but has no significant advantage in internal thrust ratio except at nozzle operating conditions where internal flow separation occurs.

The internal flow for each of the nozzle geometries is predominantly two-dimensional, except in regions of separated flow. As a result, a two-dimensional, inviscid, time-dependent computational model was applied to each

configuration. The favorable comparison of the theoretical results with the static-test data illustrates the successful application of two-dimensional inviscid theory to the prediction of internal flow characteristics of two-dimensional converging-diverging nozzles.

Langley Research Center  
National Aeronautics and Space Administration  
Hampton, VA 23665  
July 2, 1980

## REFERENCES

1. Schmeer, James W.; Lauer, Rodney F., Jr.; and Berrier, Bobby L.: Performance of Blow-in-Door Ejector Nozzles Installed on a Twin-Jet Variable-Wing-Sweep Fighter Airplane Model. NASA TM X-1383, 1967.
2. Reubush, David E.; and Mercer, Charles E.: Effects of Nozzle Interfairing Modifications on Longitudinal Aerodynamic Characteristics of a Twin-Jet, Variable-Wing-Sweep Fighter Model. NASA TN D-7817, 1975.
3. Maiden, Donald L.; and Berrier, Bobby L.: Effect of Airframe Modifications on Longitudinal Aerodynamic Characteristics of a Fixed-Wing, Twin-Jet Fighter Airplane Model. NASA TM X-2523, 1972.
4. Maiden, Donald L.; and Petit, John E.: Investigation of Two-Dimensional Wedge Exhaust Nozzles for Advanced Aircraft. J. Aircr., vol. 13, no. 10, Oct. 1976, pp. 809-816.
5. Martens, Richard E.: F-15 Nozzle/Afterbody Integration. J. Aircr., vol. 13, no. 5, May 1976, pp. 327-333.
6. Capone, Francis J.: Summary of Propulsive-Lift Research in the Langley 16-Ft Transonic Tunnel. J. Aircr., vol. 13, no. 10, Oct. 1976, pp. 803-808.
7. Hiley, P. E.; Wallace, H. W.; and Booz, D. E.: Nonaxisymmetric Nozzles Installed in Advanced Fighter Aircraft. J. Aircr., vol. 13, no. 12, Dec. 1976, pp. 1000-1006.
8. Sedgwick, T. E.: Investigation Nonaxisymmetric Two-Dimensional Nozzles Installed in Twin-Engine Tactical Aircraft. AIAA Paper No. 75-1319, Sept.-Oct. 1975.
9. Berrier, Bobby L.; Palcza, J. Lawrence; and Richey, G. Keith: Nonaxisymmetric Nozzle Technology Program - An Overview. AIAA Paper 77-1225, Aug. 1977.
10. F-15 2-D Nozzle System Integration Study. Volume I - Technical Report. NASA CR-145295, 1978.
11. Stevens, H. L.: F-15/Nonaxisymmetric Nozzle System Integration Study Support Program. NASA CR-135252, 1978.
12. Bergman, D.; Mace, J. L.; and Thayer, E. B.: Non-Axisymmetric Nozzle Concepts for an F-111 Test Bed. AIAA Paper No. 77-841, July 1977.
13. Wasson, H. R.; Hall, G. R.; and Palcza, J. L.: Results of a Feasibility Study to Add Canards and ADEN Nozzle to the YF-17. AIAA Paper 77-1227, Aug. 1977.

14. Capone, Francis J.: Static Performance of Five Twin-Engine Nonaxisymmetric Nozzles With Vectoring and Reversing Capability. NASA TP-1224, 1978.
15. Berrier, Bobby L.; and Re, Richard J.: Effect of Several Geometric Parameters on the Static Internal Performance of Three Nonaxisymmetric Nozzle Concepts. NASA TP-1468, 1979.
16. Cline, Michael C.: NAP: A Computer Program for the Computation of Two-Dimensional, Time-Dependent, Inviscid Nozzle Flow. LA-5984 (Contract W-7405-ENG. 36), Los Alamos Sci. Lab., Univ. of California, Jan. 1977.
17. Corson, Blake W., Jr.; Runckel, Jack F.; and Igoe, William, B.: Calibration of the Langley 16-Foot Transonic Tunnel With Test Section Air Removal. NASA TR R-423, 1974.
18. Carson, George T., Jr.; and Mason, Mary L.: Experimental and Analytical Investigation of a Nonaxisymmetric Wedge Nozzle at Static Conditions. NASA TP-1188, 1978.



TABLE I.- RATIO OF INTERNAL STATIC PRESSURE TO JET TOTAL PRESSURE FOR NOZZLE A1

(a) Upper-flap static pressure  $p/p_{t,j}$

$$y/w\sqrt{2.0} = 0.0$$

Point	$p_{t,j}/p_{\infty}$	$x/l_e$						
		.209	.099	.011	.077	.143	.286	.429
1	1.99	.845	.755	.346	.421	.485	.418	.407
2	2.49	.843	.756	.344	.419	.488	.418	.417
3	3.03	.844	.756	.342	.418	.487	.417	.417
4	3.48	.844	.756	.342	.419	.485	.416	.416
5	3.98	.844	.756	.342	.422	.484	.416	.415
6	4.47	.844	.756	.343	.422	.483	.416	.414
7	4.97	.844	.756	.344	.422	.482	.416	.414
8	5.47	.844	.755	.345	.421	.482	.416	.413
9	5.97	.843	.755	.346	.420	.482	.416	.413
10	6.45	.843	.755	.347	.420	.482	.417	.413
11	6.95	.843	.755	.347	.419	.482	.417	.414
12	7.44	.843	.755	.346	.419	.482	.417	.413
13	7.95	.843	.754	.346	.419	.482	.417	.413
14	8.42	.843	.754	.346	.418	.481	.417	.413
15	9.24	.843	.754	.346	.418	.481	.417	.413

$$y/w\sqrt{2.0} = 0.450$$

Point	$p_{t,j}/p_{\infty}$	$x/l_e$						
		.209	.099	.011	.077	.143	.286	.429
1	1.99	.843	.755	.354	.437	.490	.420	.414
2	2.49	.842	.755	.355	.430	.487	.421	.429
3	3.03	.841	.754	.357	.429	.486	.420	.430
4	3.48	.841	.754	.357	.428	.485	.419	.429
5	3.98	.841	.753	.357	.428	.485	.419	.428
6	4.47	.841	.753	.357	.428	.485	.419	.428
7	4.97	.841	.753	.357	.427	.485	.419	.428
8	5.47	.841	.752	.357	.427	.485	.419	.426
9	5.97	.840	.751	.357	.427	.485	.419	.426
10	6.45	.840	.751	.357	.426	.485	.419	.426
11	6.95	.840	.751	.357	.426	.485	.420	.424
12	7.44	.840	.751	.357	.426	.485	.420	.423
13	7.95	.840	.751	.356	.426	.485	.420	.423
14	8.42	.840	.751	.356	.426	.484	.420	.422
15	9.24	.839	.751	.356	.426	.484	.420	.422

$$y/w\sqrt{2.0} = 0.875$$

Point	$p_{t,j}/p_{\infty}$	$x/l_e$						
		.209	.099	.011	.077	.143	.286	.429
1	1.99	.845	.753	.343	.449	.506	.417	.418
2	2.49	.845	.753	.346	.449	.504	.418	.419
3	3.03	.845	.752	.351	.449	.501	.417	.417
4	3.48	.843	.752	.353	.452	.500	.416	.416
5	3.98	.843	.752	.353	.455	.499	.416	.416
6	4.47	.843	.751	.356	.456	.498	.416	.414
7	4.97	.842	.751	.356	.456	.497	.416	.414
8	5.47	.842	.751	.355	.456	.496	.416	.413
9	5.97	.842	.751	.355	.457	.496	.416	.412
10	6.45	.842	.751	.355	.457	.496	.417	.412
11	6.95	.842	.751	.355	.457	.495	.417	.411
12	7.44	.841	.751	.355	.457	.495	.416	.410
13	7.95	.841	.752	.355	.457	.494	.416	.410
14	8.42	.841	.752	.355	.457	.494	.417	.409
15	9.24	.841	.752	.355	.456	.494	.417	.408

TABLE I.- Continued

(b) Lower-flap static pressure  $p/p_{t,j}$ 

Point	$p_{t,j}/p_{\infty}$	$y/w\sqrt{2.0} = 0.0$									
		$x/l_e$									
		.209	.099	.011	.077	.143	.286	.429	.560	.736	.890
1	1.99	.847	.755	.392	.433	.472	.408	.417	.349	.360	.372
2	2.49	.845	.755	.391	.430	.476	.410	.414	.349	.357	.371
3	3.03	.845	.754	.391	.430	.476	.408	.412	.348	.358	.370
4	3.48	.845	.754	.391	.433	.476	.408	.409	.347	.360	.369
5	3.98	.844	.754	.393	.434	.476	.407	.409	.347	.360	.369
6	4.47	.844	.753	.394	.434	.475	.407	.408	.346	.359	.369
7	4.97	.844	.752	.395	.433	.475	.407	.407	.345	.357	.369
8	5.47	.843	.751	.396	.433	.475	.407	.406	.344	.356	.368
9	5.97	.843	.751	.396	.433	.474	.407	.406	.344	.355	.368
10	6.45	.843	.751	.396	.432	.474	.407	.405	.343	.354	.368
11	6.95	.842	.750	.396	.432	.474	.407	.404	.347	.354	.368
12	7.44	.842	.750	.395	.432	.474	.407	.404	.347	.353	.368
13	7.95	.842	.750	.395	.431	.473	.408	.404	.346	.353	.368
14	8.42	.842	.750	.395	.431	.473	.408	.404	.346	.353	.368
15	9.24	.842	.750	.395	.431	.473	.408	.403	.345	.352	.367

Point	$p_{t,j}/p_{\infty}$	$y/w\sqrt{2.0} = 0.450$									
		$x/l_e$									
		.209	.099	.011	.077	.143	.286	.429	.560	.736	.890
1	1.99	.847	.755	.388	.434	.470	.402	.438	.397	.344	.363
2	2.49	.845	.754	.387	.429	.470	.403	.436	.397	.344	.365
3	3.03	.845	.753	.387	.428	.470	.402	.435	.396	.345	.364
4	3.48	.845	.753	.387	.428	.469	.402	.435	.396	.346	.363
5	3.98	.845	.752	.388	.429	.467	.402	.434	.396	.346	.362
6	4.47	.845	.752	.388	.428	.466	.402	.434	.396	.344	.361
7	4.97	.845	.751	.387	.428	.465	.401	.433	.396	.343	.361
8	5.47	.844	.751	.387	.427	.464	.401	.433	.396	.342	.360
9	5.97	.844	.751	.387	.427	.464	.401	.433	.394	.341	.359
10	6.45	.844	.750	.387	.427	.464	.401	.432	.396	.340	.359
11	6.95	.844	.750	.387	.427	.464	.401	.432	.396	.339	.361
12	7.44	.844	.750	.387	.426	.464	.401	.431	.396	.339	.361
13	7.95	.843	.750	.386	.426	.464	.401	.431	.396	.339	.361
14	8.42	.843	.750	.386	.426	.464	.401	.431	.396	.338	.360
15	9.24	.843	.750	.386	.425	.465	.401	.430	.396	.338	.361

Point	$p_{t,j}/p_{\infty}$	$y/w\sqrt{2.0} = 0.875$									
		$x/l_e$									
		.209	.099	.011	.077	.143	.286	.429	.560	.736	.890
1	1.99	.841	.755	.379	.426	.485	.407	.419	.349	.359	.366
2	2.49	.840	.754	.376	.422	.485	.409	.419	.349	.359	.367
3	3.03	.839	.753	.375	.421	.484	.408	.417	.349	.358	.367
4	3.48	.838	.753	.374	.424	.481	.407	.416	.348	.357	.366
5	3.98	.838	.751	.375	.425	.480	.407	.415	.348	.356	.365
6	4.47	.837	.751	.377	.425	.478	.407	.414	.348	.354	.363
7	4.97	.836	.751	.378	.425	.477	.406	.414	.348	.353	.363
8	5.47	.836	.750	.378	.426	.476	.406	.413	.348	.353	.363
9	5.97	.837	.750	.379	.426	.477	.406	.413	.347	.351	.362
10	6.45	.836	.750	.379	.426	.476	.406	.412	.348	.352	.362
11	6.95	.836	.749	.379	.426	.475	.406	.412	.347	.351	.361
12	7.44	.837	.749	.379	.426	.475	.406	.412	.347	.350	.360
13	7.95	.837	.749	.379	.426	.475	.406	.411	.347	.350	.360
14	8.42	.837	.749	.379	.426	.475	.406	.411	.347	.349	.359
15	9.24	.837	.749	.379	.426	.475	.406	.411	.347	.349	.359

TABLE I.- Concluded

(c) Sidewall static pressure  $p/P_{t,j}$ Right sidewall,  $z = 0.0$ 

Point	$P_{t,j}/P_{\infty}$	$x/L_e$							
		.209	.099	.011	.077	.143	.286	.429	.560
1	1.99	.823	.739	.611	.521	.445	.434	.403	.387
2	2.49	.824	.738	.611	.520	.445	.434	.405	.387
3	3.03	.823	.738	.610	.519	.444	.434	.404	.388
4	3.48	.823	.738	.610	.519	.445	.434	.404	.388
5	3.98	.822	.737	.610	.519	.445	.434	.403	.388
6	4.47	.822	.737	.610	.519	.445	.433	.402	.388
7	4.97	.822	.737	.610	.519	.444	.433	.401	.387
8	5.47	.821	.737	.610	.519	.444	.432	.401	.387
9	5.97	.821	.737	.610	.519	.444	.432	.400	.386
10	6.45	.821	.737	.610	.519	.445	.434	.399	.386
11	6.95	.821	.737	.613	.523	.444	.433	.399	.386
12	7.44	.821	.737	.613	.523	.444	.433	.399	.385
13	7.95	.820	.737	.614	.523	.444	.433	.399	.385
14	8.42	.820	.737	.613	.523	.447	.432	.399	.385
15	9.24	.820	.737	.613	.523	.447	.432	.399	.385

Left sidewall,  $z = 0.0$ 

Point	$P_{t,j}/P_{\infty}$	$x/L_e$							
		.209	.099	.011	.077	.143	.286	.429	.429
1	1.99	.820	.742	.611	.513	.434	.440	.401	.401
2	2.49	.821	.741	.612	.511	.435	.441	.400	.400
3	3.03	.821	.741	.612	.510	.433	.440	.400	.400
4	3.48	.822	.741	.612	.510	.433	.438	.400	.400
5	3.98	.822	.741	.610	.510	.433	.437	.400	.400
6	4.47	.822	.741	.610	.510	.433	.437	.400	.400
7	4.97	.822	.741	.609	.510	.434	.436	.400	.400
8	5.47	.822	.740	.609	.511	.434	.436	.400	.400
9	5.97	.822	.740	.610	.511	.434	.435	.401	.400
10	6.45	.822	.740	.610	.511	.435	.435	.401	.401
11	6.95	.822	.741	.610	.511	.435	.435	.401	.401
12	7.44	.822	.741	.610	.511	.435	.434	.401	.401
13	7.95	.822	.741	.610	.512	.435	.434	.401	.401
14	8.42	.822	.741	.610	.512	.436	.433	.401	.401
15	9.24	.822	.741	.610	.513	.436	.433	.401	.401

TABLE II.- RATIO OF INTERNAL STATIC PRESSURE TO JET TOTAL PRESSURE FOR NOZZLE A2

(a) Upper-flap static pressure  $p/p_{t,j}$ 

Point	$P_{t,j}/P_{\infty}$	$y/w \sqrt{2.0} = 0.0$ $x/l_e$						
		.209	-.099	.011	.077	.143	.286	.429
1	1.97	.791	.572	.443	.471	.474	.435	.426
2	2.45	.790	.572	.441	.473	.473	.441	.424
3	2.92	.790	.572	.442	.473	.472	.439	.423
4	3.41	.790	.574	.441	.472	.471	.439	.423
5	3.92	.790	.574	.440	.471	.471	.437	.422
6	4.39	.789	.574	.440	.471	.471	.437	.422
7	4.87	.789	.574	.438	.470	.471	.436	.422
8	5.35	.789	.575	.438	.470	.472	.436	.421
9	5.84	.788	.575	.437	.470	.471	.435	.421
10	6.31	.788	.574	.436	.469	.472	.434	.421
11	6.80	.788	.575	.436	.469	.472	.434	.421
12	7.27	.788	.575	.435	.469	.472	.433	.421
13	7.76	.788	.574	.434	.468	.472	.433	.420
14	8.23	.788	.574	.434	.468	.472	.433	.420
15	8.49	.788	.575	.433	.468	.472	.432	.420

$$y/w \sqrt{2.0} = 0.450$$

Point	$P_{t,j}/P_{\infty}$	$x/l_e$						
		.209	-.099	.011	.077	.143	.286	.429
1	1.97	.793	.578	.453	.480	.482	.444	.418
2	2.45	.793	.578	.453	.483	.483	.443	.418
3	2.92	.793	.577	.454	.483	.482	.442	.416
4	3.41	.793	.577	.454	.482	.481	.440	.416
5	3.92	.794	.577	.454	.482	.481	.440	.415
6	4.39	.793	.577	.453	.481	.481	.439	.414
7	4.87	.793	.577	.453	.480	.481	.439	.414
8	5.35	.793	.577	.453	.480	.480	.438	.414
9	5.84	.793	.576	.453	.479	.480	.438	.414
10	6.31	.793	.576	.452	.479	.480	.437	.414
11	6.80	.793	.577	.452	.478	.479	.437	.413
12	7.27	.793	.577	.452	.478	.479	.436	.413
13	7.76	.792	.577	.451	.477	.479	.436	.413
14	8.23	.793	.577	.451	.477	.479	.436	.413
15	8.49	.793	.577	.451	.477	.479	.435	.413

$$y/w \sqrt{2.0} = 0.875$$

Point	$P_{t,j}/P_{\infty}$	$x/l_e$						
		.209	-.099	.011	.077	.143	.286	.429
1	1.97	.792	.577	.427	.507	.498	.437	.413
2	2.45	.792	.575	.422	.510	.496	.435	.413
3	2.92	.793	.575	.421	.508	.495	.433	.412
4	3.41	.791	.574	.420	.507	.494	.432	.411
5	3.92	.791	.574	.418	.506	.494	.431	.410
6	4.39	.790	.573	.417	.505	.494	.429	.410
7	4.87	.790	.573	.416	.504	.493	.429	.409
8	5.35	.790	.572	.415	.504	.493	.428	.409
9	5.84	.789	.571	.414	.503	.493	.427	.409
10	6.31	.789	.571	.413	.503	.493	.427	.408
11	6.80	.789	.570	.412	.502	.493	.426	.408
12	7.27	.788	.570	.411	.502	.493	.425	.408
13	7.76	.788	.569	.411	.501	.492	.425	.407
14	8.23	.788	.569	.411	.502	.492	.425	.407
15	8.49	.788	.569	.410	.501	.492	.424	.407

TABLE II.- Continued

(b) Lower-flap static pressure  $p/P_{t,j}$ 

$$y/w_c/2.0 = 0.0$$

Point	$P_{t,j}/P_{\infty}$	$x/l_e$						
		.209	-.099	.011	.077	.143	.286	.429
1	1.97	.792	.578	.465	.485	.478	.415	.421
2	2.45	.794	.580	.466	.487	.476	.420	.422
3	2.92	.793	.579	.468	.485	.475	.420	.420
4	3.41	.794	.582	.468	.483	.475	.418	.418
5	3.92	.794	.582	.468	.482	.474	.417	.416
6	4.39	.794	.582	.468	.481	.474	.416	.416
7	4.87	.794	.581	.469	.480	.474	.415	.415
8	5.35	.794	.581	.468	.479	.474	.414	.414
9	5.84	.793	.582	.468	.479	.473	.413	.412
10	6.31	.793	.581	.467	.478	.473	.412	.411
11	6.80	.793	.581	.467	.478	.473	.411	.411
12	7.27	.793	.581	.467	.477	.473	.410	.410
13	7.76	.793	.581	.467	.477	.473	.410	.410
14	8.23	.793	.582	.467	.477	.473	.410	.410
15	8.49	.793	.582	.466	.477	.473	.410	.410

$$y/w_c/2.0 = 0.450$$

Point	$P_{t,j}/P_{\infty}$	$x/l_e$						
		.209	-.099	.011	.077	.143	.286	.429
1	1.97	.789	.584	.486	.487	.480	.425	.415
2	2.45	.789	.586	.483	.485	.478	.440	.425
3	2.92	.789	.587	.479	.483	.477	.442	.431
4	3.41	.789	.588	.474	.483	.477	.439	.435
5	3.92	.789	.589	.471	.482	.478	.436	.438
6	4.39	.789	.589	.469	.481	.477	.433	.441
7	4.87	.789	.590	.468	.481	.478	.431	.443
8	5.35	.788	.590	.467	.480	.478	.429	.444
9	5.84	.789	.590	.466	.480	.478	.426	.445
10	6.31	.789	.591	.465	.480	.478	.423	.446
11	6.80	.789	.591	.464	.480	.478	.422	.447
12	7.27	.789	.591	.464	.480	.478	.420	.448
13	7.76	.789	.591	.463	.480	.478	.419	.448
14	8.23	.789	.592	.463	.480	.479	.418	.449
15	8.49	.789	.592	.463	.480	.479	.418	.449

$$y/w_c/2.0 = 0.875$$

Point	$P_{t,j}/P_{\infty}$	$x/l_e$						
		.209	-.099	.011	.077	.143	.286	.429
1	1.97	.774	.580	.518	.496	.462	.439	.422
2	2.45	.773	.581	.516	.494	.462	.441	.423
3	2.92	.772	.581	.514	.493	.461	.439	.422
4	3.41	.771	.583	.513	.492	.461	.438	.422
5	3.92	.770	.582	.513	.492	.460	.436	.421
6	4.39	.766	.583	.513	.492	.460	.435	.421
7	4.87	.766	.584	.513	.492	.460	.434	.421
8	5.35	.766	.584	.513	.492	.460	.434	.420
9	5.84	.766	.585	.512	.492	.460	.433	.420
10	6.31	.768	.585	.512	.492	.460	.432	.419
11	6.80	.767	.586	.512	.492	.460	.432	.419
12	7.27	.767	.586	.512	.492	.460	.432	.419
13	7.76	.766	.586	.512	.493	.460	.432	.418
14	8.23	.766	.586	.512	.493	.460	.432	.418
15	8.49	.765	.586	.511	.492	.459	.432	.418

(c) Sidewall static pressure  $p/p_t, j$

Left sidewall,  $z = 0.0$ [illegible]Right sidewall,  $z = 0.0$ 

Point	$p_{T,j}/p_{\infty}$	$x/l_e$						
		.209	.099	.011	.077	.143	.266	.429
1	1.97	.777	.682	.564	.506	.482	.442	.416
2	2.45	.778	.685	.566	.505	.483	.442	.416
3	2.92	.780	.685	.566	.504	.481	.440	.416
4	3.41	.779	.683	.566	.503	.480	.439	.415
5	3.92	.780	.683	.565	.503	.479	.438	.415
6	4.39	.780	.683	.565	.502	.479	.437	.415
7	4.87	.780	.683	.565	.501	.478	.437	.414
8	5.35	.780	.683	.563	.501	.477	.436	.414
9	5.84	.780	.683	.562	.500	.477	.436	.414
10	6.31	.780	.683	.565	.499	.477	.435	.413
11	6.80	.780	.683	.565	.499	.476	.435	.413
12	7.27	.780	.683	.564	.499	.476	.434	.413
13	7.76	.780	.683	.563	.499	.475	.433	.413
14	8.23	.780	.683	.563	.499	.475	.433	.413
15	8.49	.780	.683	.562	.499	.475	.433	.412

TABLE III.- RATIO OF INTERNAL STATIC PRESSURE TO JET TOTAL PRESSURE FOR NOZZLE B1

(a) Upper-flap static pressure  $p/p_{t,j}$

$$y/w_d/2.0 = 0.0$$

Point	$P_{t,j}/P_{\infty}$	$x/l_e$						
		.209	.099	.011	.077	.143	.286	.429
1	1.97	.842	.746	.295	.258	.287	.276	.239
2	2.46	.842	.746	.293	.259	.288	.276	.234
3	2.94	.843	.746	.292	.258	.288	.276	.234
4	3.43	.842	.746	.291	.258	.288	.276	.235
5	3.92	.842	.745	.291	.257	.287	.276	.235
6	4.39	.842	.745	.291	.256	.287	.276	.234
7	4.88	.842	.745	.290	.256	.288	.276	.234
8	5.39	.842	.744	.291	.256	.288	.275	.234
9	5.84	.842	.744	.291	.256	.288	.274	.234
10	6.32	.842	.744	.293	.256	.288	.274	.234
11	6.81	.842	.744	.293	.256	.288	.274	.234
12	7.30	.842	.744	.294	.256	.288	.274	.234
13	7.79	.842	.743	.294	.256	.288	.274	.234
14	8.53	.842	.743	.295	.256	.288	.274	.234
15	8.91	.842	.743	.295	.256	.288	.273	.234

$$y/w_d/2.0 = 0.450$$

Point	$P_{t,j}/P_{\infty}$	$x/l_e$						
		.209	.099	.011	.077	.143	.286	.429
1	1.97	.847	.757	.298	.249	.285	.274	.233
2	2.46	.848	.756	.298	.247	.286	.274	.234
3	2.94	.848	.754	.299	.246	.286	.274	.235
4	3.43	.849	.753	.299	.245	.286	.275	.235
5	3.92	.849	.752	.299	.244	.285	.275	.235
6	4.39	.849	.751	.299	.244	.285	.274	.234
7	4.88	.848	.750	.299	.243	.286	.273	.234
8	5.39	.849	.750	.299	.243	.287	.273	.234
9	5.84	.849	.749	.300	.243	.287	.273	.234
10	6.32	.849	.749	.301	.243	.287	.273	.234
11	6.81	.849	.749	.301	.243	.287	.272	.234
12	7.30	.849	.749	.301	.242	.287	.272	.233
13	7.79	.849	.748	.301	.242	.287	.272	.233
14	8.53	.849	.747	.301	.242	.287	.272	.233
15	8.91	.849	.747	.301	.242	.287	.272	.233

$$y/w_d/2.0 = 0.875$$

Point	$P_{t,j}/P_{\infty}$	$x/l_e$						
		.209	.099	.011	.077	.143	.286	.429
1	1.97	.840	.751	.277	.261	.287	.286	.233
2	2.46	.841	.750	.275	.260	.287	.286	.233
3	2.94	.840	.750	.274	.259	.287	.289	.234
4	3.43	.838	.749	.272	.257	.286	.289	.234
5	3.92	.838	.749	.271	.256	.286	.289	.234
6	4.39	.838	.749	.270	.255	.286	.289	.235
7	4.88	.837	.749	.269	.254	.286	.289	.234
8	5.39	.837	.749	.269	.253	.287	.289	.234
9	5.84	.836	.749	.269	.253	.287	.288	.234
10	6.32	.836	.749	.268	.253	.286	.288	.233
11	6.81	.836	.749	.267	.253	.285	.288	.234
12	7.30	.836	.749	.267	.252	.285	.288	.233
13	7.79	.836	.750	.266	.252	.286	.288	.233
14	8.53	.836	.750	.266	.252	.286	.288	.233
15	8.91	.835	.750	.266	.252	.286	.288	.233

TABLE III.- Continued

(b) Lower-flap static pressure  $p/p_{t,j}$ 

$$y/w_c/2.0 = 0.0$$

Point	$p_{t,j}/p_\infty$	$x/l_e$						
		.209	.099	.011	.077	.143	.286	.429
1	1.97	.849	.757	.295	.243	.272	.272	.412
2	2.46	.848	.757	.295	.244	.273	.273	.429
3	2.94	.848	.757	.295	.244	.273	.276	.429
4	3.43	.848	.758	.295	.244	.272	.277	.429
5	3.92	.847	.757	.294	.244	.272	.277	.429
6	4.39	.847	.757	.294	.244	.273	.277	.429
7	4.88	.847	.757	.295	.244	.274	.276	.429
8	5.39	.846	.757	.295	.244	.273	.276	.429
9	5.84	.846	.757	.296	.244	.273	.276	.429
10	6.32	.846	.757	.296	.244	.273	.276	.429
11	6.81	.846	.757	.296	.244	.273	.276	.429
12	7.30	.846	.758	.297	.243	.273	.276	.429
13	7.79	.846	.758	.297	.243	.273	.276	.429
14	8.23	.845	.757	.296	.243	.273	.276	.429
15	8.91	.845	.757	.296	.243	.272	.276	.429

$$y/w_c/2.0 = 0.450$$

Point	$p_{t,j}/p_\infty$	$x/l_e$						
		.209	.099	.011	.077	.143	.286	.429
1	1.97	.847	.751	.305	.249	.271	.274	.202
2	2.46	.847	.751	.299	.249	.272	.275	.213
3	2.94	.847	.752	.295	.248	.273	.276	.221
4	3.43	.846	.752	.292	.247	.273	.277	.226
5	3.92	.846	.753	.291	.246	.273	.276	.229
6	4.39	.846	.753	.290	.246	.273	.277	.232
7	4.88	.846	.753	.289	.246	.273	.276	.234
8	5.39	.846	.753	.289	.246	.272	.276	.236
9	5.84	.846	.754	.288	.245	.272	.276	.237
10	6.32	.846	.754	.288	.245	.272	.276	.237
11	6.81	.846	.754	.288	.245	.272	.276	.239
12	7.30	.846	.755	.287	.245	.271	.276	.241
13	7.79	.846	.755	.287	.244	.271	.276	.241
14	8.23	.845	.755	.286	.244	.271	.276	.243
15	8.91	.845	.756	.286	.244	.270	.276	.243

$$y/w_c/2.0 = 0.875$$

Point	$p_{t,j}/p_\infty$	$x/l_e$						
		.209	.099	.011	.077	.143	.286	.429
1	1.97	.842	.760	.304	.251	.284	.317	.453
2	2.46	.842	.758	.300	.250	.283	.319	.453
3	2.94	.841	.759	.298	.250	.283	.321	.453
4	3.43	.841	.759	.296	.250	.283	.322	.453
5	3.92	.840	.758	.295	.250	.283	.321	.453
6	4.39	.840	.758	.295	.249	.284	.320	.453
7	4.88	.839	.757	.294	.249	.284	.320	.453
8	5.39	.839	.757	.294	.249	.284	.320	.453
9	5.84	.839	.756	.294	.249	.284	.320	.453
10	6.32	.839	.756	.294	.249	.284	.320	.453
11	6.81	.840	.756	.294	.249	.283	.320	.453
12	7.30	.840	.756	.294	.249	.283	.320	.453
13	7.79	.839	.756	.294	.249	.283	.320	.453
14	8.23	.840	.756	.295	.249	.282	.320	.453
15	8.91	.839	.756	.294	.249	.282	.320	.453



TABLE III.- Concluded

(c) Sidewall static pressure  $p/p_{t,j}$ Left sidewall,  $z = 0.0$ 

Point	$p_{t,j}/p_{\infty}$	$x/l_e$							
		.209	.099	.011	.077	.143	.286	.429	.560
1	1.97	.822	.738	.610	.514	.417	.376	.463	.465
2	2.46	.823	.739	.609	.514	.417	.262	.363	.366
3	2.94	.824	.740	.609	.514	.416	.261	.171	.166
4	3.43	.823	.739	.608	.514	.416	.260	.171	.167
5	3.92	.823	.739	.608	.514	.416	.259	.171	.168
6	4.39	.823	.740	.608	.514	.417	.257	.171	.169
7	4.88	.823	.740	.607	.514	.417	.249	.171	.170
8	5.39	.823	.740	.607	.514	.417	.247	.171	.170
9	5.84	.823	.740	.607	.515	.417	.247	.171	.170
10	6.32	.823	.740	.607	.515	.417	.247	.171	.170
11	6.81	.822	.740	.608	.515	.417	.248	.171	.169
12	7.30	.820	.740	.608	.515	.417	.248	.171	.169
13	7.79	.815	.740	.607	.515	.417	.248	.171	.169
14	8.21	.807	.740	.608	.515	.417	.248	.171	.169
15	8.53	.803	.740	.608	.516	.417	.248	.170	.169
16	8.91								

Right sidewall,  $z = 0.0$ 

Point	$p_{t,j}/p_{\infty}$	$x/l_e$							
		.209	.099	.011	.077	.143	.286	.429	
1	1.97	.817	.740	.611	.510	.415	.401	.468	
2	2.46	.818	.741	.612	.508	.415	.250	.368	
3	2.94	.820	.741	.612	.507	.415	.251	.166	
4	3.43	.819	.741	.612	.506	.413	.251	.166	
5	3.92	.819	.741	.609	.506	.414	.251	.166	
6	4.39	.820	.741	.609	.505	.413	.251	.166	
7	4.88	.820	.741	.607	.505	.413	.251	.167	
8	5.39	.820	.741	.608	.505	.413	.251	.167	
9	5.84	.820	.741	.608	.505	.413	.251	.167	
10	6.32	.820	.741	.609	.505	.413	.251	.167	
11	6.81	.821	.741	.608	.505	.413	.251	.167	
12	7.30	.821	.742	.608	.505	.413	.251	.167	
13	7.79	.821	.741	.607	.505	.413	.251	.167	
14	8.21	.821	.742	.608	.505	.413	.251	.167	
15	8.53	.821	.742	.607	.505	.413	.251	.167	
16	8.91								

TABLE IV.- RATIO OF INTERNAL STATIC PRESSURE TO JET TOTAL PRESSURE FOR NOZZLE B2

(a) Upper-flap static pressure  $p/p_{t,j}$ 

$$y/w_t/2.0 = 0.0$$

Point	$p_{t,j}/p_\infty$	$x/l_e$									
		.209	.099	.011	.077	.143	.286	.429	.560	.736	.890
1	1.96	.784	.578	.430	.319	.289	.317	.452	.463	.471	.482
2	2.47	.781	.574	.424	.319	.289	.266	.225	.381	.386	.388
3	2.95	.783	.577	.424	.320	.290	.266	.225	.389	.319	.323
4	3.42	.783	.577	.424	.319	.290	.267	.225	.388	.149	.275
5	3.94	.783	.578	.424	.318	.290	.266	.223	.388	.147	.214
6	4.40	.783	.577	.424	.318	.290	.265	.223	.388	.147	.126
7	4.88	.783	.578	.424	.318	.288	.265	.223	.388	.147	.126
8	5.38	.783	.578	.423	.318	.288	.265	.223	.388	.147	.126
9	5.88	.783	.577	.423	.317	.288	.265	.222	.387	.147	.126
10	6.35	.783	.577	.423	.318	.288	.265	.223	.387	.148	.126
11	6.83	.784	.577	.424	.318	.288	.265	.223	.387	.148	.126
12	7.31	.782	.578	.424	.318	.288	.265	.222	.387	.148	.127
13	7.79	.783	.578	.424	.318	.288	.265	.222	.387	.147	.127
14	8.54	.783	.578	.424	.317	.288	.265	.222	.386	.147	.126
15	8.73	.783	.578	.423	.317	.288	.265	.222	.386	.147	.126

$$y/w_t/2.0 = 0.450$$

Point	$p_{t,j}/p_\infty$	$x/l_e$									
		.209	.099	.011	.077	.143	.286	.429	.560	.736	.890
1	1.96	.787	.568	.420	.326	.290	.286	.448	.460	.469	.482
2	2.47	.784	.568	.422	.327	.291	.258	.226	.380	.385	.388
3	2.95	.786	.569	.422	.327	.292	.258	.226	.388	.318	.322
4	3.42	.787	.568	.420	.327	.292	.258	.225	.388	.147	.275
5	3.94	.786	.568	.420	.325	.291	.258	.225	.387	.146	.211
6	4.40	.787	.568	.420	.326	.291	.257	.225	.387	.146	.123
7	4.88	.785	.568	.420	.326	.291	.257	.225	.387	.146	.123
8	5.38	.786	.568	.420	.326	.291	.256	.224	.387	.146	.123
9	5.88	.786	.566	.420	.326	.291	.255	.224	.387	.146	.124
10	6.35	.786	.566	.420	.326	.291	.255	.224	.387	.146	.124
11	6.83	.786	.566	.420	.326	.291	.255	.224	.387	.146	.124
12	7.31	.787	.567	.420	.326	.292	.255	.224	.387	.146	.124
13	7.79	.787	.566	.420	.326	.291	.255	.223	.387	.146	.124
14	8.54	.788	.567	.421	.326	.292	.255	.223	.387	.146	.124
15	8.73	.788	.567	.421	.326	.292	.255	.223	.387	.146	.124

$$y/w_t/2.0 = 0.875$$

Point	$p_{t,j}/p_\infty$	$x/l_e$									
		.209	.099	.011	.077	.143	.286	.429	.560	.736	.890
1	1.96	.788	.583	.407	.333	.302	.269	.439	.453	.468	.482
2	2.47	.788	.583	.406	.331	.302	.269	.224	.370	.374	.381
3	2.95	.790	.583	.403	.331	.301	.269	.225	.389	.306	.314
4	3.42	.790	.583	.403	.329	.301	.269	.225	.389	.145	.270
5	3.94	.787	.582	.403	.328	.301	.269	.225	.389	.146	.187
6	4.40	.787	.582	.403	.328	.300	.270	.225	.389	.147	.124
7	4.88	.787	.582	.403	.329	.299	.268	.225	.389	.147	.124
8	5.38	.788	.582	.403	.329	.299	.269	.224	.389	.148	.125
9	5.88	.787	.582	.402	.329	.298	.268	.224	.389	.148	.125
10	6.35	.788	.583	.402	.329	.299	.268	.224	.389	.149	.125
11	6.83	.787	.583	.402	.329	.299	.268	.224	.389	.149	.125
12	7.31	.787	.584	.402	.329	.299	.268	.224	.389	.149	.125
13	7.79	.787	.582	.402	.329	.298	.268	.224	.389	.149	.126
14	8.54	.788	.583	.402	.329	.298	.269	.224	.388	.149	.125
15	8.73	.788	.583	.403	.329	.298	.268	.224	.388	.149	.125

TABLE IV.- Continued

(b) Lower-flap static pressure  $p/P_{t,j}$ 

Point	$P_{t,j}/P_{\infty}$	$y/w_c/2.0 = 0.0$									
		$x/l_e$									
		.209	.099	.011	.077	.143	.286	.429	.560	.736	.890
1	1.96	.790	.563	.408	.322	.300	.270	.398	.424	.443	.469
2	2.47	.790	.565	.409	.325	.301	.271	.227	.378	.385	.386
3	2.95	.787	.566	.407	.326	.300	.273	.227	.378	.318	.323
4	3.42	.788	.566	.408	.326	.300	.273	.228	.378	.148	.275
5	3.94	.788	.566	.408	.325	.299	.273	.227	.378	.147	.217
6	4.40	.787	.566	.409	.325	.299	.273	.228	.378	.147	.118
7	4.88	.788	.567	.409	.325	.299	.273	.227	.378	.147	.118
8	5.38	.788	.566	.410	.323	.299	.273	.227	.378	.147	.118
9	5.88	.787	.565	.410	.323	.298	.272	.226	.378	.147	.118
10	6.35	.787	.565	.410	.323	.298	.271	.226	.378	.147	.119
11	6.83	.787	.566	.410	.323	.299	.271	.226	.378	.147	.119
12	7.31	.787	.566	.410	.323	.298	.272	.226	.378	.147	.119
13	7.79	.787	.566	.410	.323	.298	.272	.226	.378	.147	.119
14	8.54	.788	.567	.411	.324	.298	.272	.226	.378	.147	.119
15	8.73	.786	.567	.411	.324	.298	.272	.226	.378	.147	.118

 $y/w_c/2.0 = 0.450$ 

Point	$P_{t,j}/P_{\infty}$	$x/l_e$									
		$x/l_e$									
		.209	.099	.011	.077	.143	.286	.429	.560	.736	.890
1	1.96	.785	.571	.416	.333	.296	.269	.419	.433	.442	.465
2	2.47	.784	.571	.413	.333	.299	.270	.207	.376	.383	.386
3	2.95	.784	.570	.411	.333	.300	.271	.214	.376	.316	.322
4	3.42	.784	.571	.409	.330	.301	.271	.219	.376	.149	.274
5	3.94	.783	.571	.407	.329	.300	.270	.223	.376	.149	.216
6	4.40	.784	.571	.406	.329	.298	.270	.226	.376	.149	.121
7	4.88	.784	.572	.405	.329	.298	.270	.228	.376	.149	.121
8	5.38	.782	.571	.404	.329	.298	.270	.230	.376	.149	.122
9	5.88	.782	.571	.403	.328	.298	.270	.231	.376	.149	.122
10	6.35	.782	.572	.402	.328	.298	.270	.232	.376	.149	.122
11	6.83	.783	.572	.402	.328	.298	.270	.233	.376	.149	.122
12	7.31	.784	.571	.402	.328	.298	.270	.234	.376	.149	.122
13	7.79	.784	.572	.402	.328	.298	.270	.235	.376	.149	.122
14	8.54	.784	.573	.402	.328	.298	.271	.236	.376	.149	.122
15	8.73	.783	.573	.402	.328	.298	.271	.236	.376	.149	.122

 $y/w_c/2.0 = 0.875$ 

Point	$P_{t,j}/P_{\infty}$	$x/l_e$									
		$x/l_e$									
		.209	.099	.011	.077	.143	.286	.429	.560	.736	.890
1	1.96	.783	.592	.409	.328	.300	.274	.406	.425	.447	.471
2	2.47	.781	.593	.408	.328	.301	.275	.226	.368	.372	.378
3	2.95	.781	.595	.405	.328	.302	.277	.226	.368	.305	.313
4	3.42	.781	.595	.405	.328	.300	.276	.227	.368	.154	.268
5	3.94	.780	.595	.404	.328	.299	.276	.227	.368	.154	.203
6	4.40	.779	.596	.404	.326	.300	.275	.227	.368	.154	.166
7	4.88	.779	.597	.404	.326	.300	.275	.227	.368	.154	.127
8	5.38	.777	.597	.403	.327	.300	.274	.227	.368	.155	.127
9	5.88	.777	.595	.403	.326	.299	.274	.226	.368	.154	.128
10	6.35	.777	.596	.402	.326	.299	.274	.227	.368	.154	.128
11	6.83	.778	.596	.402	.327	.299	.274	.226	.368	.154	.127
12	7.31	.779	.597	.403	.327	.299	.273	.227	.368	.154	.128
13	7.79	.779	.597	.402	.327	.299	.273	.227	.368	.154	.128
14	8.54	.779	.598	.402	.327	.299	.273	.227	.368	.154	.128
15	8.73	.780	.598	.402	.327	.299	.273	.227	.368	.154	.128

TABLE IV.- Concluded

(c) Sidewall static pressure  $p/p_{t,j}$ Left sidewall,  $z = 0.0$ 

Point	$P_{t,j}/P_{\infty}$	$x/l_e$									
		-.209	-.099	.011	.077	.143	.286	.429	.560	.736	.890
1	1.96	.783	.676	.559	.483	.407	.281	.207	.138	.493	.510
2	2.47	.782	.678	.556	.483	.407	.281	.205	.153	.323	.390
3	2.95	.783	.679	.557	.483	.406	.281	.206	.145	.297	.309
4	3.42	.784	.680	.557	.483	.407	.281	.206	.156	.153	.262
5	3.94	.783	.680	.556	.483	.407	.280	.206	.165	.154	.136
6	4.40	.782	.680	.556	.482	.407	.278	.206	.163	.154	.136
7	4.88	.782	.681	.556	.483	.407	.277	.206	.178	.154	.136
8	5.38	.782	.681	.555	.483	.407	.276	.206	.171	.154	.136
9	5.88	.782	.681	.555	.483	.407	.276	.205	.181	.154	.136
10	6.35	.782	.680	.556	.483	.407	.276	.205	.174	.154	.136
11	6.83	.783	.681	.556	.483	.407	.276	.205	.179	.154	.136
12	7.31	.781	.681	.556	.482	.407	.276	.205	.175	.154	.136
13	7.79	.780	.681	.556	.483	.407	.276	.205	.182	.154	.136
14	8.54	.775	.682	.556	.483	.407	.276	.204	.187	.154	.136
15	8.73	.772	.682	.556	.483	.407	.276	.204	.182	.154	.136

Right sidewall,  $z = 0.0$ 

Point	$P_{t,j}/P_{\infty}$	$x/l_e$							
		-.209	-.099	.011	.077	.143	.286	.429	
1	1.96	.771	.681	.558	.479	.411	.283	.233	
2	2.47	.772	.681	.558	.478	.412	.282	.208	
3	2.95	.774	.681	.559	.478	.411	.283	.209	
4	3.42	.775	.682	.560	.477	.409	.284	.208	
5	3.94	.774	.682	.559	.476	.409	.283	.208	
6	4.40	.774	.680	.552	.475	.408	.283	.208	
7	4.88	.775	.681	.552	.475	.408	.282	.208	
8	5.38	.776	.681	.553	.475	.408	.282	.208	
9	5.88	.774	.680	.553	.474	.407	.282	.208	
10	6.35	.775	.681	.553	.475	.408	.282	.208	
11	6.83	.775	.681	.554	.474	.408	.282	.208	
12	7.31	.776	.681	.554	.474	.408	.282	.208	
13	7.79	.776	.681	.554	.474	.408	.282	.208	
14	8.54	.777	.681	.554	.475	.408	.282	.208	
15	8.73	.777	.681	.555	.475	.408	.282	.208	

TABLE V.- RATIO OF INTERNAL STATIC PRESSURE TO JET TOTAL PRESSURE FOR NOZZLE B3

(a) Upper-flap static pressure  $p/p_{t,j}$

$$y/w_c/2.0 = 0.0$$

Point	$P_{t,j}/p_{\infty}$	$x/l_e$									
		.199	.093	.013	.077	.141	.279	.417	.545	.715	.864
1	1.98	.795	.596	.375	.341	.306	.280	.246	.213	.187	.164
2	2.48	.794	.597	.372	.342	.308	.280	.238	.205	.179	.156
3	2.96	.795	.599	.371	.343	.308	.280	.239	.206	.180	.157
4	3.46	.795	.600	.369	.343	.308	.281	.240	.207	.181	.158
5	3.95	.796	.600	.368	.343	.308	.280	.240	.207	.181	.158
6	4.44	.796	.600	.367	.344	.307	.280	.240	.207	.181	.158
7	4.93	.796	.600	.367	.345	.307	.280	.240	.207	.181	.158
8	5.42	.796	.600	.366	.344	.306	.280	.240	.207	.181	.158
9	5.92	.796	.600	.365	.344	.306	.280	.240	.207	.181	.158
10	6.41	.796	.601	.365	.345	.306	.280	.240	.207	.181	.158
11	6.89	.797	.601	.364	.345	.306	.280	.240	.207	.181	.158
12	7.38	.797	.601	.364	.345	.306	.280	.240	.207	.181	.158
13	7.87	.797	.601	.364	.345	.306	.280	.240	.207	.181	.158
14	8.35	.797	.601	.363	.345	.306	.280	.240	.207	.181	.158
15	8.81	.797	.601	.363	.345	.306	.280	.240	.207	.181	.158

$$y/w_c/2.0 = 0.450$$

Point	$P_{t,j}/p_{\infty}$	$x/l_e$									
		.199	.093	.013	.077	.141	.279	.417	.545	.715	.864
1	1.98	.797	.591	.400	.329	.310	.284	.231	.204	.179	.156
2	2.48	.796	.591	.400	.328	.312	.285	.242	.215	.190	.167
3	2.96	.796	.591	.398	.327	.313	.287	.244	.218	.193	.170
4	3.46	.796	.592	.397	.327	.313	.287	.245	.219	.194	.171
5	3.95	.796	.592	.396	.326	.313	.287	.245	.219	.194	.171
6	4.44	.796	.592	.395	.325	.313	.288	.245	.219	.194	.171
7	4.93	.796	.592	.394	.325	.313	.288	.245	.219	.194	.171
8	5.42	.796	.592	.394	.324	.313	.288	.245	.219	.194	.171
9	5.92	.795	.592	.394	.324	.313	.288	.245	.219	.194	.171
10	6.41	.796	.592	.392	.323	.313	.288	.245	.219	.194	.171
11	6.89	.796	.592	.392	.323	.313	.288	.245	.219	.194	.171
12	7.38	.795	.593	.392	.322	.313	.288	.245	.219	.194	.171
13	7.87	.795	.593	.392	.322	.313	.288	.245	.219	.194	.171
14	8.35	.795	.593	.391	.322	.313	.288	.245	.219	.194	.171
15	8.81	.795	.593	.391	.322	.313	.288	.245	.219	.194	.171

$$y/w_c/2.0 = 0.875$$

Point	$P_{t,j}/p_{\infty}$	$x/l_e$									
		.199	.093	.077	.141	.279	.417	.545	.715	.864	
1	1.98	.801	.379	.330	.320	.275	.237	.210	.185	.160	.137
2	2.48	.801	.377	.329	.321	.276	.231	.204	.179	.154	.131
3	2.96	.801	.375	.328	.320	.276	.232	.205	.180	.155	.132
4	3.46	.800	.374	.327	.320	.276	.232	.205	.180	.155	.132
5	3.95	.800	.373	.325	.319	.276	.231	.204	.179	.154	.131
6	4.44	.800	.372	.324	.318	.275	.231	.204	.179	.154	.131
7	4.93	.800	.371	.324	.317	.275	.231	.204	.179	.154	.131
8	5.42	.800	.370	.323	.316	.274	.229	.203	.178	.153	.130
9	5.92	.800	.370	.322	.316	.274	.229	.203	.178	.153	.130
10	6.41	.799	.369	.322	.315	.274	.229	.203	.178	.153	.130
11	6.89	.799	.369	.322	.315	.273	.229	.203	.178	.153	.130
12	7.38	.799	.368	.321	.315	.273	.228	.202	.177	.152	.129
13	7.87	.799	.368	.321	.315	.273	.228	.202	.177	.152	.129
14	8.35	.799	.368	.321	.315	.273	.228	.202	.177	.152	.129
15	8.81	.799	.368	.320	.315	.273	.228	.202	.177	.152	.129

(b) Lower-flap static pressure  $p/p_t, j$

Point	$P_{T,j}/P_{\infty}$	$x/1_e$						
		.199	.093	.013	.077	.141	.279	.417
1	1.96	.792	.615	.399	.333	.301	.275	.443
2	2.48	.792	.615	.400	.336	.303	.275	.443
3	2.96	.791	.615	.400	.337	.303	.276	.444
4	3.46	.791	.614	.401	.338	.304	.276	.444
5	3.95	.791	.614	.401	.338	.303	.276	.444
6	4.44	.791	.614	.401	.338	.303	.275	.443
7	4.93	.791	.613	.400	.338	.303	.275	.443
8	5.42	.791	.613	.401	.338	.303	.275	.443
9	5.92	.790	.613	.401	.338	.303	.275	.443
10	6.41	.790	.613	.400	.338	.303	.275	.443
11	6.89	.790	.613	.400	.338	.303	.274	.442
12	7.38	.790	.613	.400	.338	.303	.274	.442
13	7.87	.790	.613	.400	.338	.303	.274	.442
14	8.35	.790	.612	.400	.338	.303	.274	.442
15	8.81	.790	.612	.399	.338	.302	.274	.442

Point	$P_{L,j}/P_{\infty}$	$y/w\sqrt{2.0} = 0.450$ $x/L_e$									
		.199	.093	.013	.077	.141	.279	.417	.545	.715	.864
1	1.98	.788	.616	.401	.336	.307	.278	.423	.430	.449	.466
2	2.48	.787	.619	.401	.335	.309	.280	.232	.371	.380	.381
3	2.96	.788	.621	.402	.334	.310	.281	.232	.371	.381	.381
4	3.46	.789	.621	.402	.333	.310	.281	.233	.366	.371	.371
5	3.95	.788	.621	.402	.332	.308	.281	.233	.366	.371	.371
6	4.44	.789	.622	.401	.332	.307	.281	.233	.367	.371	.371
7	4.93	.789	.621	.401	.332	.306	.281	.233	.367	.371	.371
8	5.42	.788	.621	.401	.331	.306	.281	.233	.367	.371	.371
9	5.92	.788	.621	.401	.331	.305	.282	.232	.367	.371	.371
10	6.41	.788	.621	.401	.330	.305	.282	.232	.367	.371	.371
11	6.89	.788	.621	.401	.330	.305	.282	.232	.367	.371	.371
12	7.38	.788	.621	.401	.330	.305	.282	.232	.367	.371	.371
13	7.87	.788	.622	.401	.330	.305	.282	.232	.367	.371	.371
14	8.35	.788	.621	.401	.329	.305	.282	.232	.367	.371	.371
15	8.81	.788	.623	.401	.329	.305	.282	.232	.367	.371	.371

[illegible]

TABLE V.- Concluded

(c) Sidewall static pressure  $p/p_{t,j}$ Left sidewall,  $z = 0.0$ 

Point	$P_{t,j}/P_{\infty}$	$x/l_e$						
		.199	.093	.013	.077	.141	.279	.417
1	1.98	.778	.680	.551	.469	.398	.294	.234
2	2.48	.778	.678	.551	.469	.399	.295	.236
3	2.96	.779	.679	.551	.469	.399	.297	.237
4	3.46	.780	.679	.551	.469	.400	.297	.237
5	3.95	.778	.678	.551	.469	.400	.297	.238
6	4.44	.779	.678	.551	.469	.400	.296	.237
7	4.93	.779	.678	.551	.469	.400	.296	.237
8	5.42	.779	.678	.551	.469	.400	.295	.237
9	5.92	.779	.678	.552	.469	.400	.295	.237
10	6.41	.779	.678	.552	.469	.400	.295	.237
11	6.89	.779	.678	.552	.469	.400	.295	.236
12	7.38	.779	.678	.552	.469	.400	.295	.236
13	7.87	.779	.678	.552	.469	.400	.295	.236
14	8.35	.778	.678	.552	.469	.400	.295	.236
15	8.81	.779	.678	.552	.468	.400	.294	.236

Right sidewall,  $z = 0.0$ 

Point	$P_{t,j}/P_{\infty}$	$x/l_e$						
		.199	.093	.013	.077	.141	.279	.417
1	1.98	.779	.681	.556	.474	.402	.285	.223
2	2.48	.779	.681	.555	.474	.403	.287	.224
3	2.96	.780	.682	.556	.474	.402	.288	.225
4	3.46	.780	.682	.556	.474	.401	.289	.226
5	3.95	.780	.682	.557	.474	.401	.288	.226
6	4.44	.781	.682	.554	.474	.401	.288	.226
7	4.93	.781	.682	.555	.474	.401	.287	.226
8	5.42	.781	.682	.555	.474	.400	.287	.226
9	5.92	.781	.682	.555	.474	.400	.287	.226
10	6.41	.781	.682	.555	.474	.400	.287	.226
11	6.89	.781	.682	.556	.474	.400	.287	.226
12	7.38	.781	.682	.556	.474	.400	.287	.226
13	7.87	.781	.682	.556	.475	.400	.287	.226
14	8.35	.781	.682	.555	.475	.400	.287	.226
15	8.81	.781	.682	.555	.475	.400	.287	.226

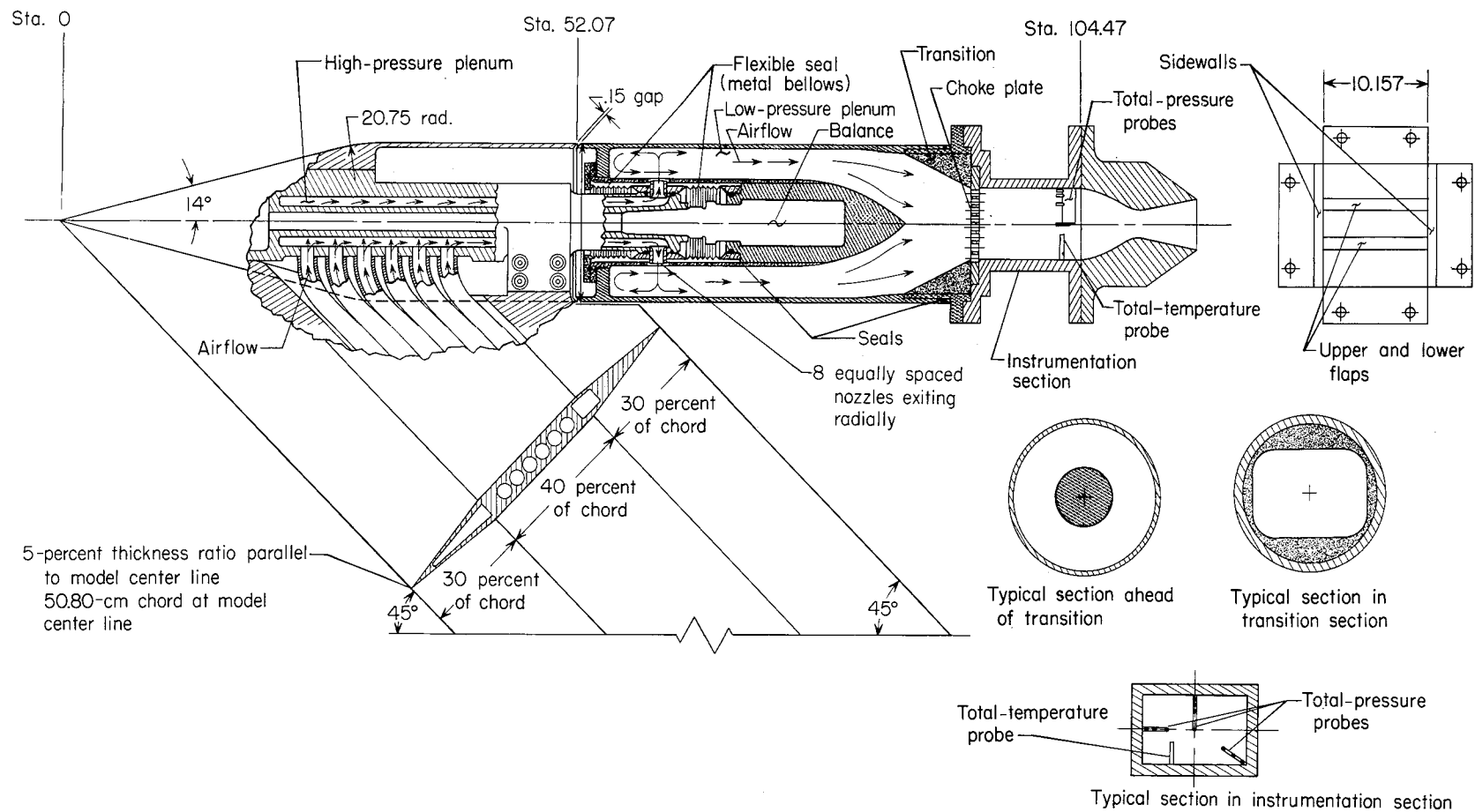
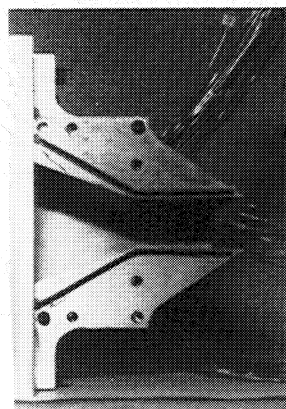
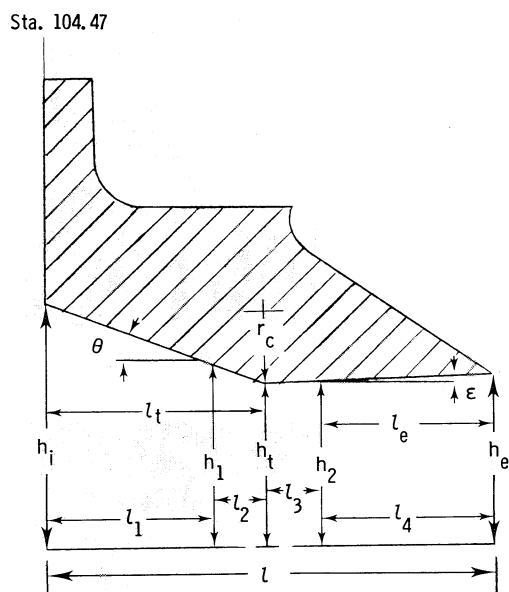


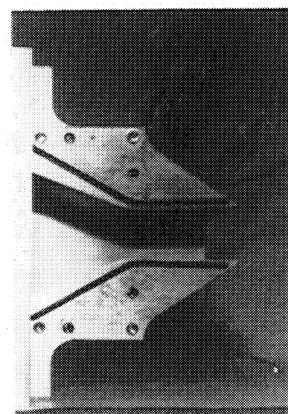
Figure 1.- Sketch of air-powered nacelle model with typical nozzle configuration installed. All dimensions are in centimeters unless otherwise noted.





Configuration A1

Parameter	A1	A2	Parameter	A1	A2
$A_e, \text{cm}^2$	30.29	30.29	$l_t$	5.78	5.78
$A_t, \text{cm}^2$	27.81	27.81	$l_1$	5.54	4.74
$A_e/A_t$	1.09	1.09	$l_2$	.24	1.04
$h_e$	1.49	1.49	$l_3$	.01	.06
$h_i$	3.52	3.52	$l_4$	5.76	5.72
$h_t$	1.37	1.37	$M_d$	1.35	1.35
$h_1$	1.41	1.57	$\text{NPR}_d$	2.97	2.97
$h_2$	1.37	1.37	$r_c$	.68	2.74
$l$	11.56	11.56	$\theta, \text{deg}$	20.84	22.33
$l_e$	5.78	5.78	$\epsilon, \text{deg}$	1.21	1.21



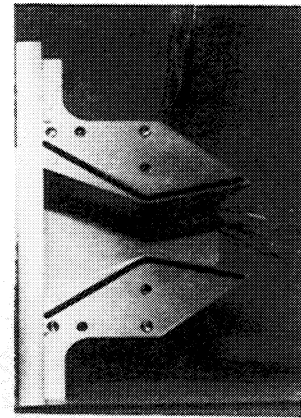
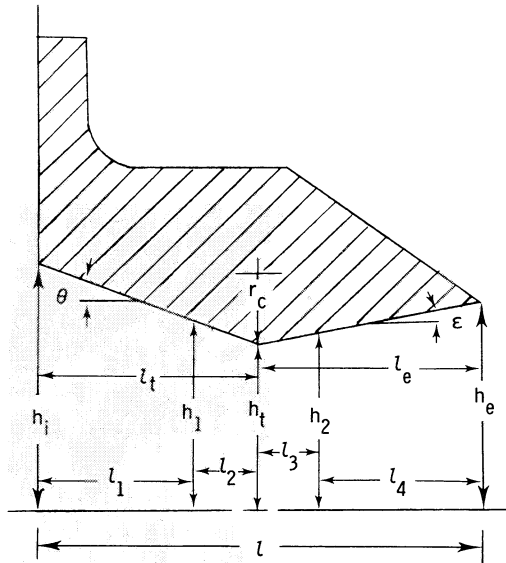
Configuration A2

L-80-174

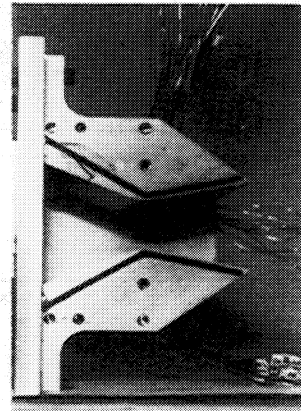
(a) Configurations A1 and A2.

Figure 2.- Sketches of nonaxisymmetric converging-diverging nozzle configurations showing important parameters. All dimensions are in centimeters unless otherwise noted.

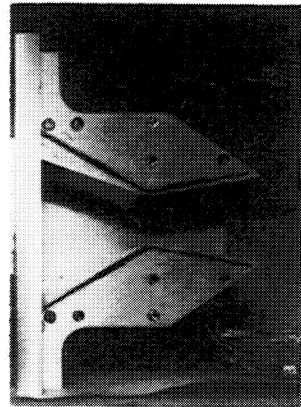
Sta. 104.47



Configuration B1



Configuration B2



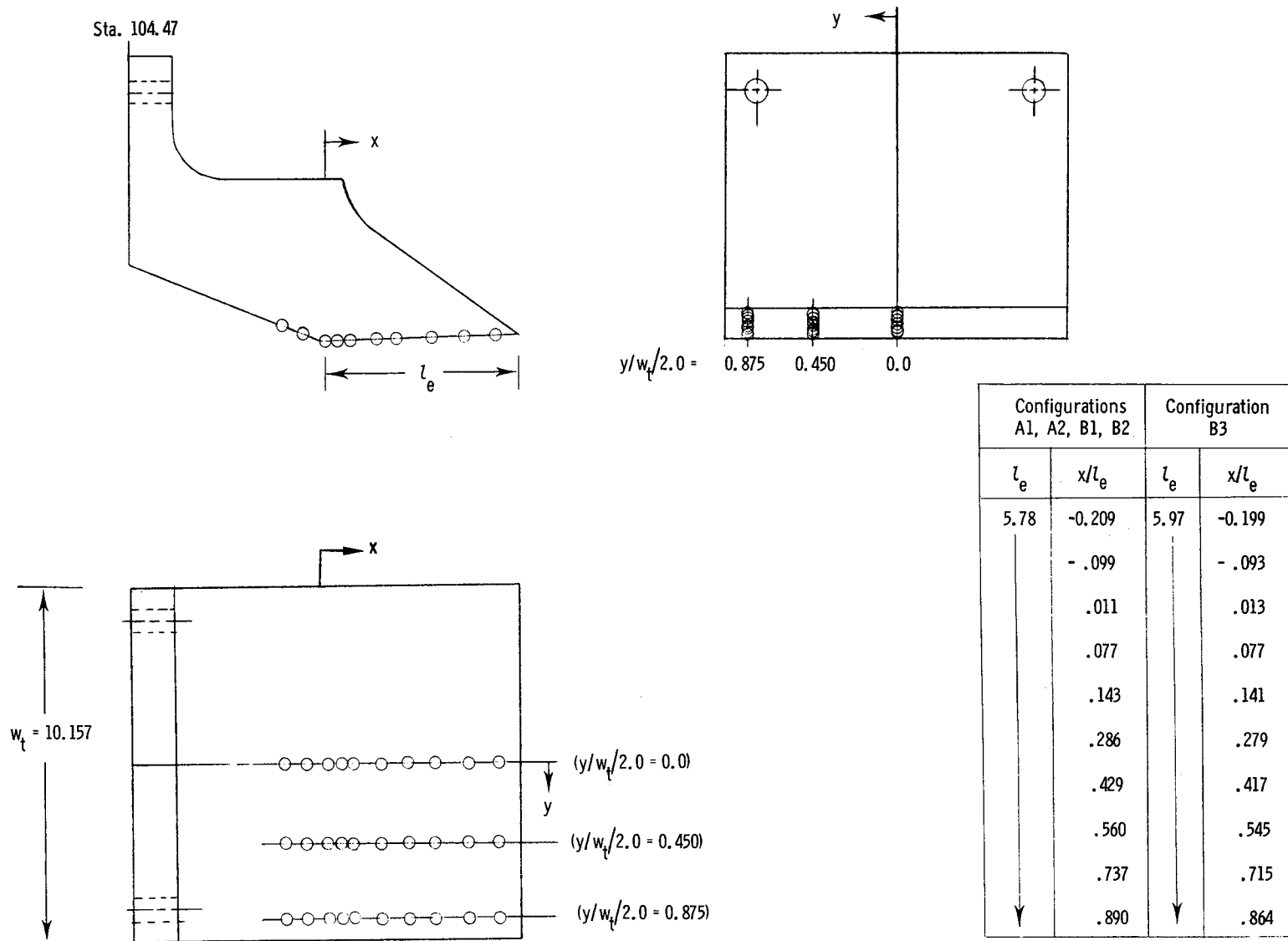
Configuration B3

	B1	B2	B3		B1	B2	B3
$A_e, \text{cm}^2$	50.06	50.06	50.06	$l_t$	5.78	5.78	6.27
$A_t, \text{cm}^2$	27.81	27.81	27.81	$l_1$	5.54	4.74	5.32
$A_e/A_t$	1.80	1.80	1.80	$l_2$	.24	1.04	.96
$h_e$	2.46	2.46	2.46	$l_3$	.13	.53	.52
$h_i$	3.52	3.52	3.52	$l_4$	5.65	5.25	5.46
$h_t$	1.37	1.37	1.37	$M_d$	2.08	2.08	2.08
$h_1$	1.41	1.57	1.54	$\text{NPR}_d$	8.81	8.81	8.81
$h_2$	1.38	1.42	1.42	$r_c$	.68	2.74	2.74
$l$	11.56	11.56	12.25	$\theta, \text{deg}$	20.84	22.33	20.42
$l_e$	5.78	5.78	5.97	$\epsilon, \text{deg}$	10.85	11.24	10.85

(b) Configurations B1, B2, and B3.

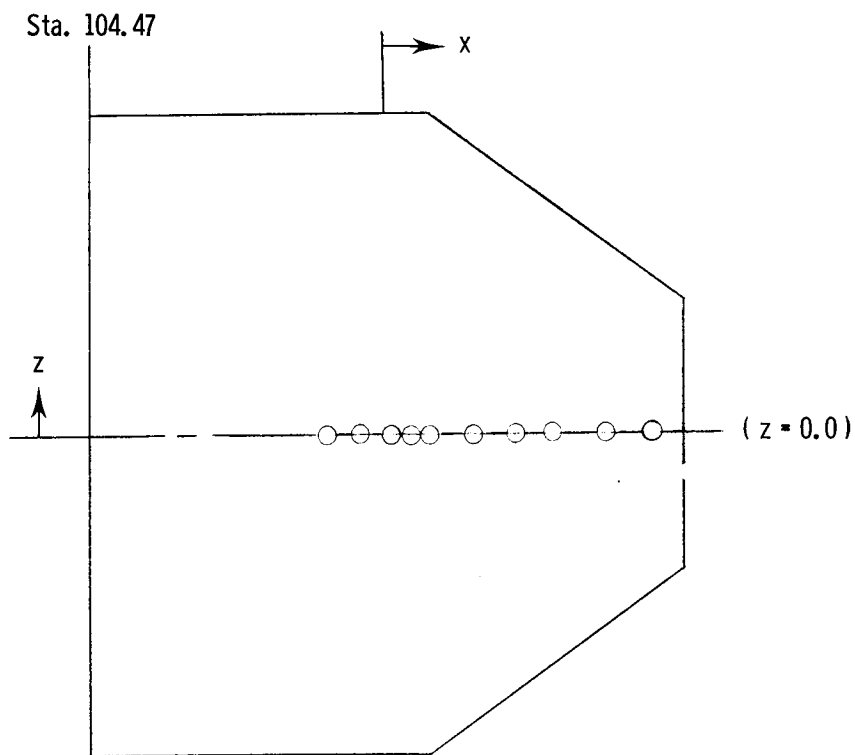
L-80-175

Figure 2.- Concluded.



(a) Flap static-pressure instrumentation.

Figure 3.- Sketches of 2-D C-D nozzle components showing internal static-pressure orifice locations. All dimensions are in centimeters unless otherwise noted.



Configurations A1, A2, B1, B2		Configuration B3	
Left	Right	Left	Right
$x/l_e$	$x/l_e$	$x/l_e$	$x/l_e$
-0.209	-0.209	-0.199	-0.199
-.099	-.099	-.093	-.093
.011	.011	.013	.013
.077	.077	.077	.077
.143	.143	.141	.141
.286	.286	.279	.279
.429	.429	.417	.417
.560		.545	
.736		.715	
.890		.864	

(b) Sidewall static-pressure instrumentation.

Figure 3.- Concluded.

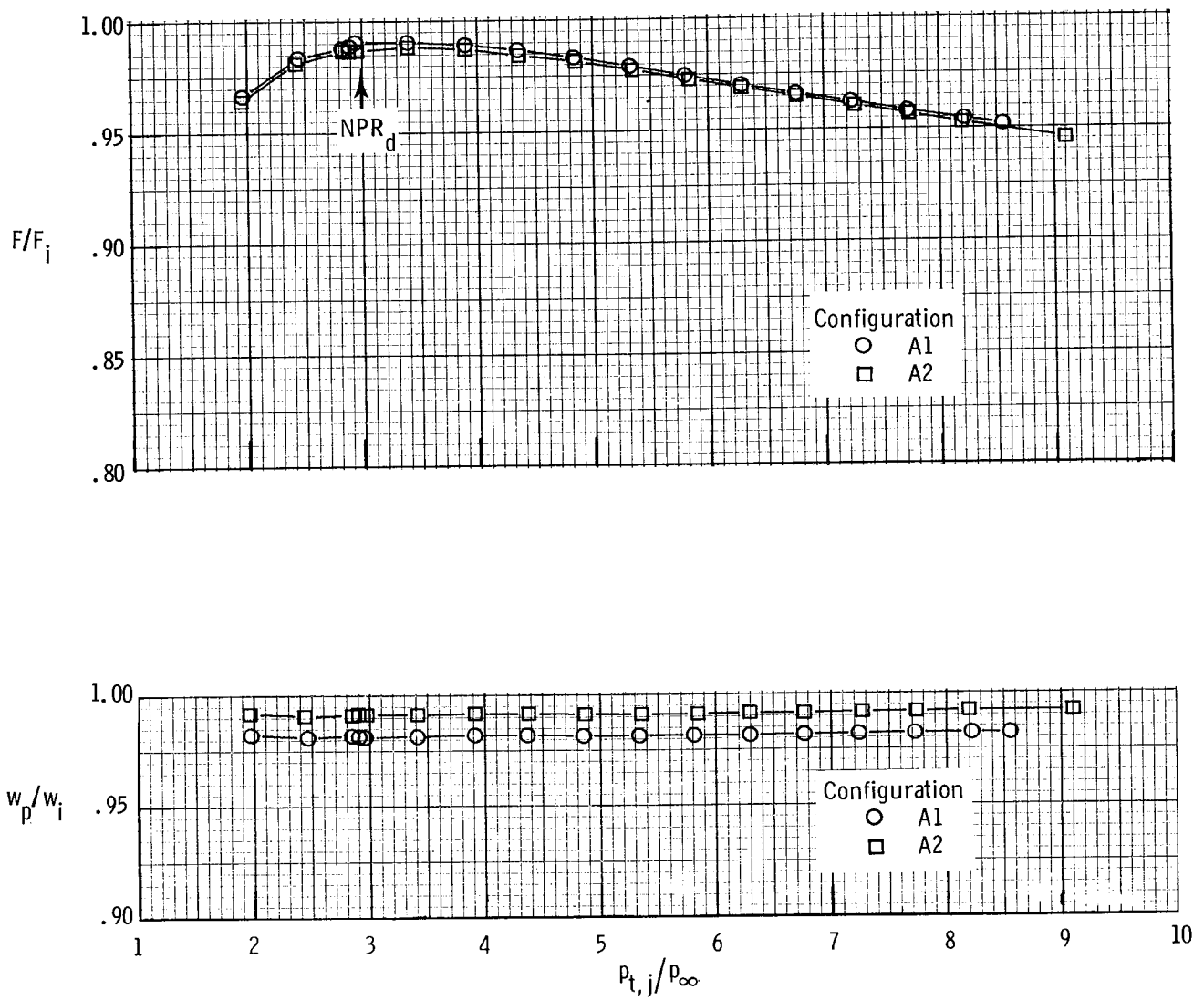


Figure 4.- Variation of nozzle internal thrust ratio and discharge coefficient with nozzle pressure ratio for 2-D C-D nozzles with low divergence angle.

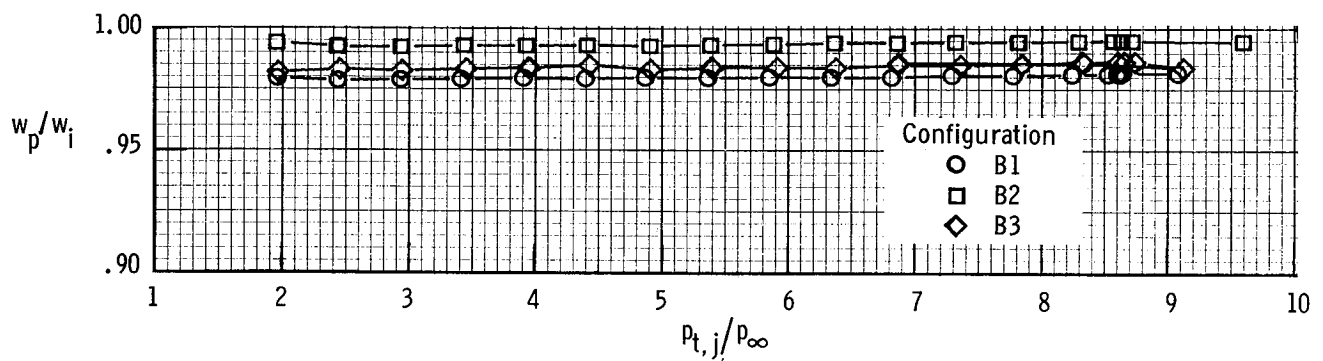
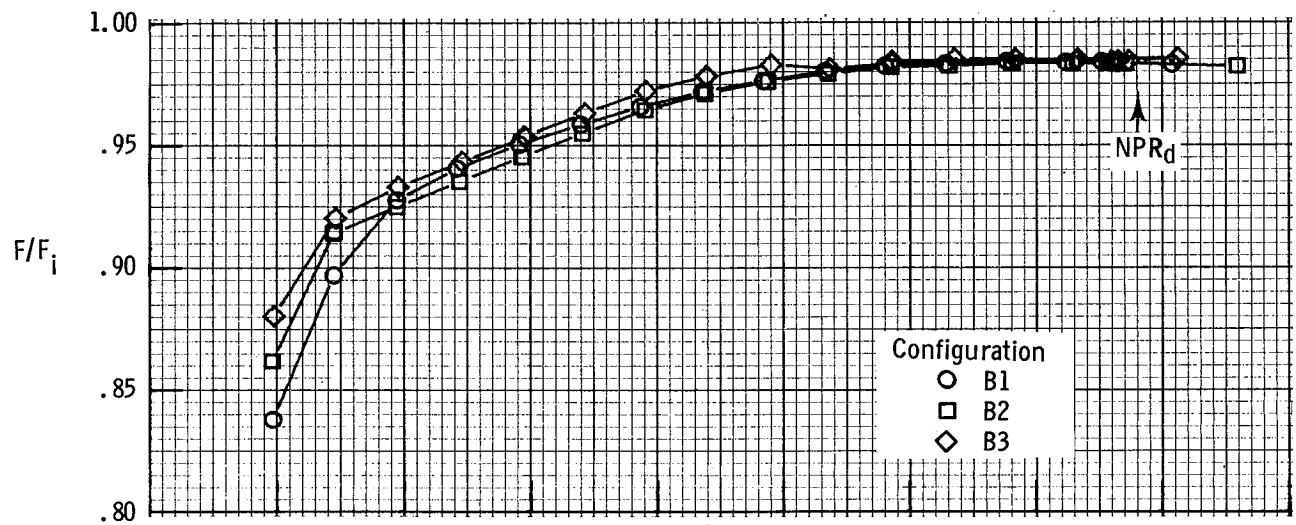


Figure 5.- Variation of internal thrust ratio and discharge coefficient with nozzle pressure ratio for 2-D C-D nozzles with high divergence angle.

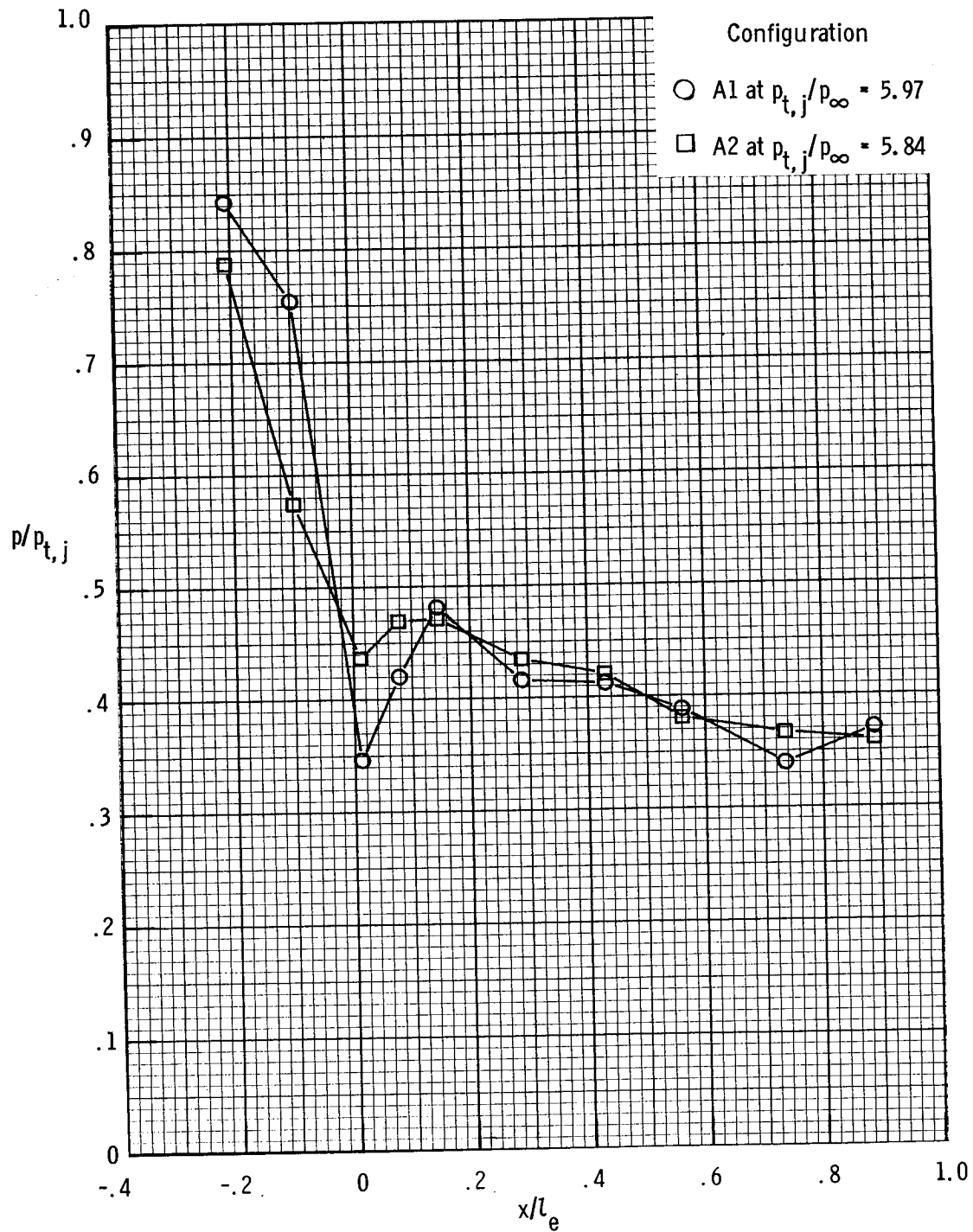


Figure 6.- Comparison of internal static-pressure distributions along upper-flap center line for nozzles A1 and A2.

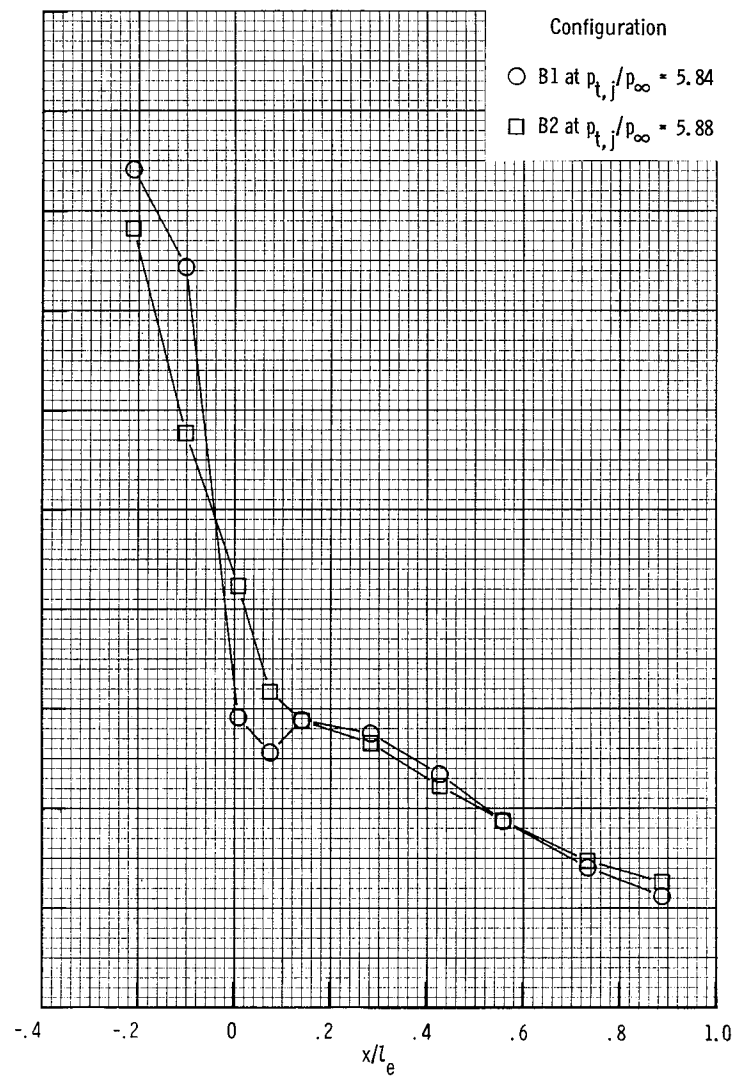
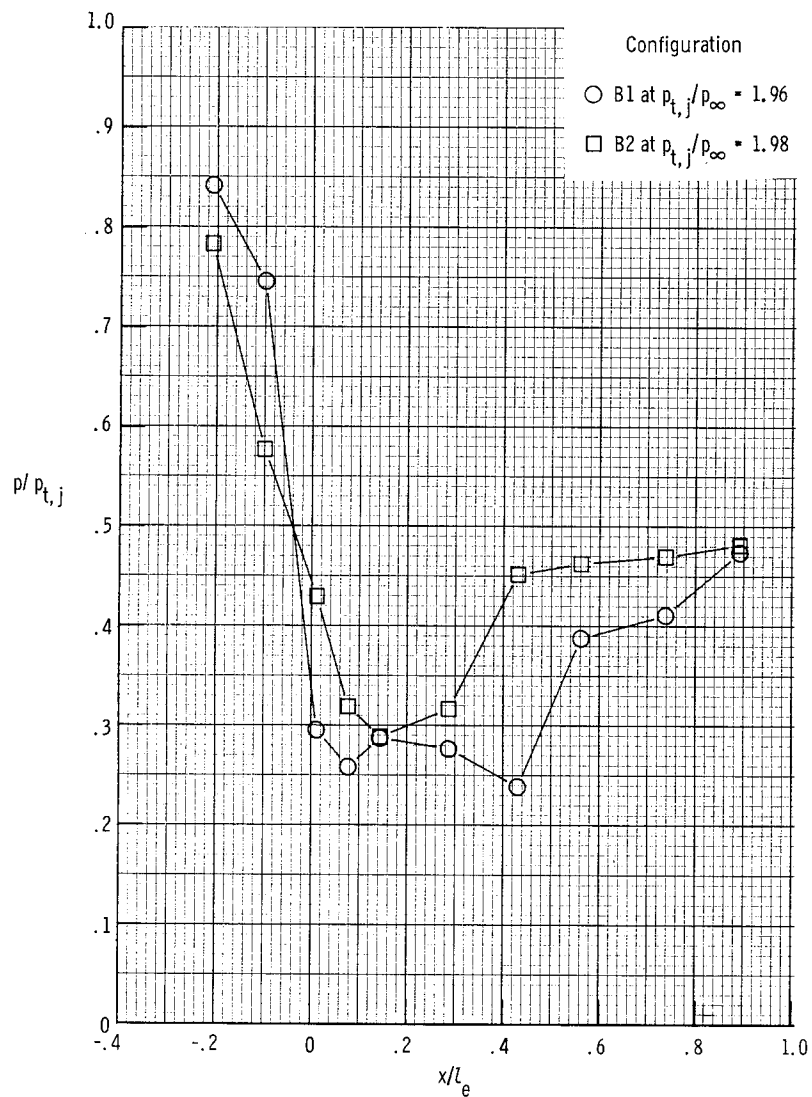


Figure 7.- Comparison of internal static-pressure distributions along upper-flap center line for nozzles B1 and B2.



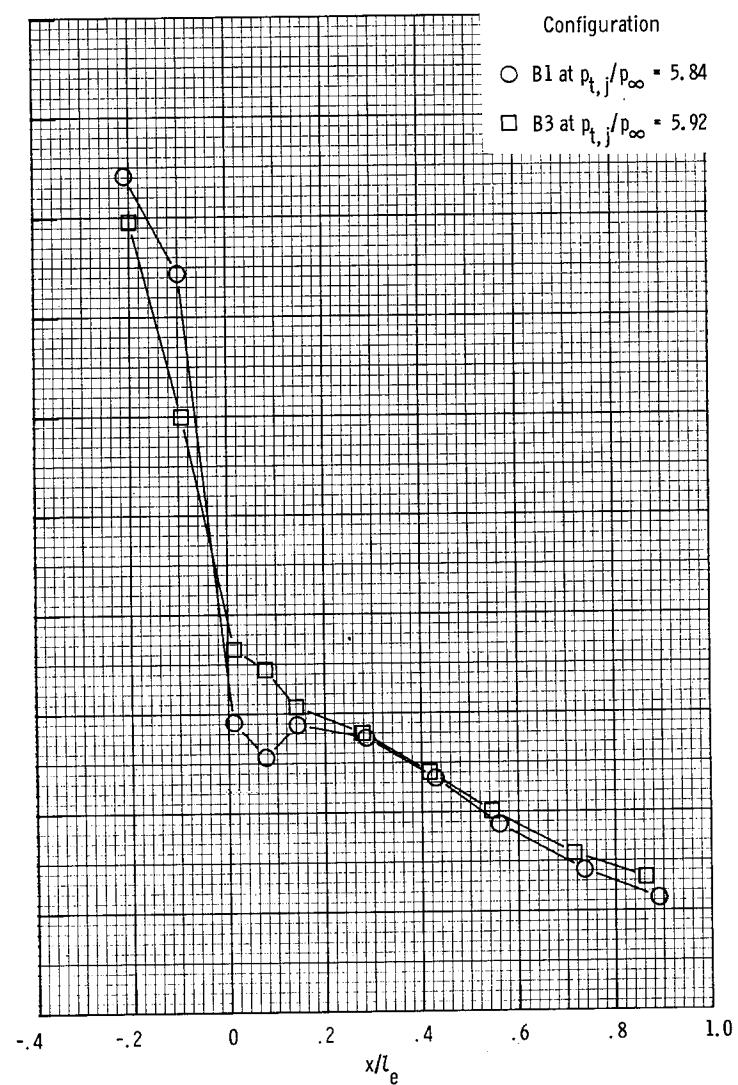
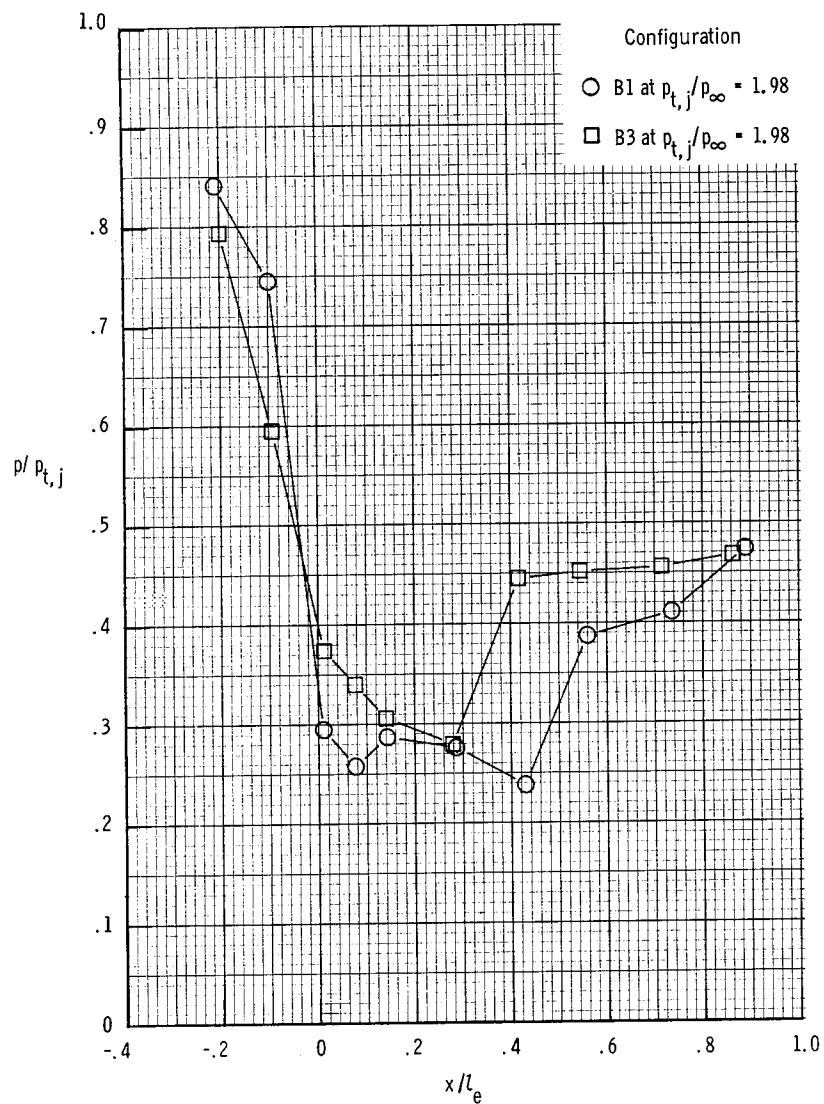
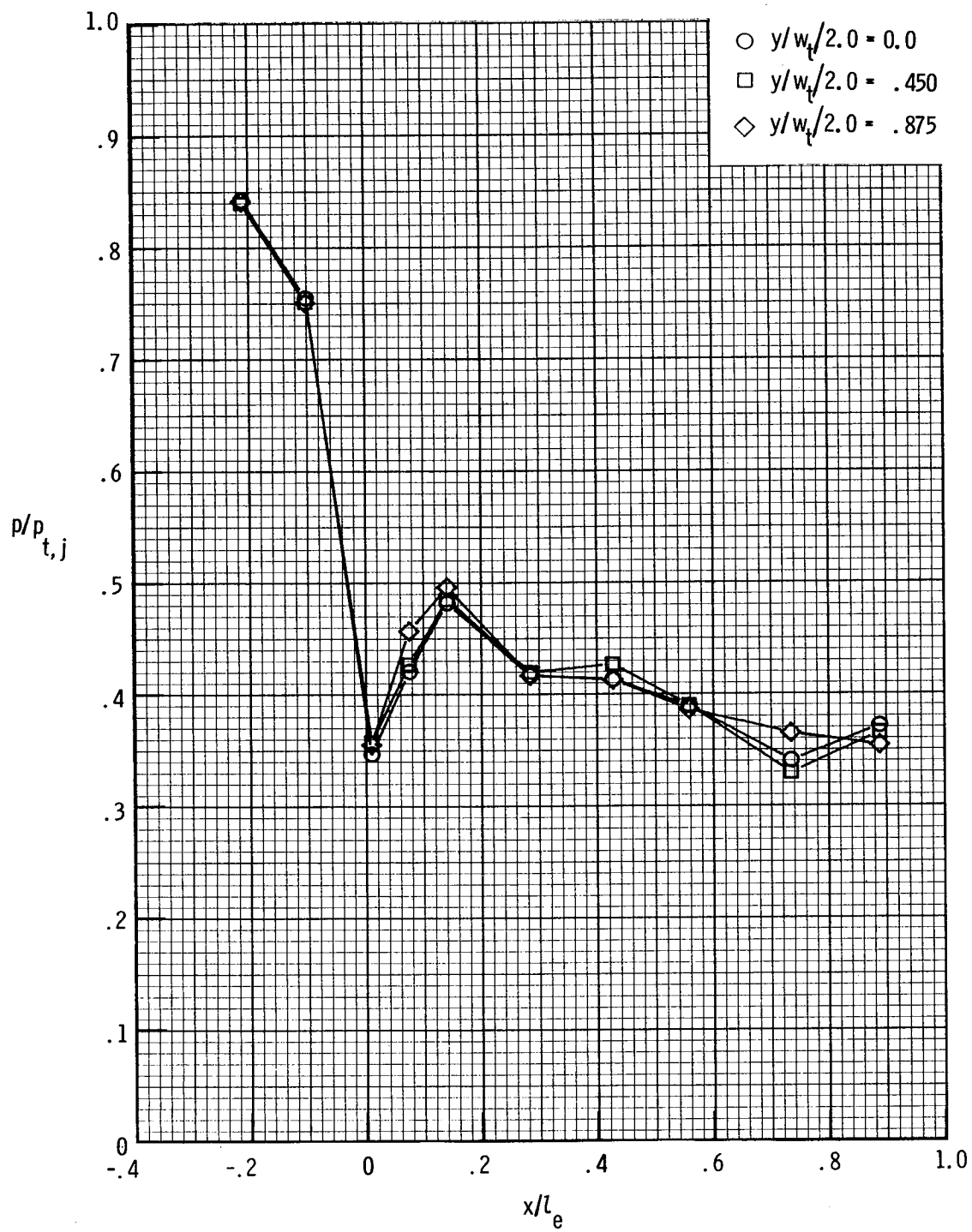
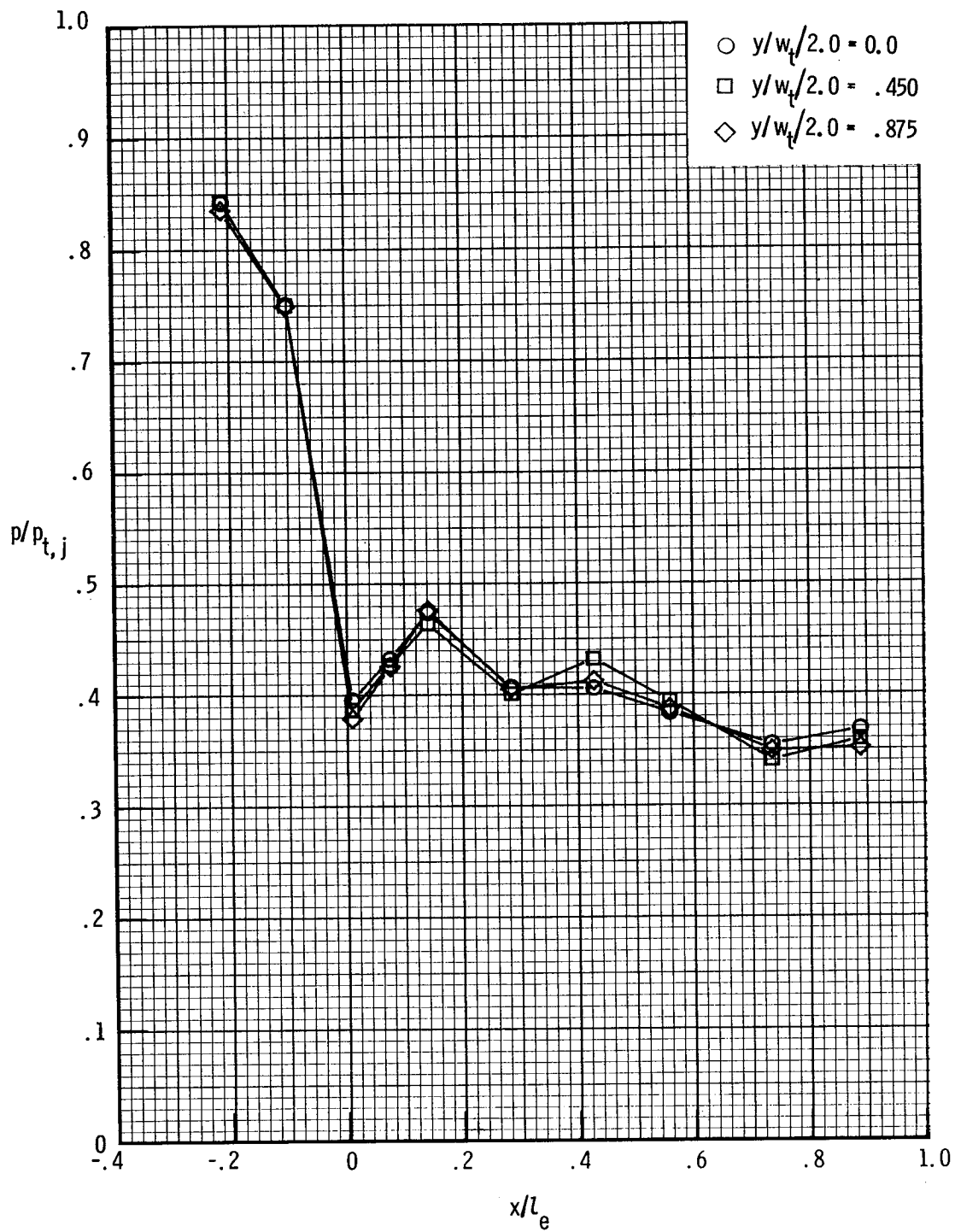


Figure 8.- Comparison of internal static-pressure distributions along the upper-flap center line for nozzles B1 and B3.



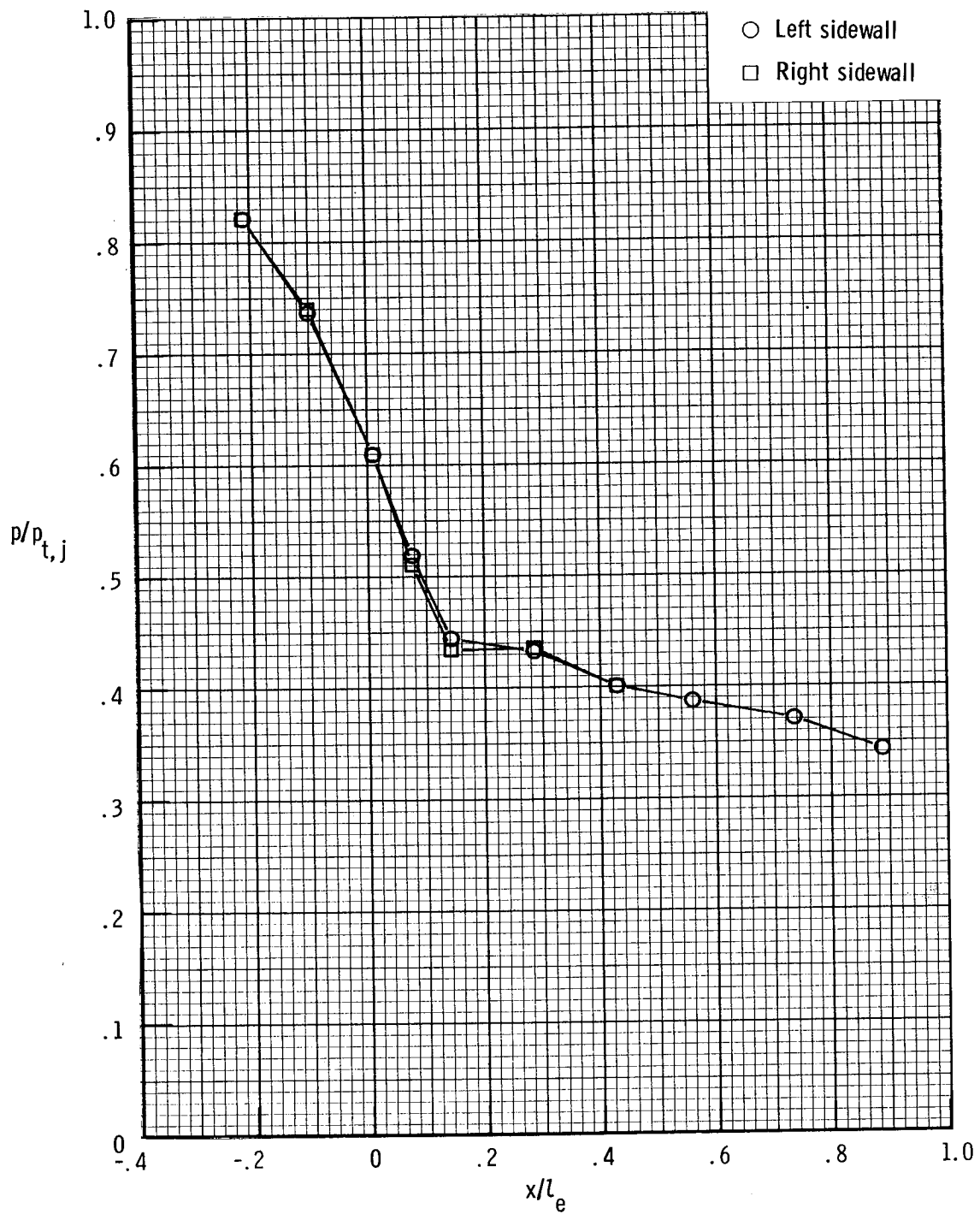
(a) Upper flap.

Figure 9.- Internal static-pressure distributions for nozzle A1 at  $P_{t,j}/P_{\infty} = 5.97$ .



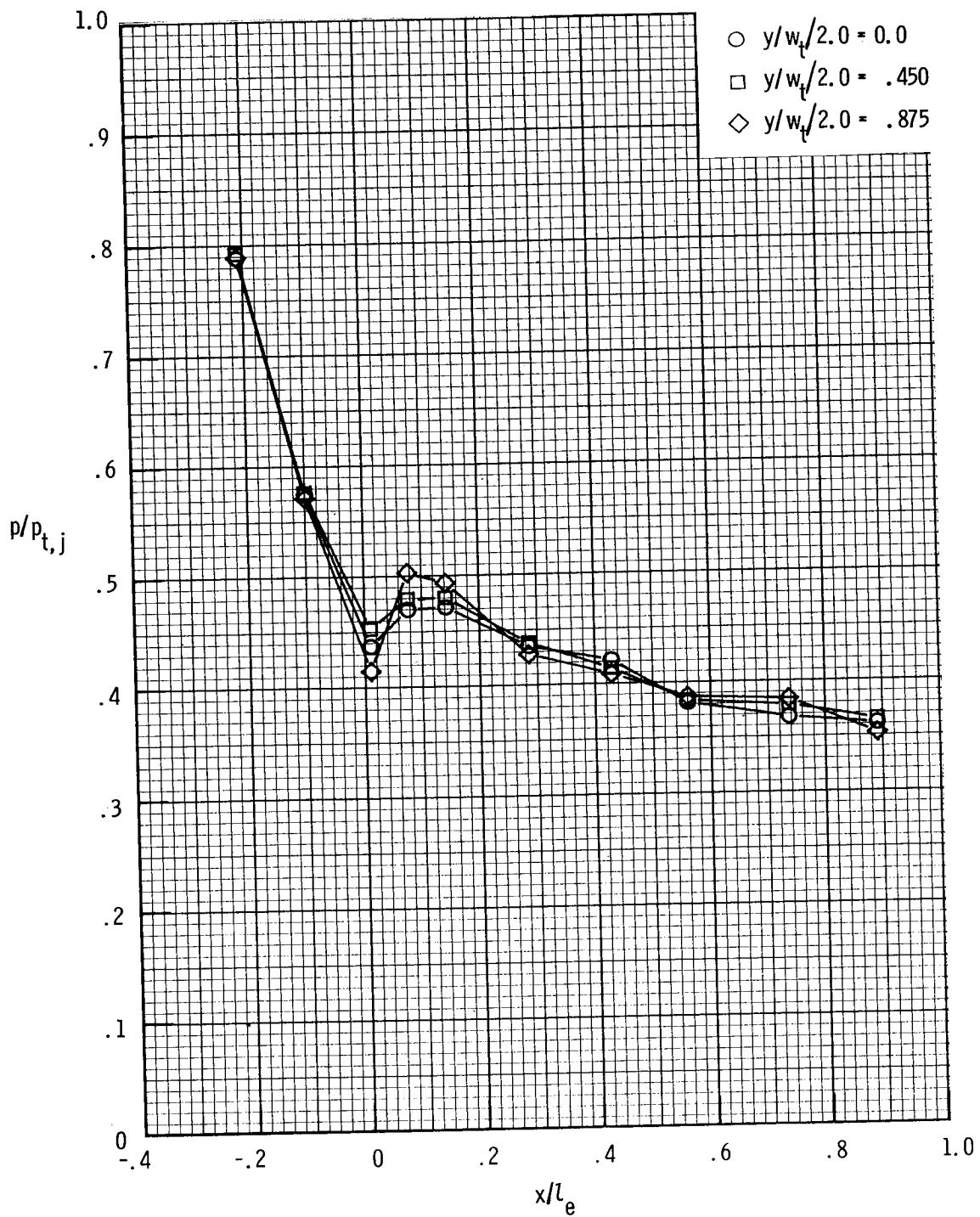
(b) Lower flap.

Figure 9.- Continued.



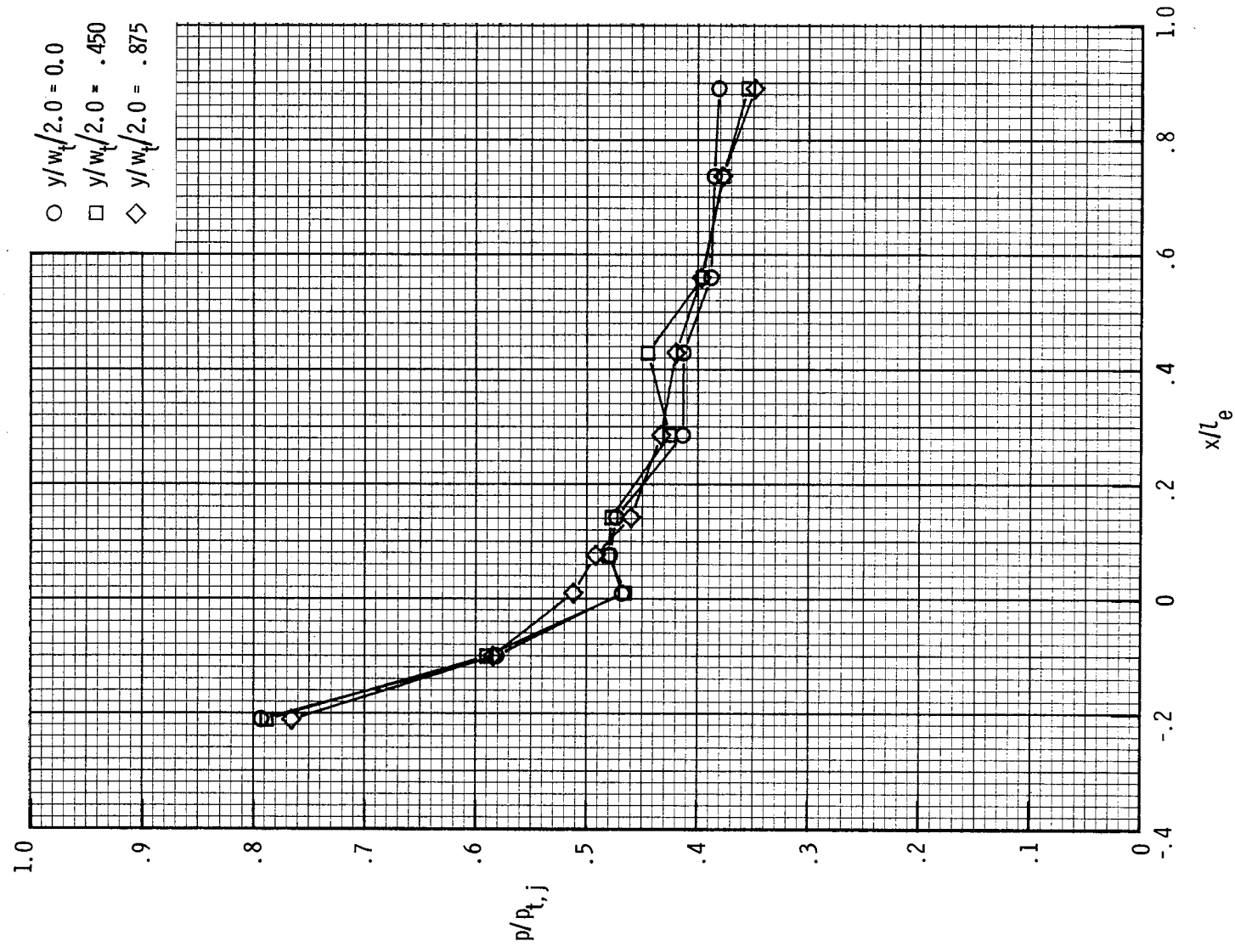
(c) Sidewalls.

Figure 9.- Concluded.



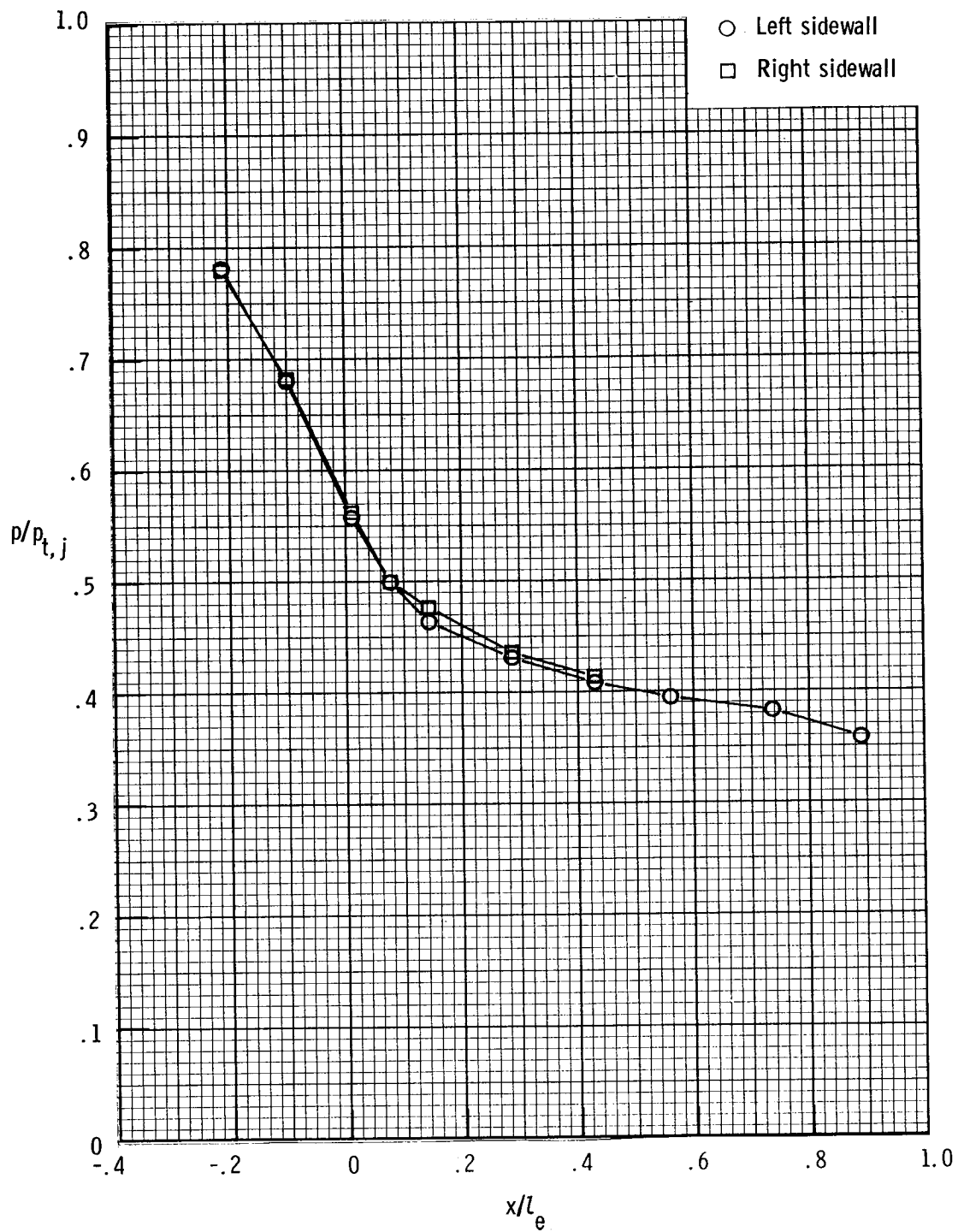
(a) Upper flap.

Figure 10.- Internal static-pressure distributions for nozzle A2 at  $p_{t,j}/p_\infty = 5.84$ .



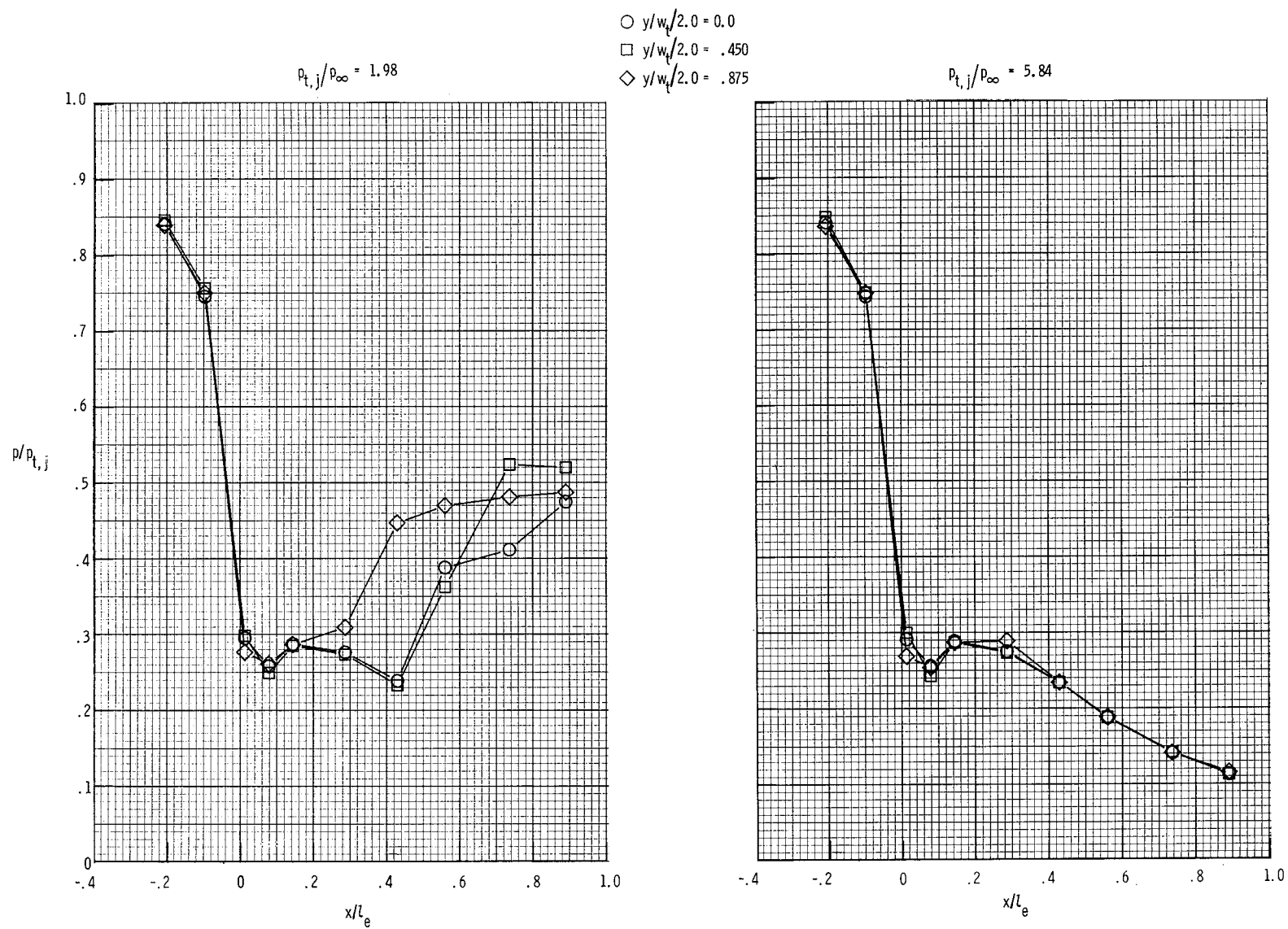
(b) Lower flap.

Figure 10.- Continued.



(c) Sidewalls.

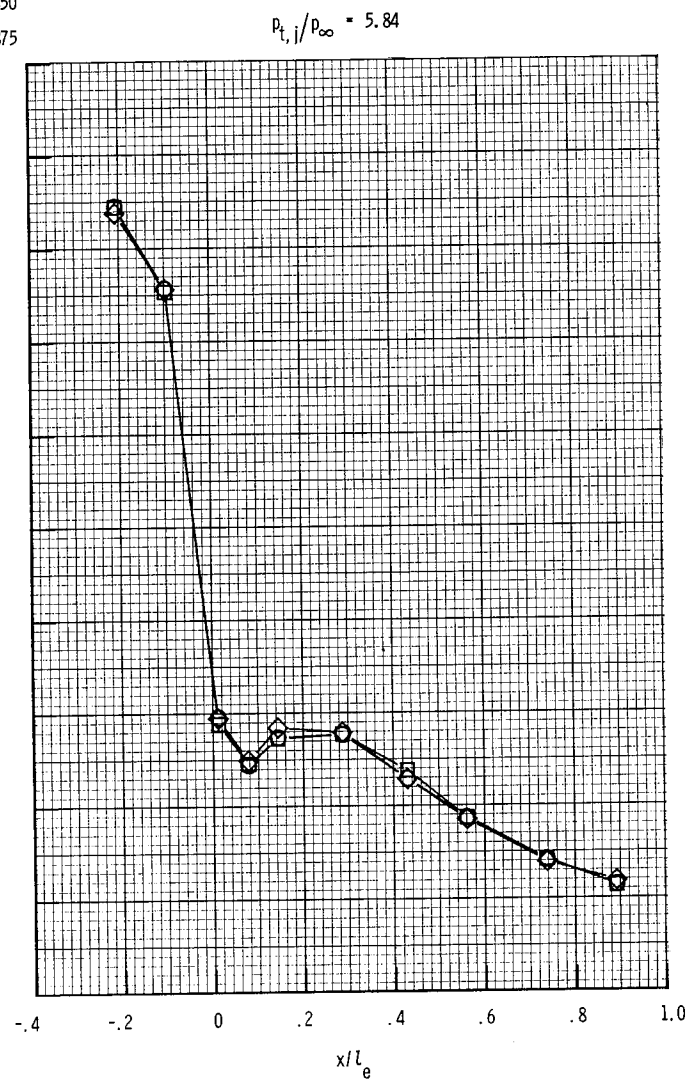
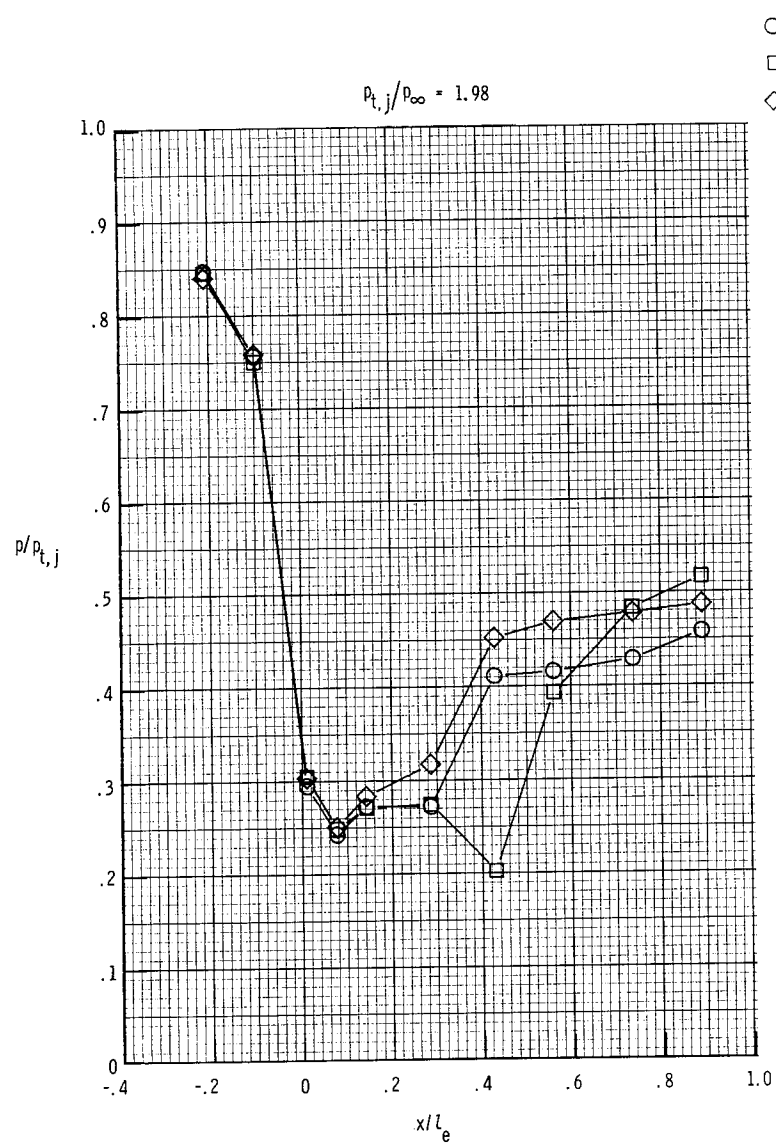
Figure 10.- Concluded.



(a) Upper flap.

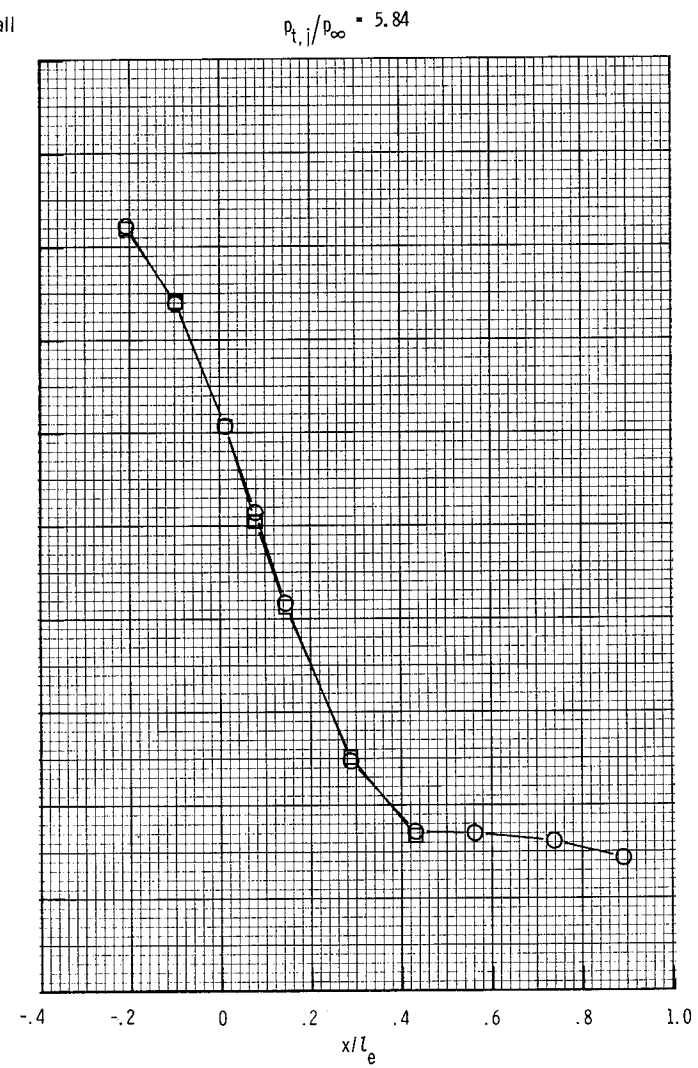
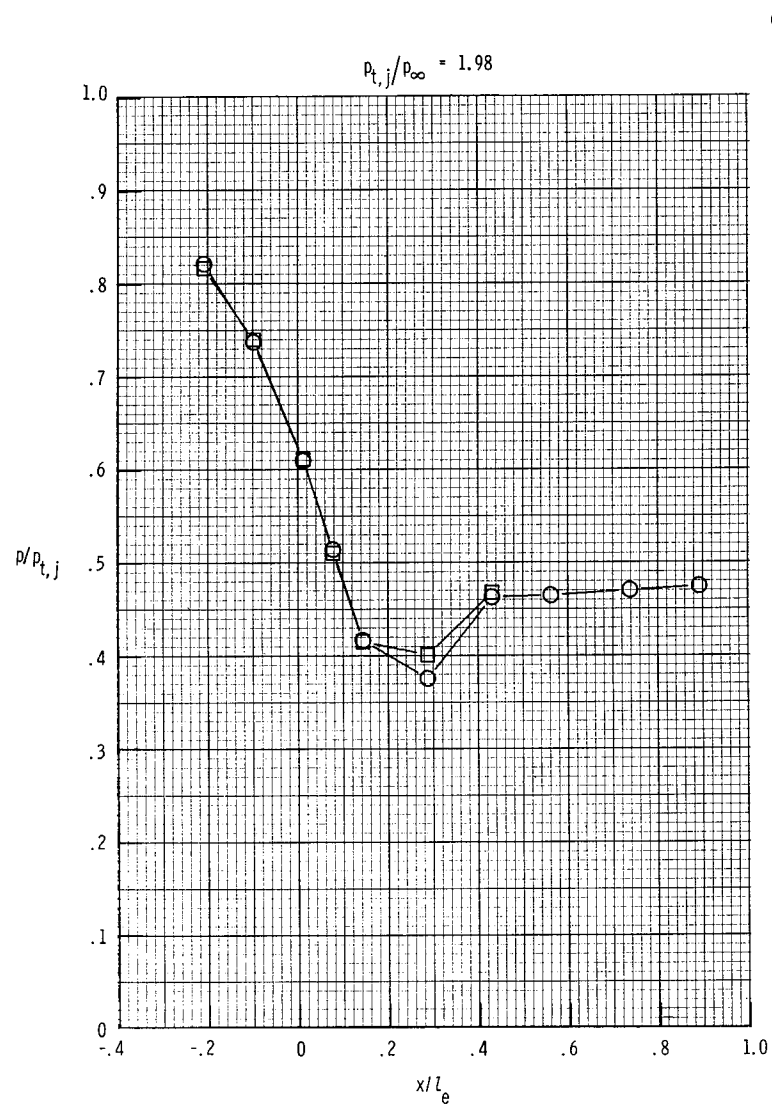
Figure 11.- Internal static-pressure distributions for nozzle B1 at  $p_{t,j}/p_\infty = 1.98$  and  $p_{t,j}/p_\infty = 5.84$ .





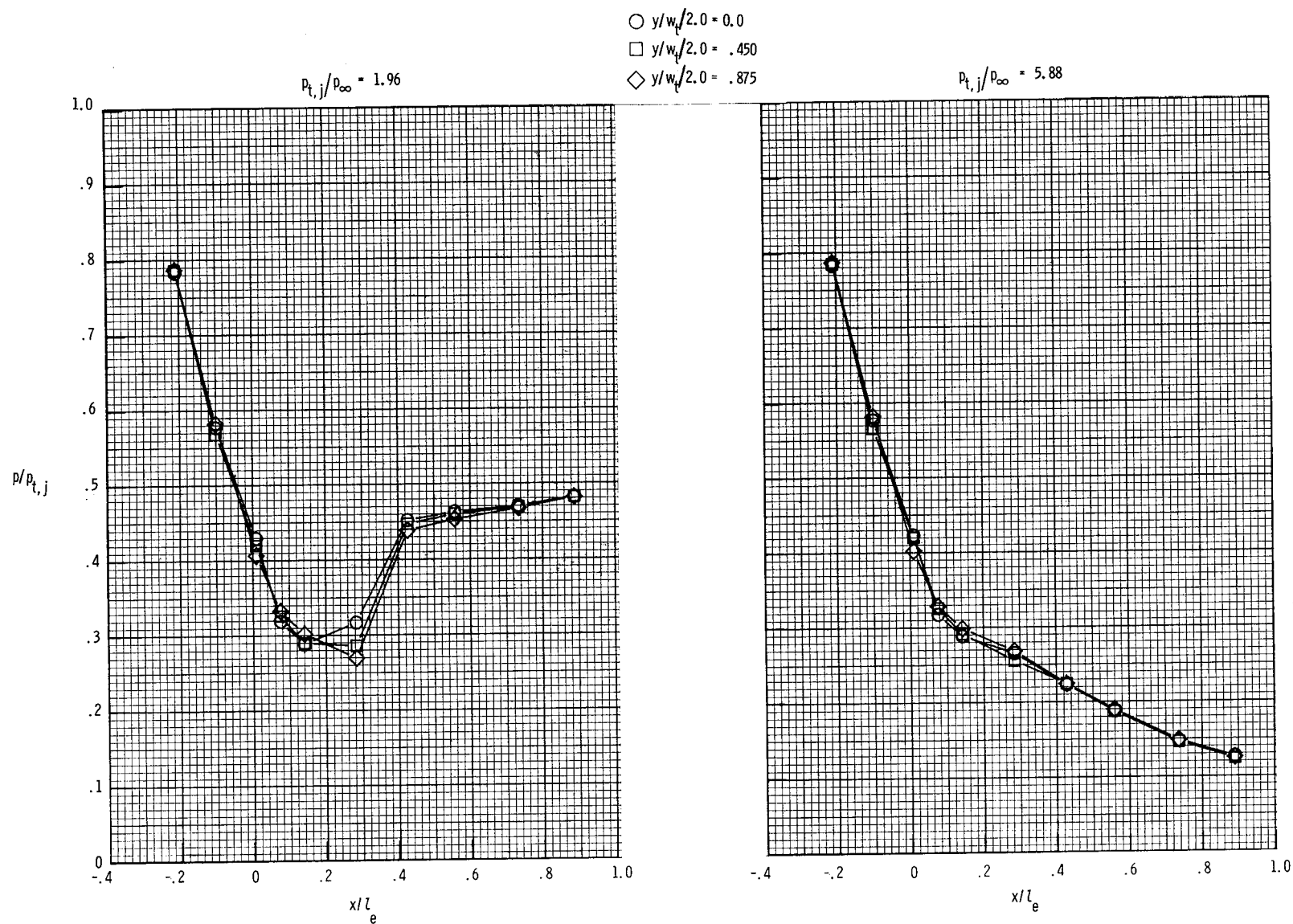
(b) Lower flap.

Figure 11.- Continued.



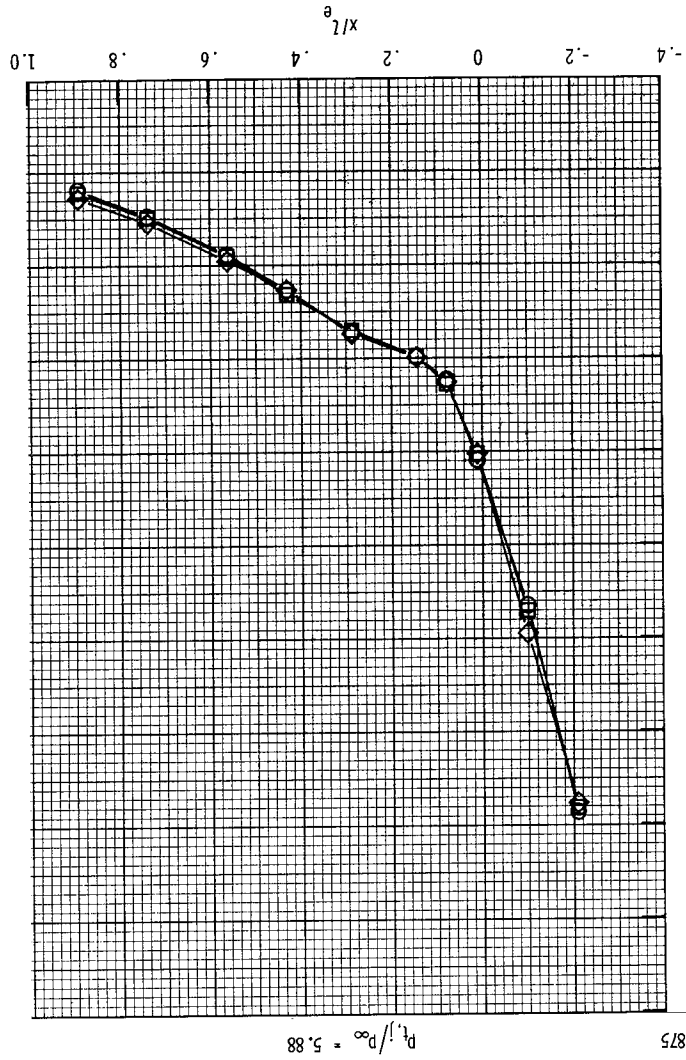
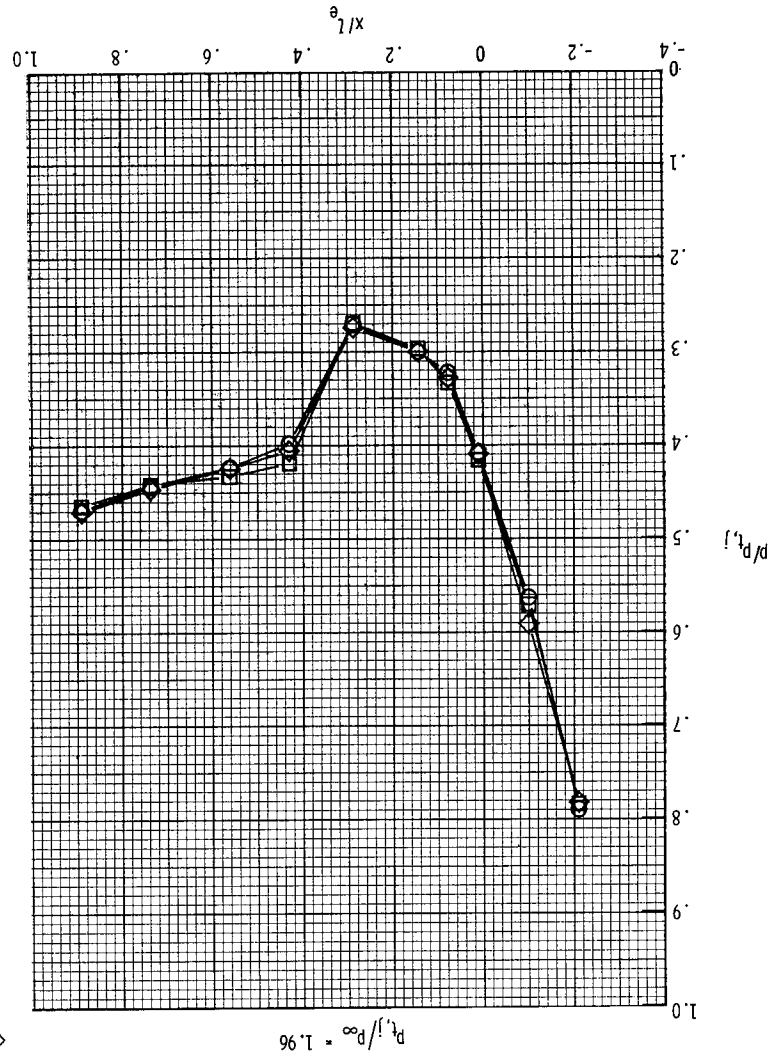
(c) Sidewalls.

Figure 11.- Concluded.

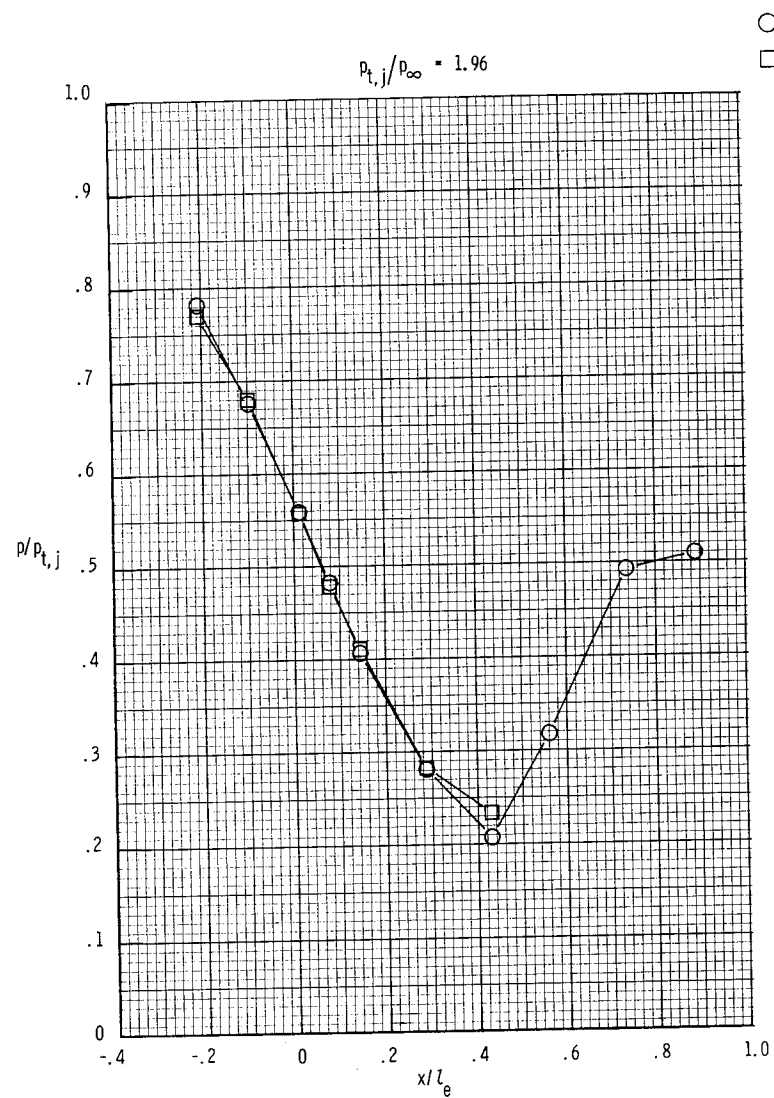


(a) Upper flap.

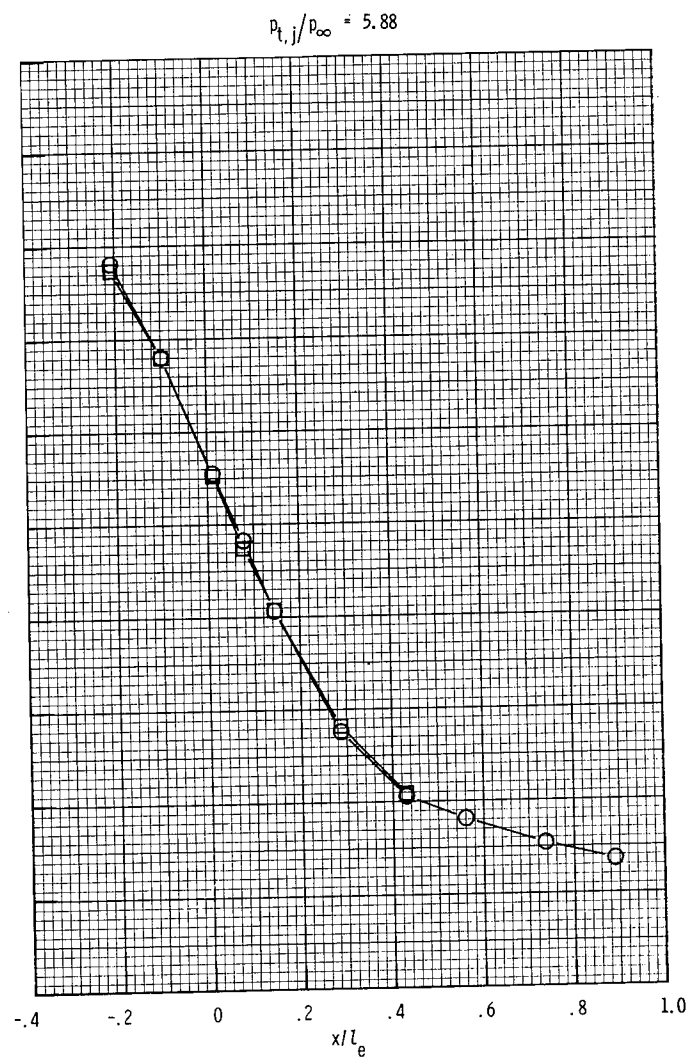
Figure 12.- Internal static-pressure distributions for nozzle B2 at  $p_{t,j}/p_\infty = 1.96$  and  $p_{t,j}/p_\infty = 5.88$ .



(b) Lower flap.  
Figure 12.- Continued.

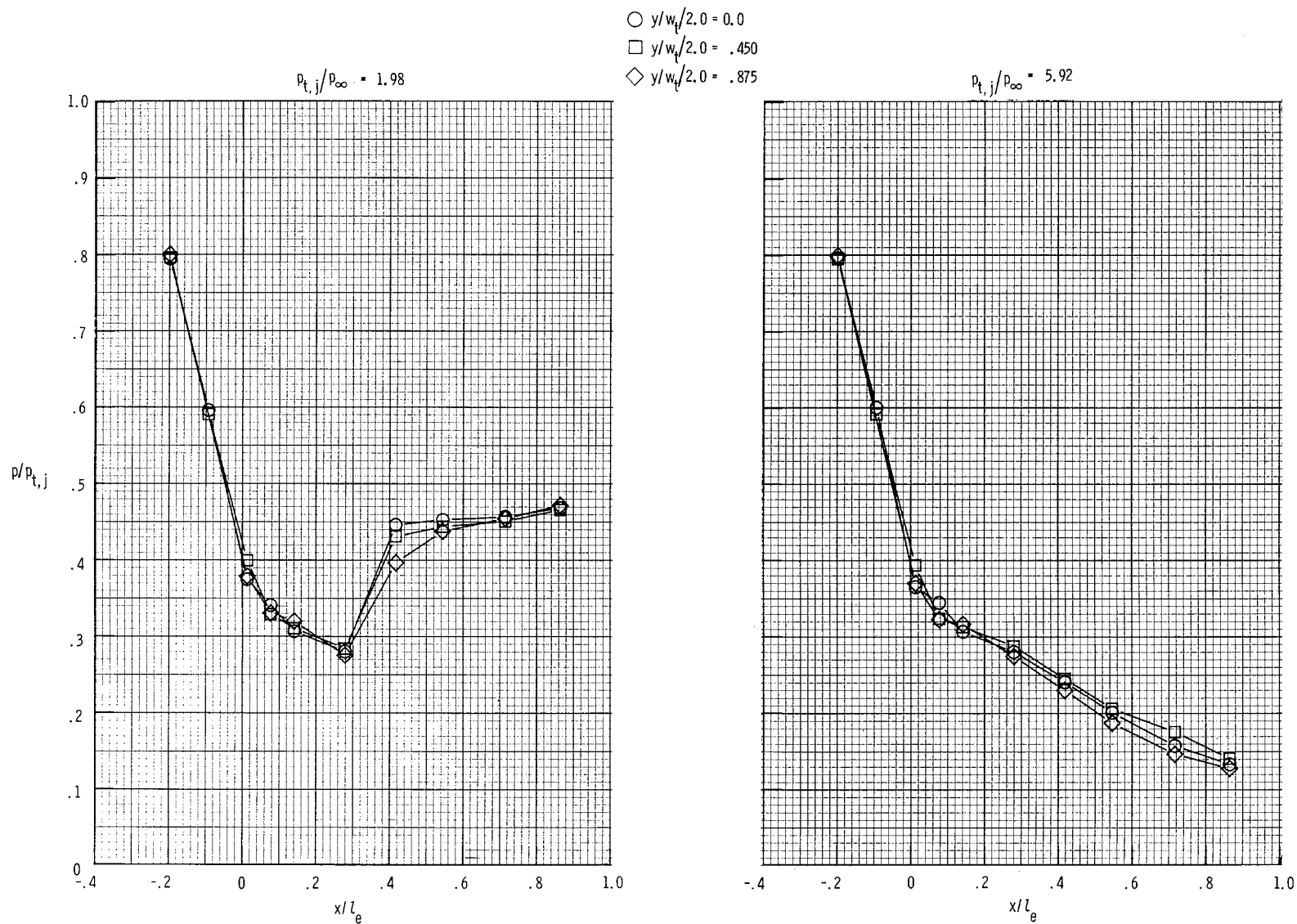


○ Left sidewall  
□ Right sidewall



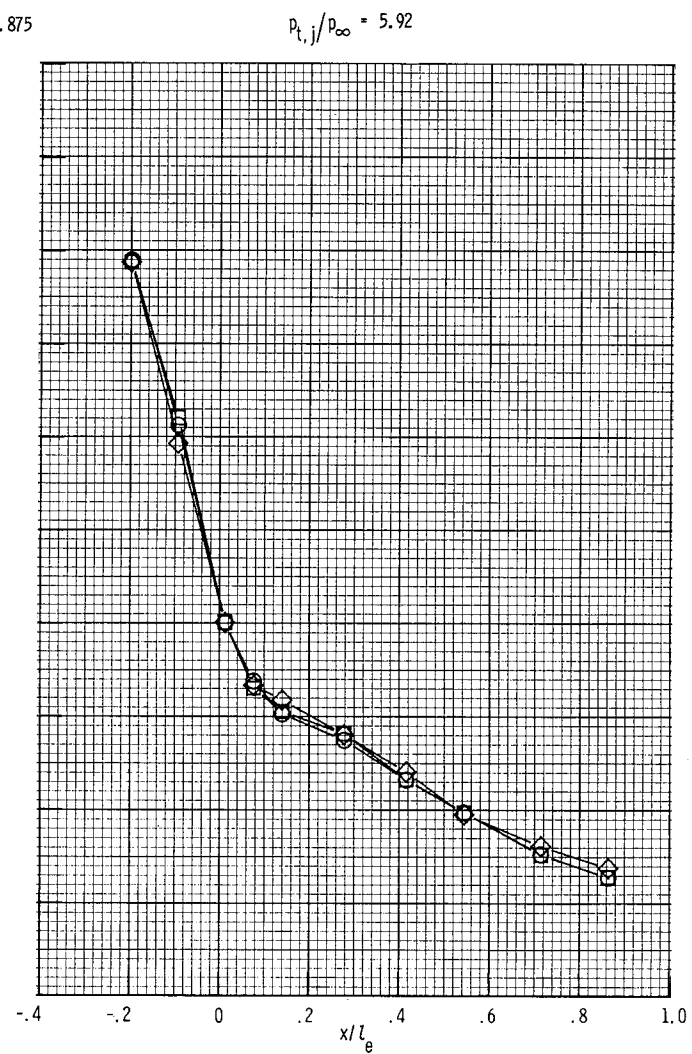
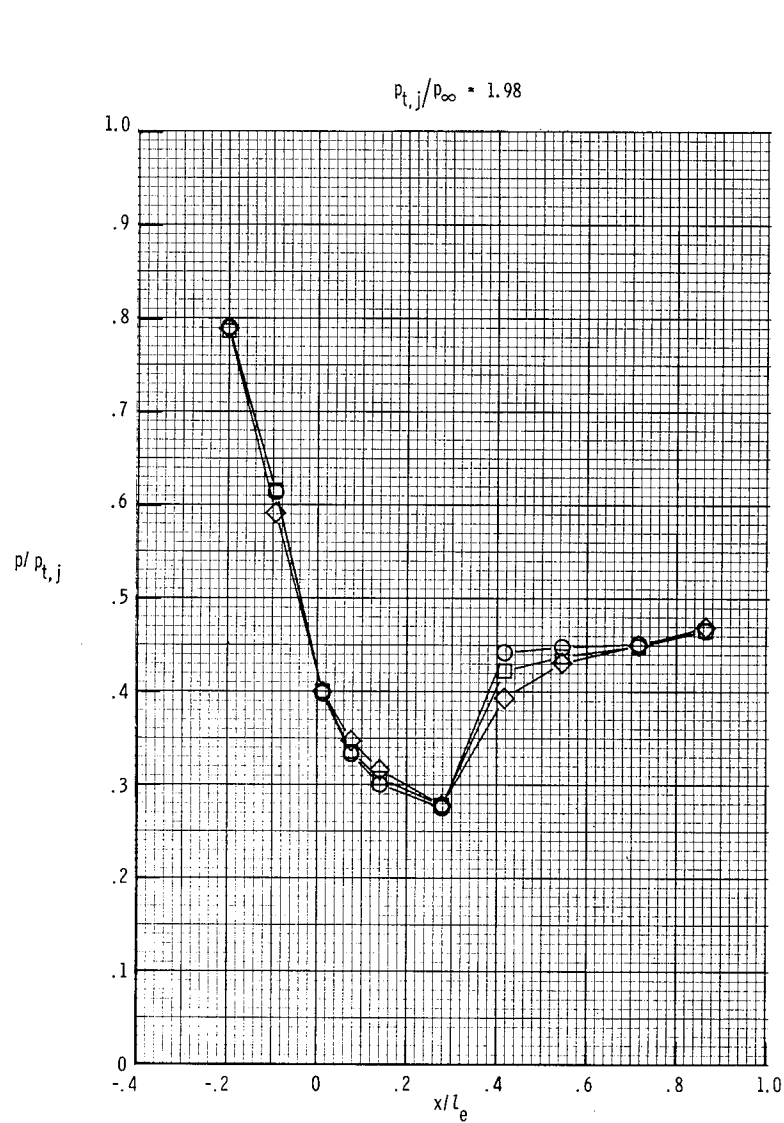
(c) Sidewalls.

Figure 12.- Concluded.



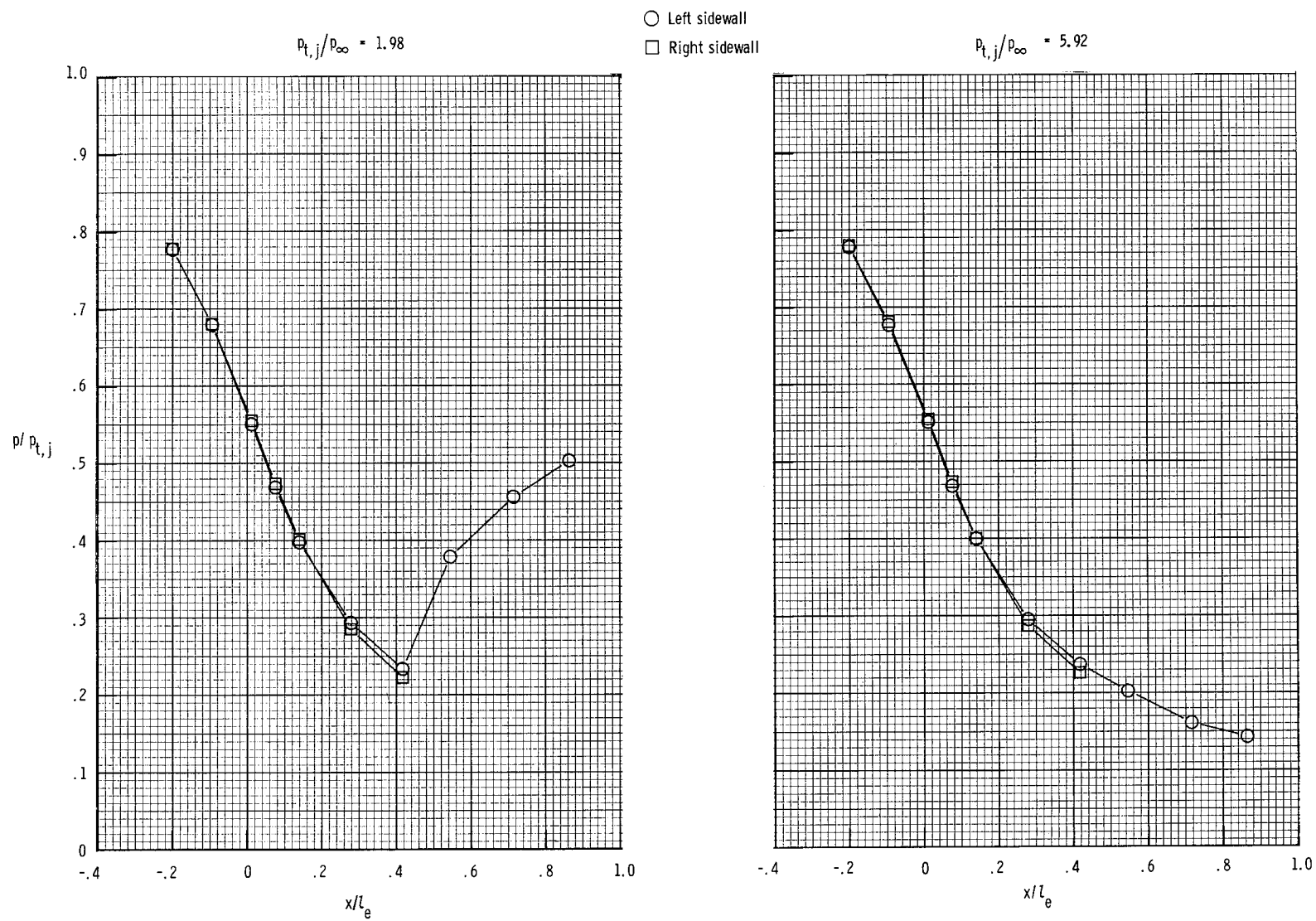
(a) Upper flap.

Figure 13.- Internal static-pressure distributions for nozzle B3 at  $p_{t,j}/p_{\infty} = 1.98$  and  $p_{t,j}/p_{\infty} = 5.92$ .



(b) Lower flap.

Figure 13.- Continued.



(c) Sidewalls.

Figure 13.- Concluded.



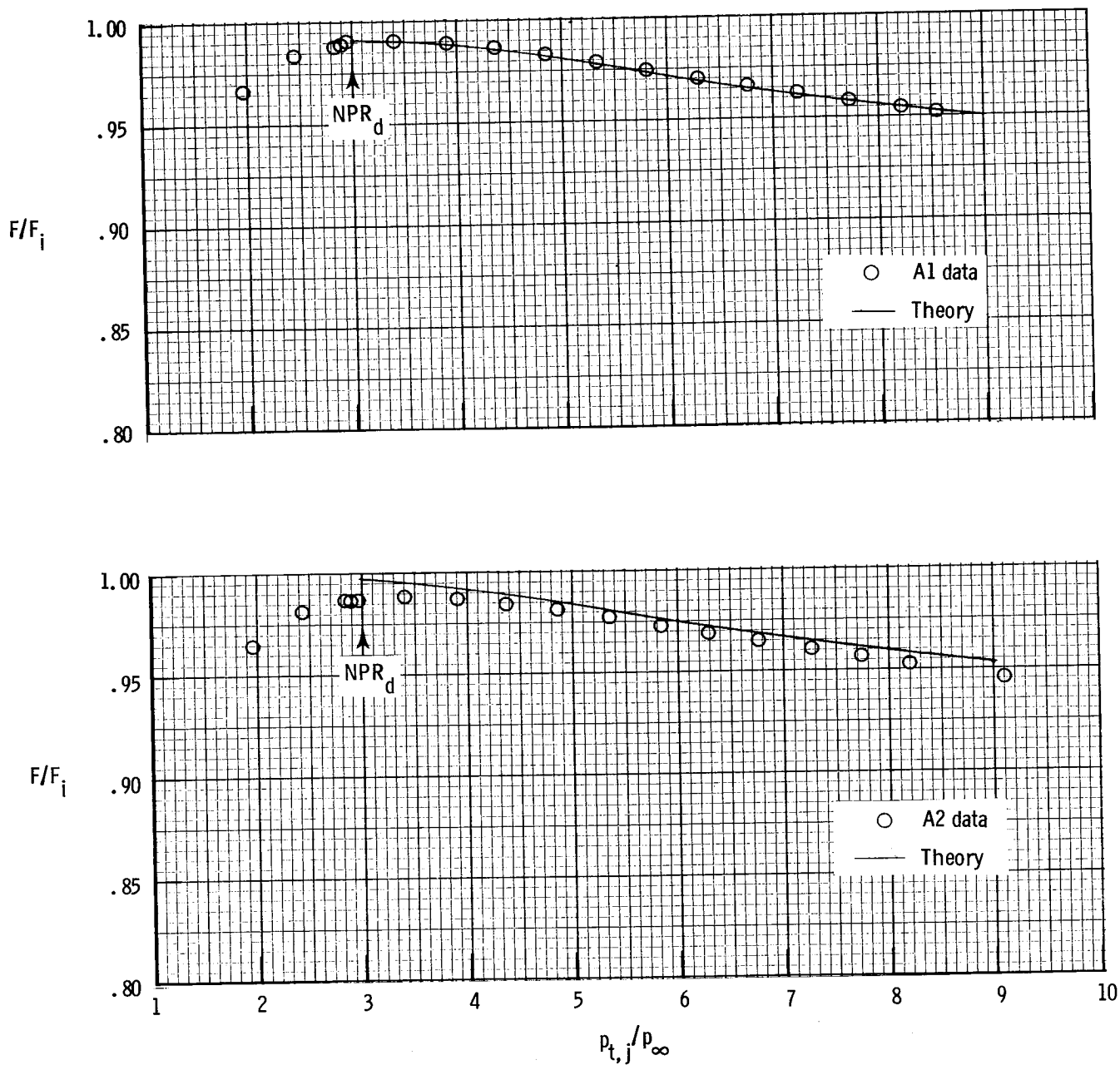


Figure 14.- Comparison of theoretical and experimental internal thrust ratios for nozzles with low divergence angles.

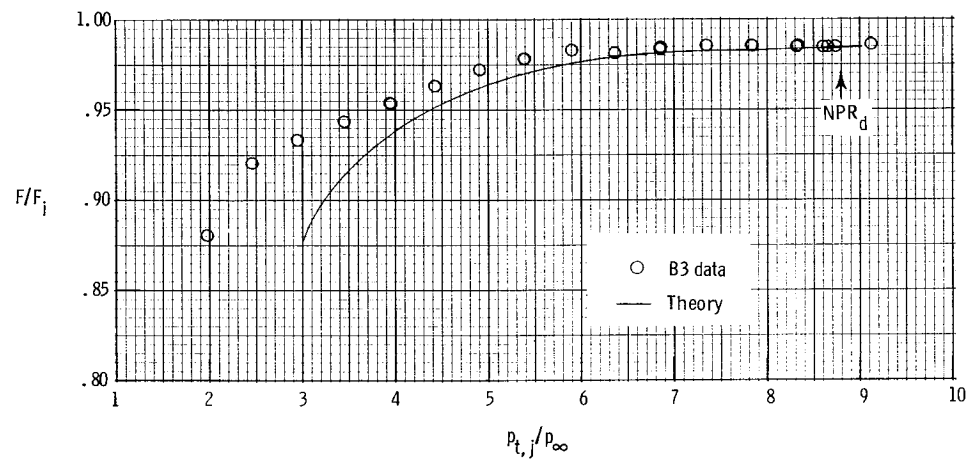
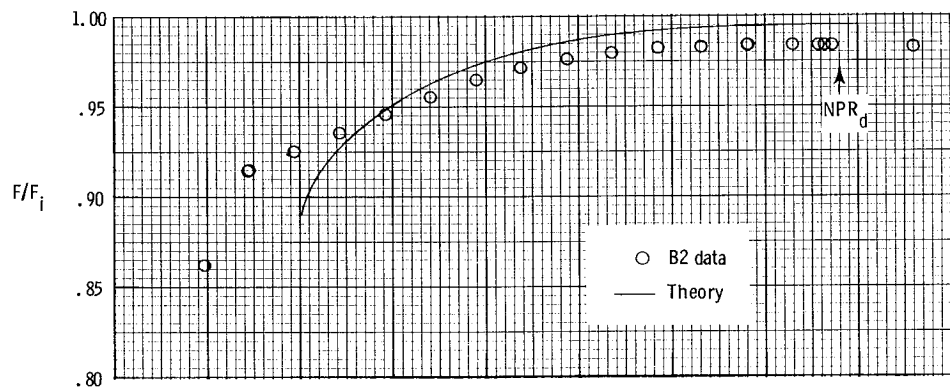
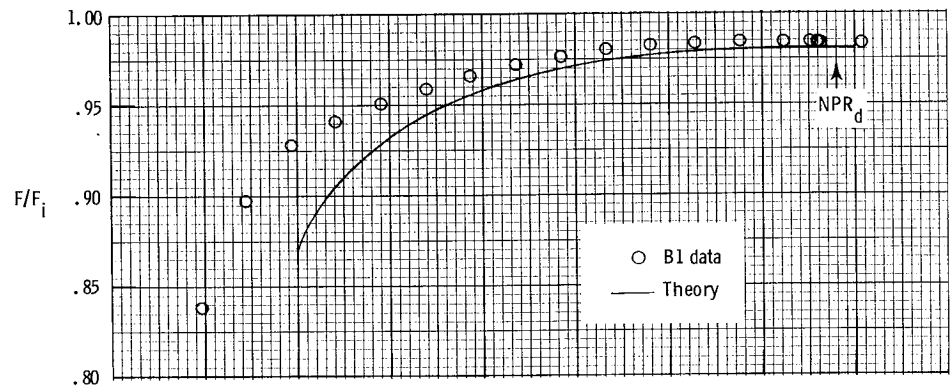


Figure 15.- Comparison of theoretical and experimental internal thrust ratios for nozzles with high divergence angles.

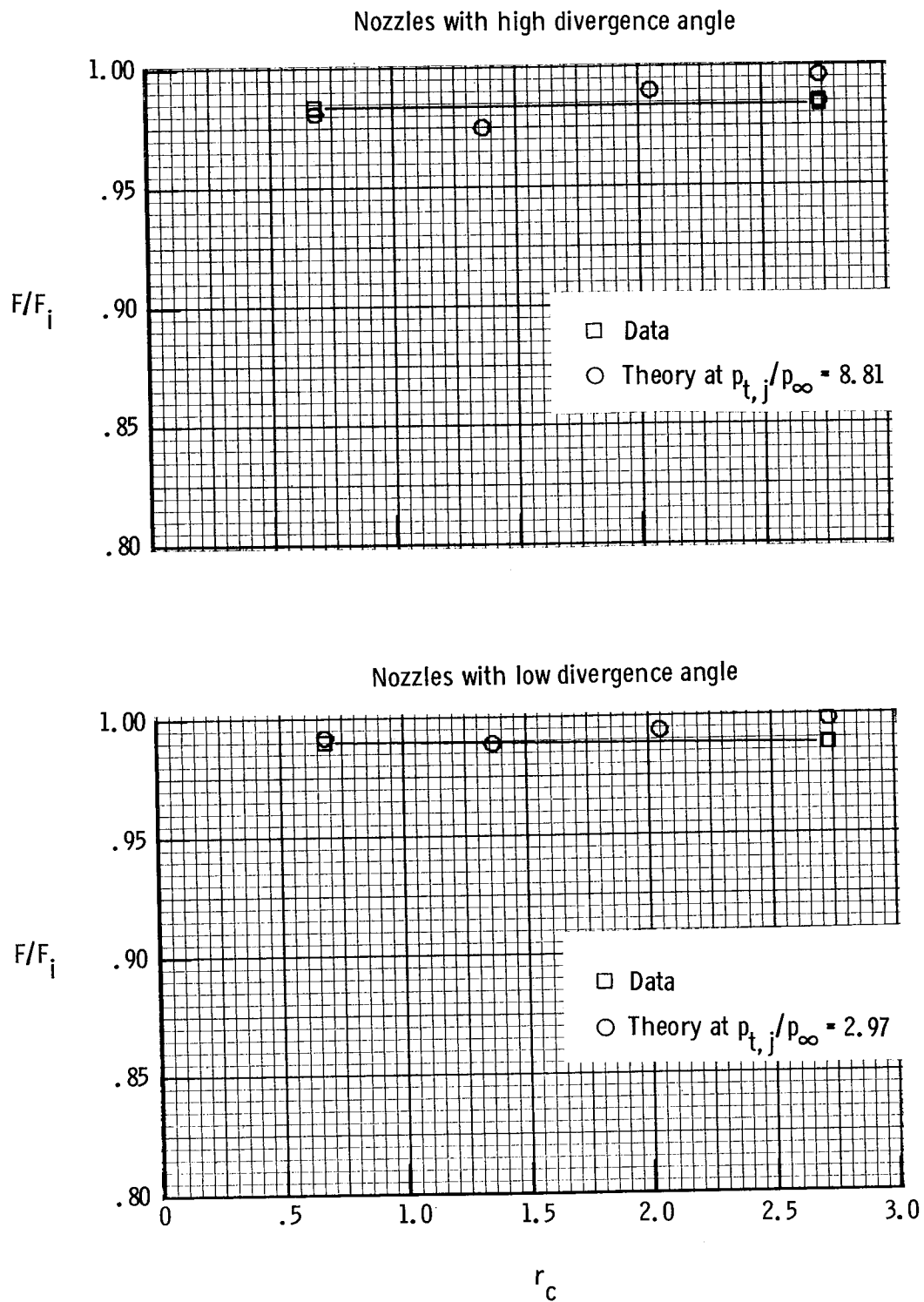


Figure 16.- Effect of throat radius on experimental and theoretical internal thrust ratio.

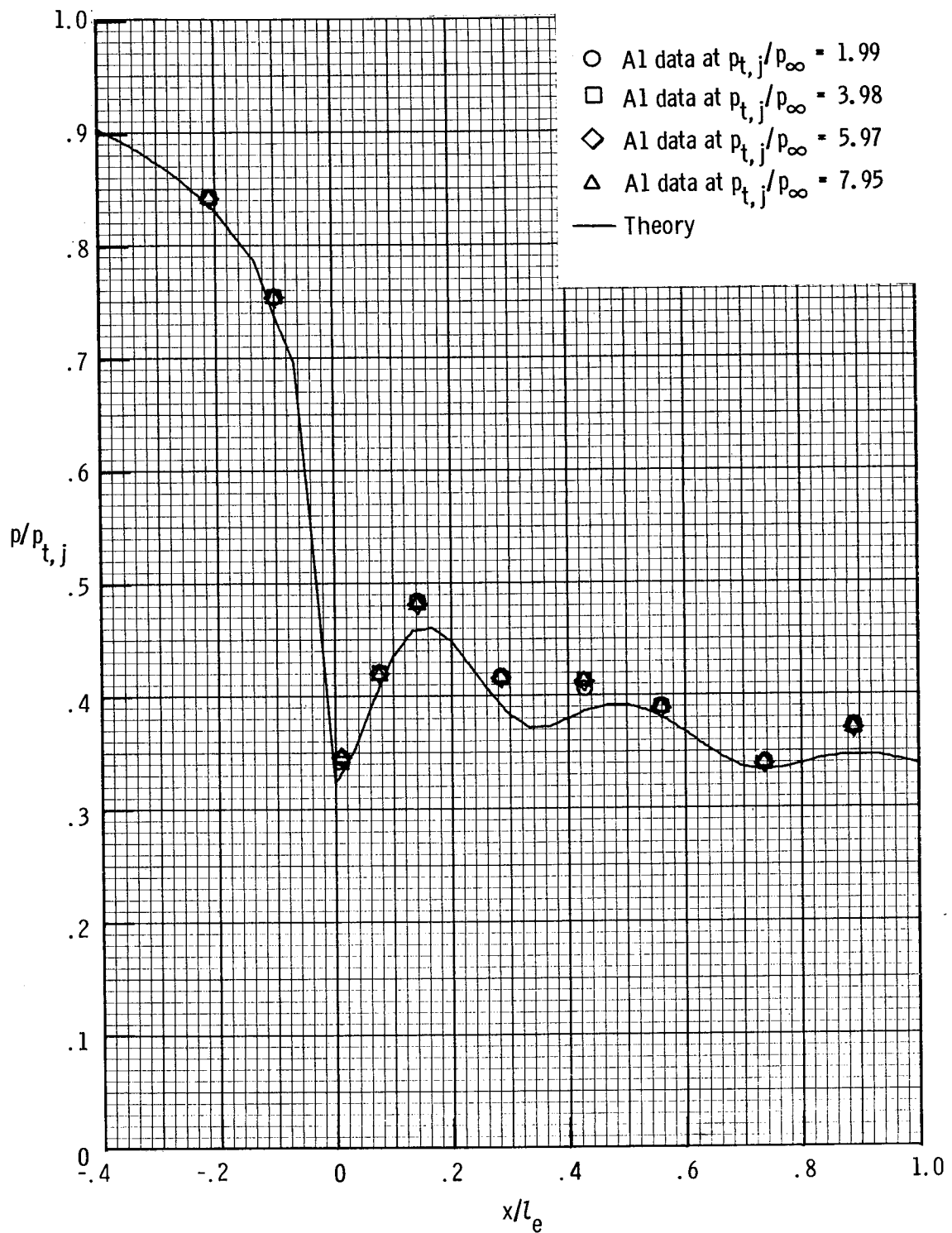


Figure 17.- Comparison of theoretical and experimental static-pressure distributions on upper-flap center line for nozzle A1.

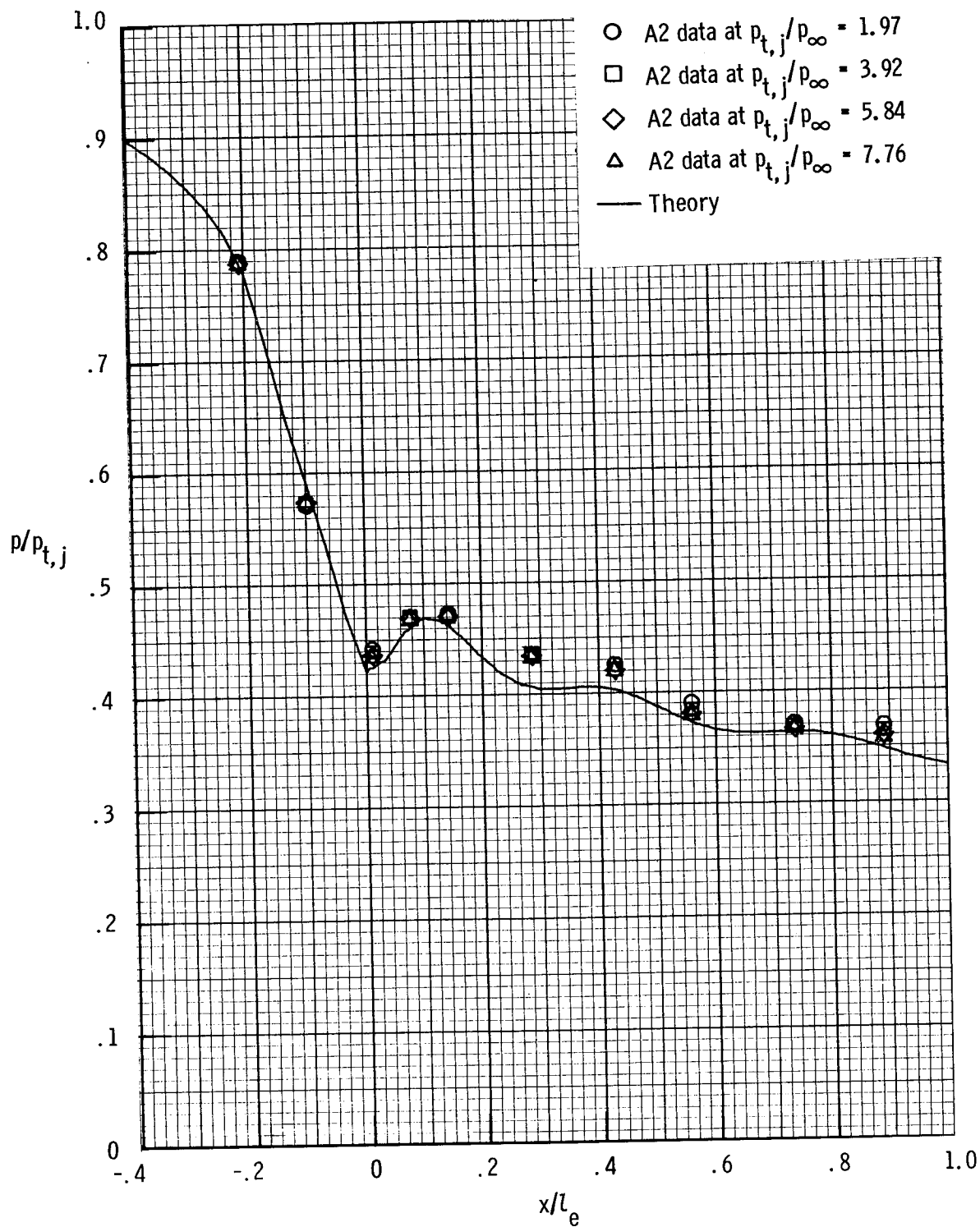


Figure 18.- Comparison of theoretical and experimental static-pressure distributions on upper-flap center line for nozzle A2.

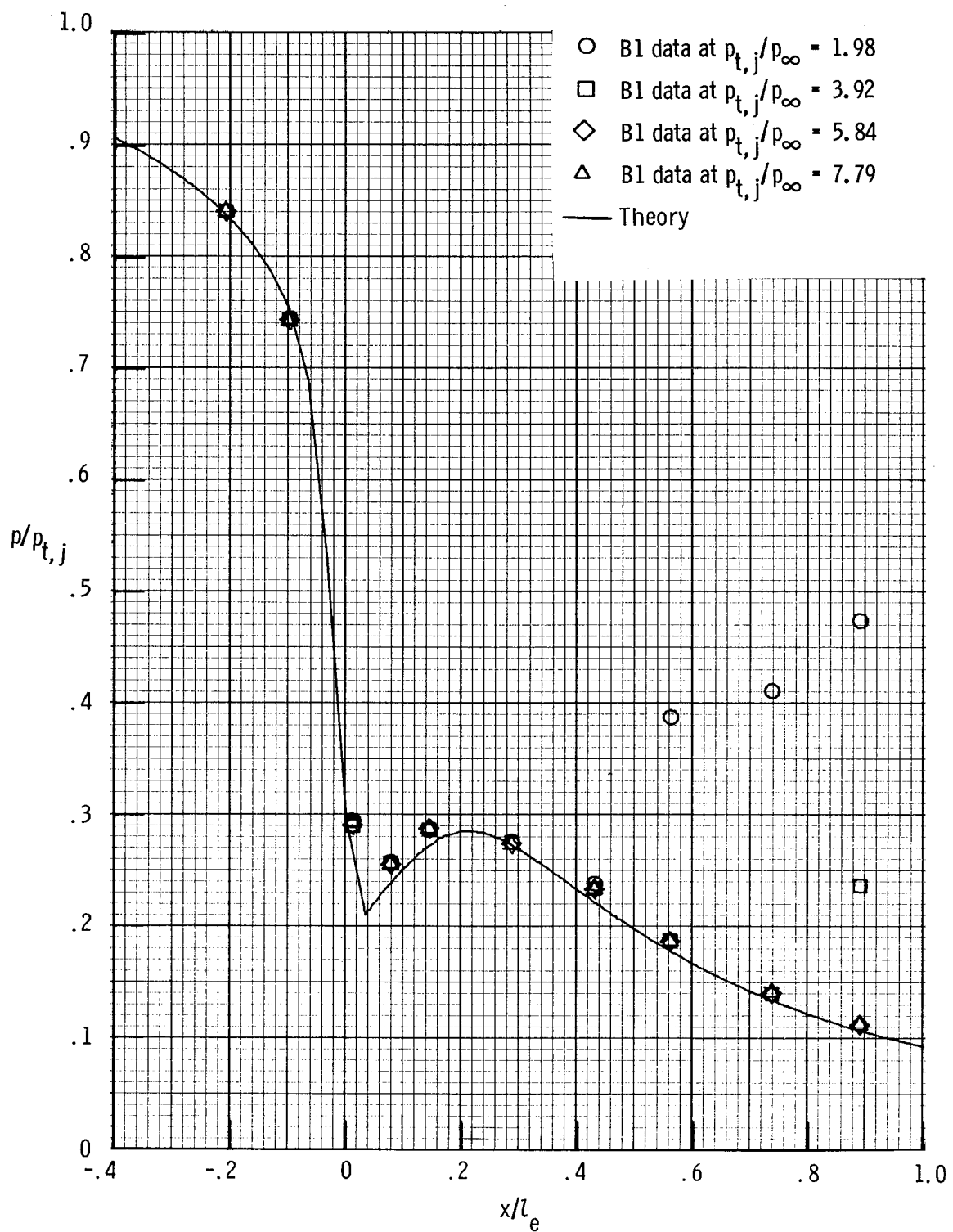


Figure 19.— Comparison of theoretical and experimental static-pressure distributions on upper-flap center line for nozzle B1.

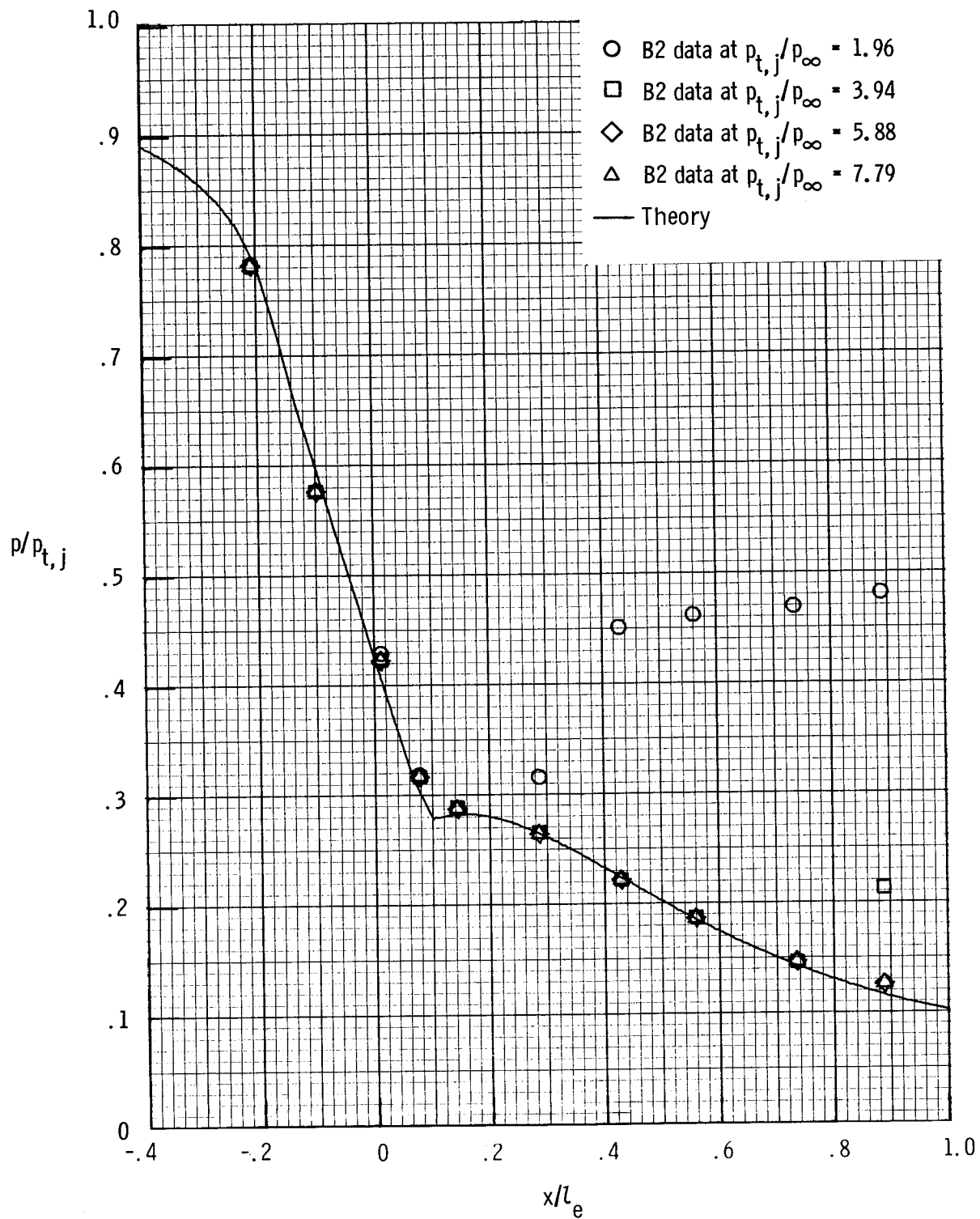


Figure 20.— Comparison of theoretical and experimental static-pressure distributions on upper-flap center line for nozzle B2.

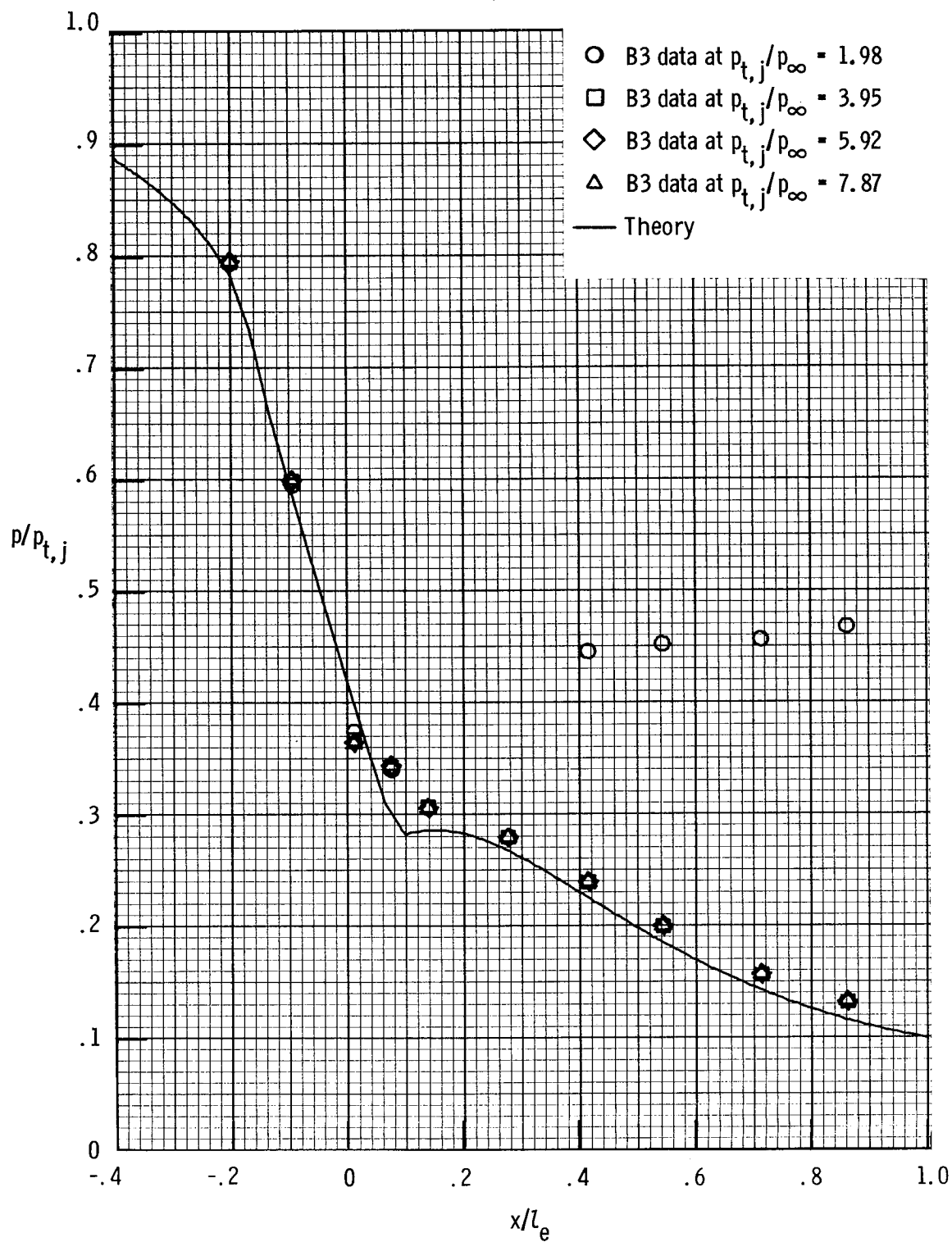


Figure 21.— Comparison of theoretical and experimental static-pressure distributions on upper-flap center line for nozzle B3.



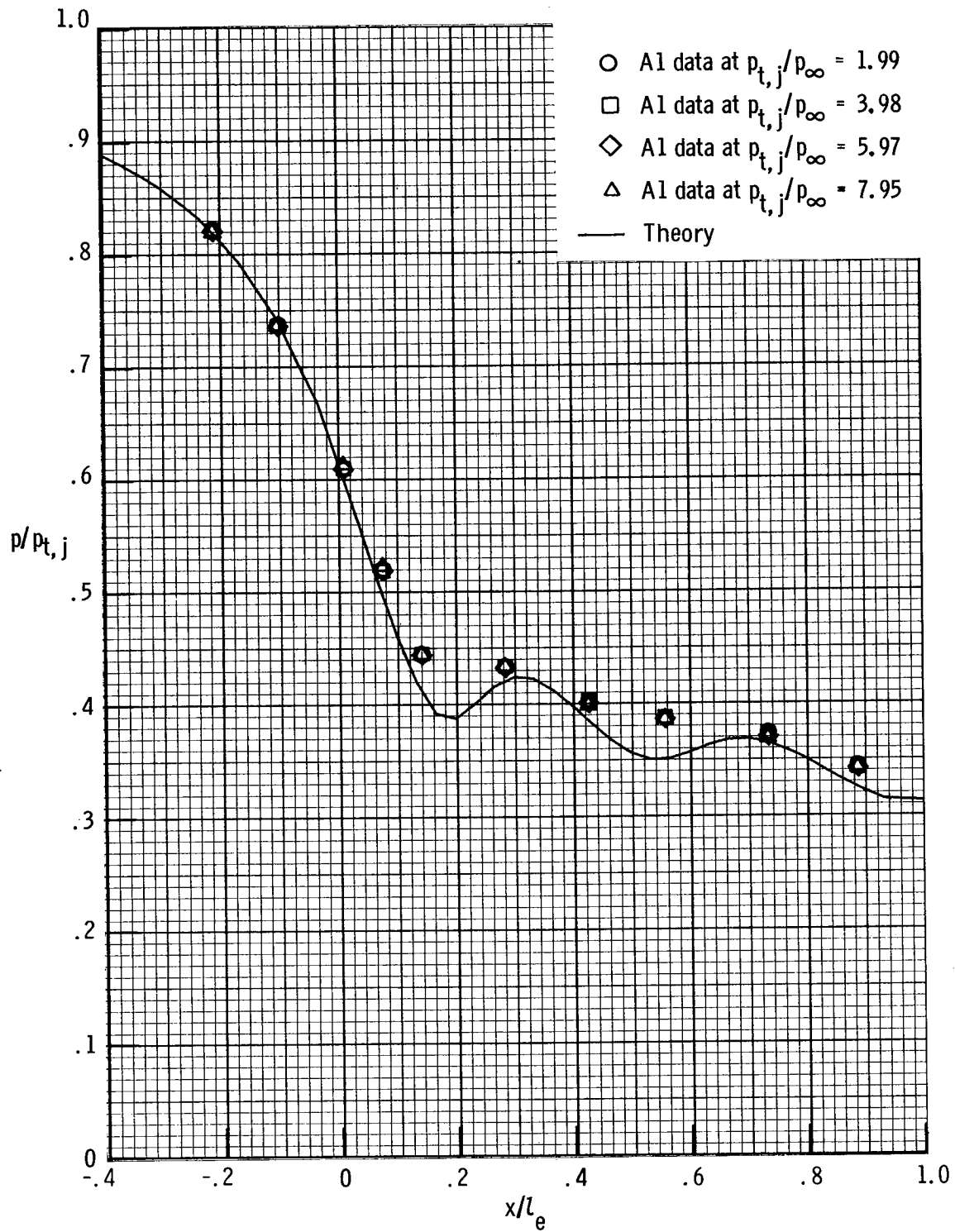


Figure 22.- Comparison of theoretical center-line static-pressure distributions with experimental static-pressure distributions on left sidewall center line for nozzle A1.

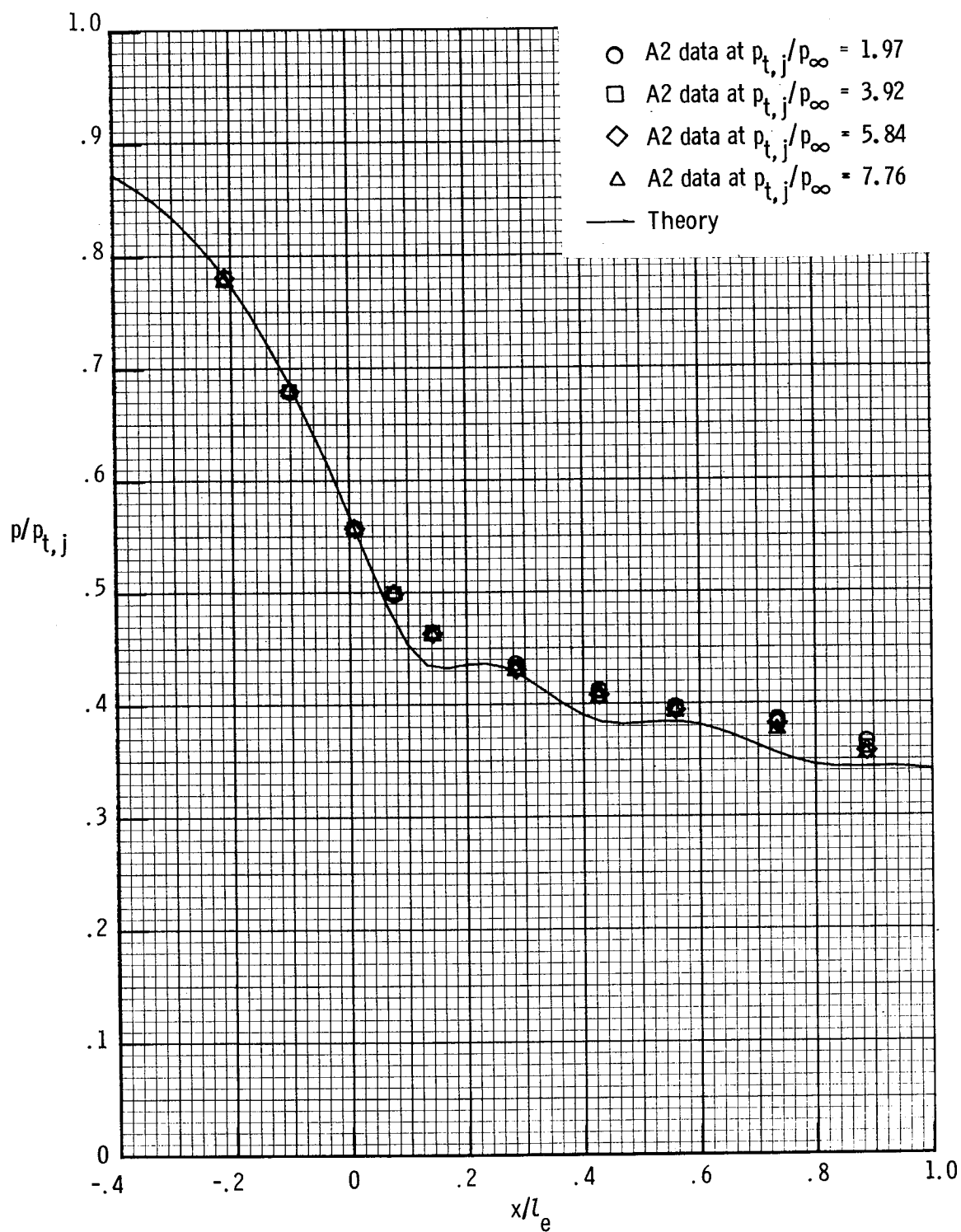


Figure 23.- Comparison of theoretical center-line static-pressure distributions with experimental static-pressure distributions on left sidewall center line for nozzle A2.

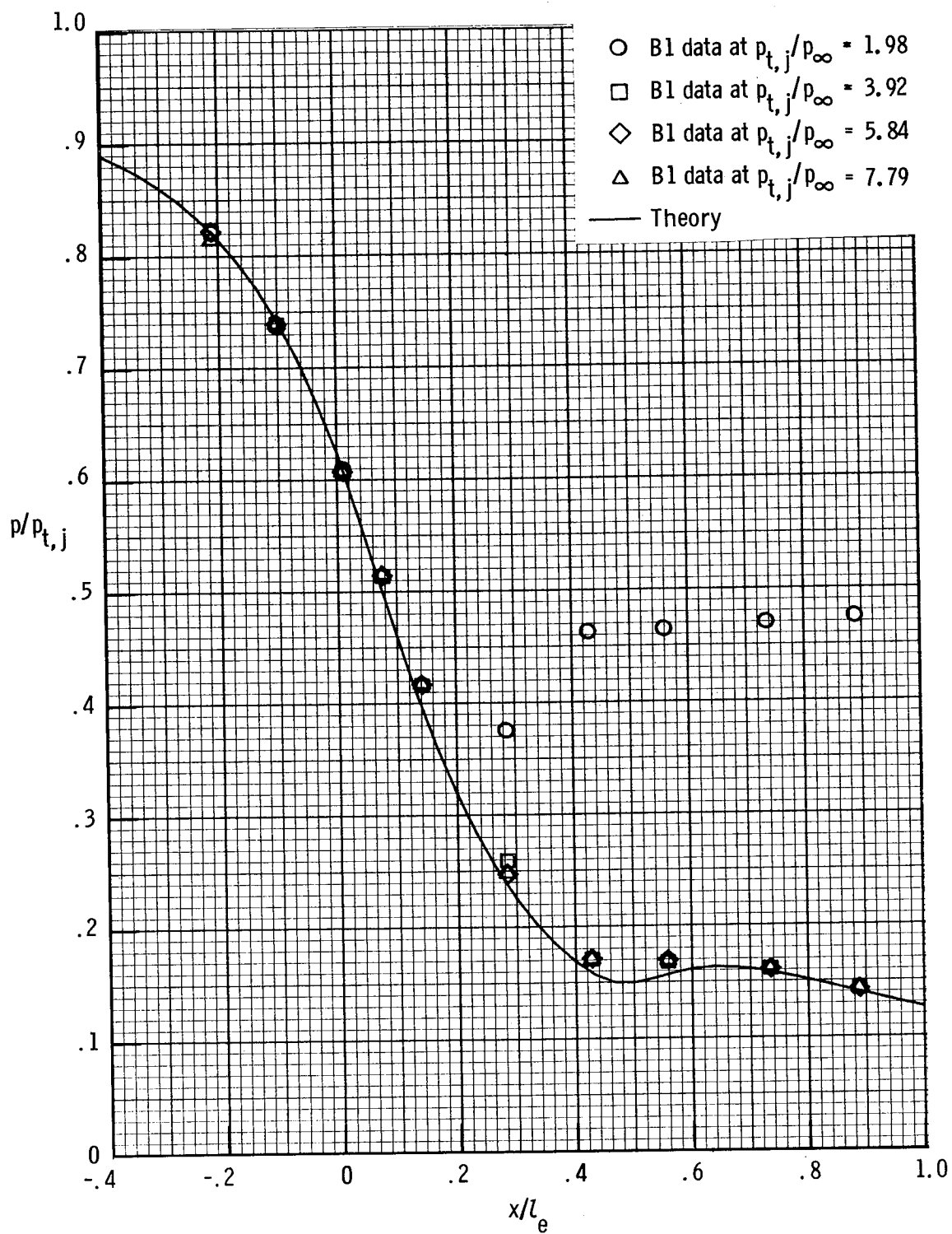


Figure 24.- Comparison of theoretical center-line static-pressure distributions with experimental static-pressure distributions on left sidewall center line for nozzle B1.

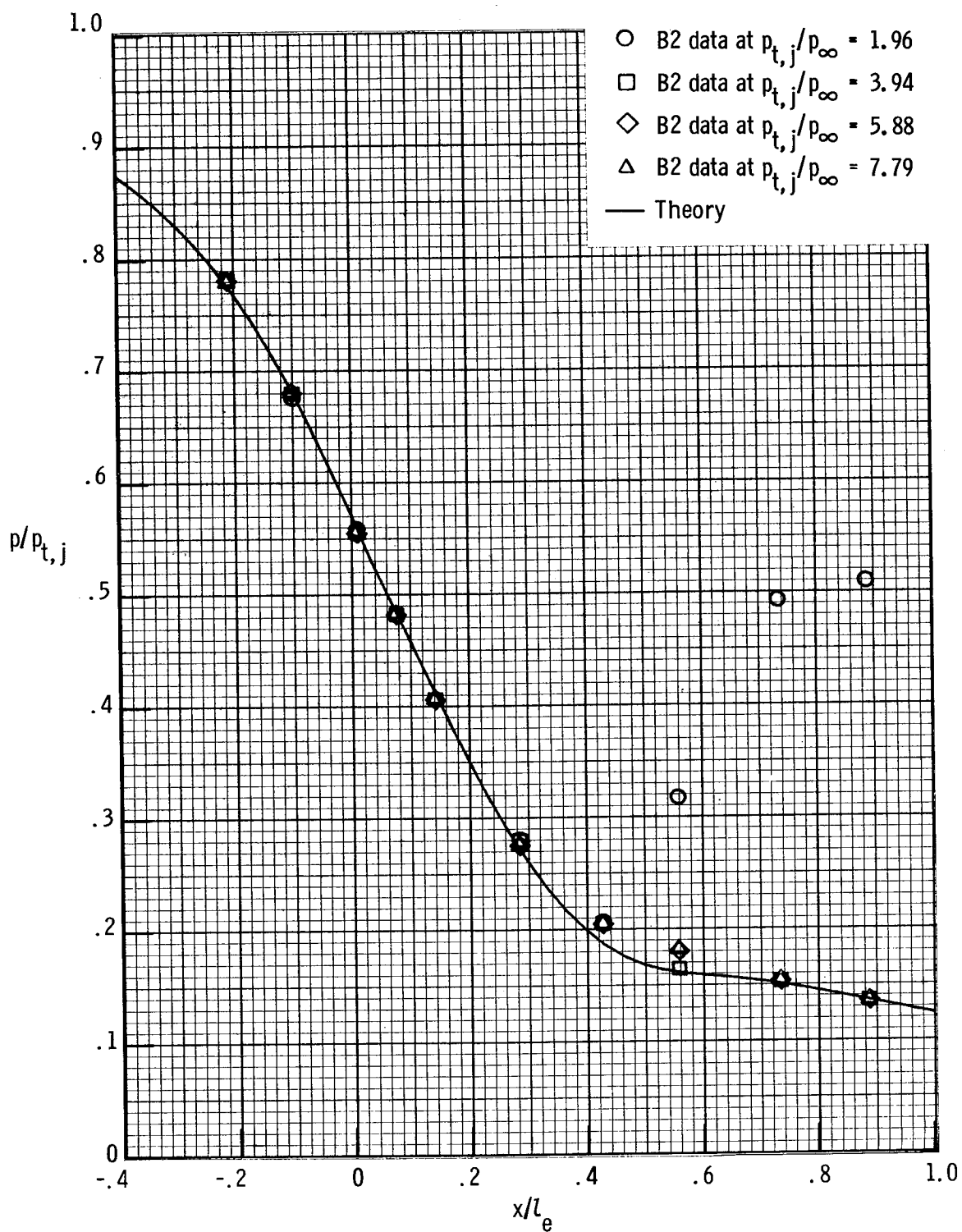


Figure 25.- Comparison of theoretical center-line static-pressure distributions with experimental static-pressure distributions on left sidewall center line for nozzle B2.

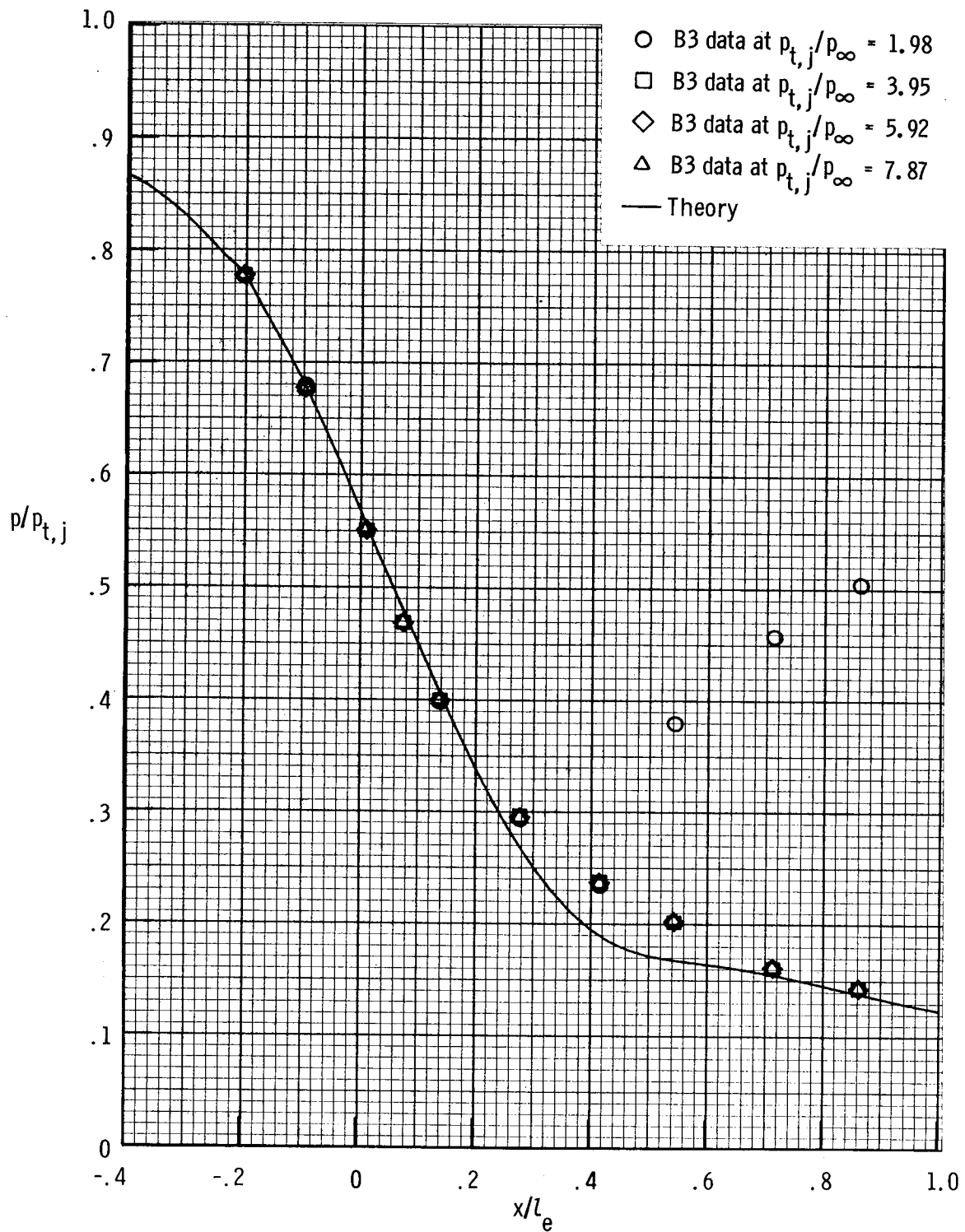


Figure 26.— Comparison of theoretical center-line static-pressure distributions with experimental static-pressure distributions on left sidewall center line for nozzle B3.

1. Report No. NASA TP-1704		2. Government Accession No.		3. Recipient's Catalog No.	
4. Title and Subtitle  THE EFFECT OF THROAT CONTOURING ON TWO-DIMENSIONAL CONVERGING-DIVERGING NOZZLES AT STATIC CONDITIONS				5. Report Date August 1980	
				6. Performing Organization Code	
7. Author(s)  Mary L. Mason, Lawrence E. Putnam, and Richard J. Re				8. Performing Organization Report No. L-13591	
9. Performing Organization Name and Address  NASA Langley Research Center Hampton, VA 23665				10. Work Unit No. 505-32-13-01	
				11. Contract or Grant No.	
12. Sponsoring Agency Name and Address  National Aeronautics and Space Administration Washington, DC 20546				13. Type of Report and Period Covered Technical Paper	
				14. Sponsoring Agency Code	
15. Supplementary Notes					
16. Abstract  An experiment has been conducted at static conditions to determine the internal performance effects of nozzle throat contouring, the result of increasing the circular-arc throat radius. Five nonaxisymmetric converging-diverging nozzles were tested at nozzle pressure ratios up to 9.0. Data are presented as internal thrust ratios, discharge coefficients, and static-pressure distributions. Comparisons of internal performance data for the five nozzles show that throat contouring increases the value of discharge coefficient but has no significant effect on internal thrust ratio except in cases of internal flow separation. To illustrate the use of the two-dimensional converging-diverging (2-D C-D) nozzle data base, a two-dimensional inviscid theory was applied to the five configurations. The generally good agreement of data with theoretical results indicates that two-dimensional inviscid theory can be successfully applied to the prediction of 2-D C-D nozzle internal flow.					
17. Key Words (Suggested by Author(s))  Nonaxisymmetric nozzles Internal performance Static performance NAP			18. Distribution Statement  Unclassified - Unlimited  Subject Category 02		
19. Security Classif. (of this report) Unclassified	20. Security Classif. (of this page) Unclassified	21. No. of Pages 67	22. Price A04		